A smart sensing platform for the discrimination of human movement

Mark Tristan Elliott

Engineering Systems and Management

ASTON UNIVERSITY

Doctor of Philosophy

April 2007

A smart sensing platform for the discrimination of human movement

Mark Tristan Elliott

Engineering Systems and Management

ASTON UNIVERSITY

Doctor of Philosophy

April 2007

This thesis documents the design, implementation and testing of a smart sensing platform that is able to discriminate between differences or small changes in a person's walking. The distributive tactile sensing method is used to monitor the deflection of the platform surface using just a small number of sensors and, through the use of neural networks, infer the characteristics of the object in contact with the surface.

The thesis first describes the development of a mathematical model which uses a novel method to track the position of a moving load as it passes over the smart sensing surface.

Experimental methods are then described for using the platform to track the position of swinging pendulum in three dimensions. It is demonstrated that the method can be extended to that of real-time measurement of balance and sway of a person during quiet standing.

Current classification methods are then investigated for use in the classification of different gait patterns, in particular to identify individuals by their unique

gait pattern. Based on these observations, a novel algorithm is developed that is able to discriminate between abnormal and affected gait. This algorithm, using the distributive tactile sensing method, was found to have greater accuracy than other methods investigated and was designed to be able to cope with any type of gait variation.

The system developed in this thesis has applications in the area of medical diagnostics, either as an initial screening tool for detecting walking disorders or to be able to automatically detect changes in gait overtime. The system could also be used as a discrete biometric identification method, for example identifying office workers as they pass over the surface.

Keywords: Gait Classification, Distributive Tactile Sensing, Pattern Recognition, Smart Sensing.

Dedicated to Amy and my Family

Acknowledgements

Contents

List of Figures

List of Tables

Chapter 1

Introduction

1.1 Force plates and their limitations

Gait analysis laboratories are essential for the detection of walking disorders in people and the monitoring of their rehabilitation process post-operation. One of the most important instruments present in a gait analysis laboratory is the force plate. Force plates are rigid platforms, usually around $0.5m^2$ that measure the ground reaction force (GRF) created by the subject as they walk over the plate. Most modern force plates can accurately measure the ground reaction force and moments in all three dimensions. Force plates operate using four piezo-type force transducers connected in each corner between the platform and the base-plate (which is in contact with the floor). Each transducer measures the applied force as the subject walks over the plate. The resultant forces are calculated as the sum of the four sets of transducer forces. Force plates can provide very accurate measures of the force and moment components generated as a person walks over a surface and hence can be used as a tool for diagnosing walking disorders along with changes in walking over time by analysing the data generated. However, there are several limitations of force plates that still have not yet been resolved.

Limited Dimensions. Force plates have limited dimensions and so can only capture one foot strike. Also, their design means that even if a larger plate was manufactured, then it wouldn't be possible to separate the forces generated during the double stance phase of walking. Therefore, for most walking applications a pair of force plates must be used. To reduce noise, most force plates need to be embedded or secured to the floor they are mounted on. This leads to the issue of how should the plates be positioned relative to each other? People have different stride lengths, yet the semi-permanent installation and limited plate dimensions mean that only a narrow range of stride can be properly accommodated. In the worst case this can cause the subject to shorten or lengthen their normal stride and result in measurements being taken that are not representative of the subject's natural gait. In a similar sense, it has been noted that the prominence of two force plates embedded into the walkway can lead to the subject 'aiming' for the plate or even stamping onto the plate to 'ensure a reading is taken'. The solution is to hide the plates, by covering the surface with carpet for example. However, although this helps in achieving the measurement of natural gait, the limited plate dimensions mean that multiple measurements are required to increase the chance of capturing a direct hit of the foot onto the force plate.

Raw Data Output. The primary disadvantage with force plates however is that they only produce raw measurement data, there is no intelligence in the system to aid with the analysis. A lab analyst will have to compile and examine the six sets of time series data (three dimensions of forces and moments) for *each* capture. The captured data may then be compared to previous datasets, if say, a pre and post operation analysis was being carried out. This could take several hours to examine and report back on. The extra time taken to analyse the data results in less time available for patients to use the gait analysis laboratory and hence increased patient waiting times.

1.2 Overview of a novel gait analysis platform

In this thesis, the development of a novel gait analysis platform is described. The platform aims to resolve the identified issues relating to the current force plate instruments. First, the design of the physical sensing platform addresses the dimension problem with force plates. A large walkway type platform was developed which could capture a full gait cycle (i.e a left and right foot strike) on a single continuous plate with low levels of cross talk. This eliminated the spacing problem by accommodating a much larger range of stride lengths.

Force plates, rely on their stiffness and high natural frequency to capture accurate GRF measurements. Ideally, they are required to be embedded into the surface of a solid floor to ensure they are not affected by external noise. This can make installation of force plates complex and in some cases impractical. Therefore, rather than develop the sensing platform using standard force plate technology, the distributive tactile sensing method is investigated as an alternative. The distributive tactile sensing method utilises a small number of sensors to capture the deflection of a continuous surface. The sensor data is then analysed, usually using neural network algorithms to infer the characteristics of the object in contact with the surface, causing the deflection. Note therefore, with this method a flexible surface is required in contrast to a stiff surface used by force plates. The final prototype developed was a self contained system and therefore was very resilient to external movement or noise.

The majority of this thesis concentrates on the development of algorithms that will take the sensor data from the platform and perform some form of intelligent analysis. The algorithms developed are able to compare the captured gait patterns created by a subject walking over the platform and compare them to a stored database of templates. Small differences in the gait pattern are recognised and can therefore be used to classify the pattern to one of two (e.g normal/abnormal) or one of several (e.g person identification) classes.

The system developed means the identified class can be presented to the user

around three seconds after the subject has walked over the platform. Therefore, the system has potential to greatly reduce analysis times and increase the number of patients tested in a gait analysis laboratory. It has applications as an initial screening tool, where the system could identify and provide possible suggestions to the cause of any deviation away from normal walking that the patient is exhibiting. Alternatively, it could be used to compare a subject's gait pattern post-operation to that measured pre-operation and identify any differences. All this would save the gait analyst large amounts of work and would direct them towards a quicker diagnosis.

It should be noted that measurement of ground reaction forces and moments was not one of the aims of the project, therefore although with detailed calibration it would be possible to produce these measurements from the system developed, it is not the intention to re-create or improve the measurements provided by the force plate. Instead, the sensor outputs are used as abstract, dimensionless values to take gait analysis a step further by being able to discriminate and classify gait patterns rather than just provide raw measurements.

1.3 Objectives

The objectives of the work in this thesis may be summarised as follows:

a). Establish the viability of the Distributive Tactile Sensing method when applied to a large scale plate subjected to dynamic loads.

b). Develop a sensing platform that overcomes the limitations of the force plate caused by its physical dimensions and therefore be able to capture gait patterns without restricting a person's natural walking style.

c). Investigate appropriate sensor methods and implement the required electronic hardware to capture accurate time series data for analysis.

d). Develop algorithms that can discriminate and classify between different gait patterns. In particular it must be able to discriminate between small changes in a person's gait and also be an algorithm that can be easily generalised to different gait pattern classifications.

1.4 Structure of thesis

In Chapter 2 current literature relating to the research is reviewed. First, current research into gait analysis instruments is investigated, with a particular focus on research into overcoming the limitations of force plates. Next some of the previous applications of the Distributive Tactile Sensing method are discussed, showing how the method has developed over the last thirteen years. The remainder of the chapter reviews the literature related to each of the experiments undertaken and described in this thesis. This includes the areas of moving force identification, balance and sway and finally gait discrimination.

The first task involved testing the potential viability of using the Distributive Tactile Sensing method to infer the characteristics of an object or person ambulating over the surface of a plate. In Chapter 3 a mathematical model is developed that attempts to track a moving load as it passes over the surface of a plate. The amplitude of the force applied varies harmonically. The model is split into two parts, with the plate response first being modeled mathematically followed by a technique which is developed that uses the captured deflection data to track the load position as it moves across the surface.

Next, in Chapter 4 an experiment is developed that tests the ability to infer the characteristics of an object through the deflection of a plate it was mounted on. In this case the experiment was designed to be relatively controllable with few variables such that the mechanical construction, electronics and algorithms could all be developed and thoroughly tested. The set up consisted of a swing construction, mounted on to a supported plate. The experiment investigates whether the position of the swing can be tracked in real-time using the distributive tactile sensing method. The results can be easily applied to the area of balance and sway measurement of people during quiet standing.

In Chapter 5, the issues discovered in the swing experiment are identified and improved upon where necessary. This experiment moves from measuring the position of an object to the classifying of a person's gait. The experiment described

in this chapter investigates the viability of using the measured gait pattern to identify a person. A convenient sample of people are tested against, with two different classification algorithms tested: Dynamic Time Warping and feature extraction methods. Both algorithms are found to produce reasonable results. However, it is found that certain types of walking present in the sample can affect the accuracy of the whole system.

In Chapter 6, the findings from the previous experiments are used to work towards the main aim of being able to discriminate between different gait patterns. In this experiment a test is developed to determine whether small changes in gait can be detected in a person's walking. To do this, a volunteer's walking is subtly affected by making them carry a heavy tray or wear a heavy backpack. Two classes are defined as normal walking (without tray/backpack) and abnormal walking (with tray/backpack). Feature extraction algorithms are tested again along with a normalised distance calculation algorithm. The distance algorithm is found to achieve the best results and is also determined to be the most likely to be the most generalisable algorithm to different scenarios.

Finally, conclusions are drawn from the research in Chapter 7 along with suggestions on how the research could be developed further in the future to produce a practical and commercially viable system.

Chapter 2

Literature Review

2.1 Introduction

The wide scope of the research in this thesis leads to several areas of the literature being reviewed. The primary application of the system developed is in the area of gait analysis. In the first section of the literature review, instruments currently used in a gait analysis laboratory are reviewed along with current research being undertaken to improve them. The force plate is identified as the primary tool for measuring ground reaction forces of a person. These ground reaction forces are then used to analyse the patient's gait and provide a diagnosis of any walking disorder. Whereas force plates use a stiff plate, the platform developed in this thesis uses a flexible surface and hence uses the distributive sensing method to capture the gait profile through the plate deflection. In section 2.3 the previous applications of distributive tactile sensing are reviewed, showing how this technique has developed over the last decade or so.

In Chapter 3, a mathematical model is developed that enables the tracking of a moving force as it progresses over a plate. Section 2.4 investigates other research

into the area of dynamic plate response due to a moving load. Several papers are also discussed where the plate response is used to identify the applied force or the force impact location. It's interesting to note however, that there appears to be no current literature regarding the tracking of the force location as it traverses the surface of a plate.

Another potential application of the platform developed is in the measurement of balance and sway during quiet standing (see Chapter 4). Therefore current measurement techniques are reviewed in section 2.5, with most of the literature stating the use of force plates or accelerometers to measure postural instability. It appears there is much less research on balance and sway measurement than gait measurement.

Finally, the area of gait classification is reviewed in section 2.6. The ultimate project aim was to develop the platform based system such that it is able to discriminate between normal and affected gait or to be able to detect a change in gait, rather than just provide raw data measurements. There have been a small number of attempts to do this using GRF data captured by force plates. Most research has investigated the discrimination between normal gait and some specific pathological gait, such as that caused by ankle arthrodesis or neurological disorders such as cerebral palsy. The results presented are mixed and in some cases ambiguous, suggesting further research into classification techniques are required.

2.2 Gait Analysis

The ultimate application of this research is to provide a system that can be used for gait analysis and which has several advantages and novel features over the systems currently available. In this section, the current systems are evaluated with examples of their use and any limitations they may have.

One of the most widely used pieces of equipment for gait analysis is the Force Plate. This is a well established technology such that there is minimal academic research taking place to actually improve the measurement accuracy of a force plate. There are two dominant companies that manufacture force plates for use in a gait laboratory, AMTI (Virginia, USA) and Kistler (New York, USA). A force plate consists of a stiff plate mounted onto a base using force transducers in each corner. Using the force transducer data, three dimensional ground reaction forces (GRF) and moments can be calculated. The main advantage of force plates is that they are able to produce these measurements accurately and relatively simply, with little extra data processing required on the user side. However, force plates have some limitations. Each plate has limited dimensions (usually $0.5m^2$) and can only measure the GRF of one foot strike. Therefore, a gait lab will nearly always have at least a pair of force plates in use. This leads to a second problem of spacing the force plates an acceptable distance apart, such that the patient can strike each force plate correctly without inhibiting their natural gait. Further to this, instances where the patient strikes the plate abnormally hard to insure recording of the data would also create false readings [1]. For optimum performance, a force plate is required to be embedded in the floor where they are to be used, hence making it impractical for temporary installation or usage. Despite these shortcomings however, virtually all gait laboratories will regularly use force plates for accurate GRF measurement.

Some of the shortcomings of the force plate approach can be solved by combining force plate technology with a treadmill. This has the advantage of being able to capture repeated measures of the patients' ground reaction force without having to create an excessively long walkway or having the problem of requiring the patient to strike the force plate correctly. There has been extensive research into the production of an instrumented treadmill (ITM) and this has brought with it a whole new set of measurement issues.

One of the earliest attempts was produced by Kram and Powell [2] who mounted a force plate onto a treadmill underneath the belt. This was able to successfully measure the vertical GRF of the patient, but not the horizontal forces due to the

effects of the moving belt. Kram *et al* [3] and a similar attempt by Dierick *et al* [4] get around this problem by mounting the whole treadmill structure onto a set of force transducers anchored to the floor. This enabled the forces and moments to be measured in three dimensions. However, by using a single force plate it is only possible to measure the combined GRF, it is not possible to get the GRF of each individual foot during the periods when both feet are in contact with the surface. A partial solution was suggested by Davis and Cavanagh [5], who derived an algorithm to decompose the individual vertical GRFs. But it was not possible to extend this to the horizontal components. Belli *et al* [6] provided a novel solution to this problem, by building a treadmill isolated into two halves. A separate belt was driven on each of the separate frames at an identical speed. The two frames were both mounted on force transducers and were separated by just 7mm, in an attempt to minimise any gait altering effects. The isolated segments meant that individual left and right GRFs and moments could be measured.

Another inherent issue with the ITM designs is that of the large mass and low stiffness affecting the natural frequency of the device. Both Kram and Dierick address this issue in detail in their papers, with Kram [3] building the treadmill from scratch, while Dierick [4] attempted to modify a commercially available model. Both claim to have achieved a natural frequency which does not affect the force measurements.

The most recent and certainly the most extravagant attempt at producing an instrumented treadmill is that presented by Paolini *et al* [7]. This treadmill consists of three independent force plates (and hence three individual, synchronised treadmill belts). The force plates are arranged such that the first force plate (FP1) is positioned towards the front of the treadmill and is full width and half the total length. FP2 and FP3 are placed side-by-side behind FP1, each one being half width and half length. FP2 and FP3 are able to provide individual GRFs in the same way as Belli's treadmill [6]. The extra, full width, front force plate makes it also possible to accurately measure the force when the patient's foot crosses the mid-line, stated to be a common occurrence in healthy subjects. This treadmill was designed and manufactured professionally by AMTI. Therefore, the natural

frequencies of the unit were found to be up to three times higher than the other designs mentioned here. The design of the system could lead to some potential issues however. For example it is questionable whether some patients, especially the infirm or those running, would be confident with ambulating over a surface made up of three independent belts with a gap of several millimetres between each one. Also, it is not mentioned whether a strict fail safe system is in place to ensure that the speed of each belt is kept within a matched tolerance at all times.

A highly debated question regarding gait analysis using instrumented treadmills is, whether treadmill locomotion is representative of overground walking. Many experiments have been carried out to investigate whether treadmills do cause an alteration of natural gait and what those changes are. Wank *et al* [8] claims that when using a treadmill, subjects 'favoured a type of running that provided them with a higher level of security'. This caused a reduced swing amplitude of the leg and lower vertical foot displacement on the treadmill in comparison to overground walking. They also found that upper body forward lean was higher and foot contact time was shorter. Several papers are found to be in agreement with changes in time-distance parameters. These include higher cadence [9; 10; 11; 12], shorter step length [10; 11] and shorter stance time [9; 12]. However, there are contradictions. For example, Riley et. al [13] claim that they found no significant differences between any time-distance parameters, while Schache *et al* [11] claim that the stance phase was shorter for overground walking, which is an opposing finding to Alton [9] and Warabi [12].

There have also been several investigations into whether significant changes occur in various peak joint angles. Significant changes in the hip joint angle were found [9; 13; 14], although again with contradictory findings such that Riley *et al* state a significant decrease in hip flexion with treadmill walking, while Alton claims a greater range of motion on the treadmill. Similarly, significant differences in knee flexion angles were found, with Riley *et al* [13] stating that peak knee flexion angle was reduced in treadmill walking. Matsas *et al* [10] notes significant differences in knee flexion angles during the first minute of treadmill walking to that of

overground walking. However, they observe that over time the difference reduces. Along with Lavcanska *et al* [15], who carried out a very similar experiment, they conclude that at least six minutes of treadmill familiarisation should be made available to subjects before data is captured. It is claimed that most of the aforementioned publications do not implement this familiarisation period and therefore could be the reason for the observed differences in the majority of cases.

Savelberg *et al* offer an alternative explanation for the cause of the differences between treadmill and overground gait. They claim that significant kinematic variations were attributable to the variation of the treadmill's belt speed during locomotion. The mass of the subject, speed and power of the treadmill motor were found to be the main factors affecting the variation in belt speed. They conclude that belt speed variation needs to be minimised, possibly through the use of a high powered motor, in order to mimic overground walking. Similarly, Schache *et al* [11] suggest that a high powered treadmill, with a minimal belt speed fluctuation is capable of being used to obtain a representation of the typical 3D kinematic pattern of the lumbo-pelvic-hip complex during running.

This overview suggests that it can be claimed with reasonable confidence that treadmill locomotion does affect gait kinematics and kinetics in comparison to overground walking. Despite, the numerous experiments undertaken however, the literature does not offer a general agreement on what factors are affected. Therefore, the differences cannot be suitably characterised in order to make appropriate adjustments to measurements when a treadmill is used for gait analysis. In addition to this, treadmill walking still presents a greater challenge to older adults and those with balance instabilities.

Another instrument commonly found in a gait lab is the in-shoe pressure measurement system. The two most common systems are the FSCAN (TekScan, Massachusetts, USA) and Pedar (Novel, Munich, Germany). The instrument consists of a flexible substrate containing a matrix of small thin-film force sensitive resistive sensors. These are cut to size and inserted on top of the inner-sole of the shoe. The main advantage of these systems are that they enable the subject

to walk around freely without restriction (assuming a wireless logging module is used). The output of the system provides a graphical pressure map applied by the foot as the subject is in motion. Unfortunately, these devices and the FSCAN in particular, have been found to have large inaccuracies. It has been reported that non-linearities, high hysteresis and inconsistent calibration have severely impeded the reliability of the devices. Nicolopoulos *et al* [16] gives a comprehensive review of the current literature and concludes that although the 'accuracy of the FSCAN system was found to be strongly dependent on a variety of factors... information such as pressure pattern recognition can still be obtained'.

2.3   Distributive Tactile Sensing

The experiments undertaken in this thesis have primarily used the principles of distributive tactile sensing in attempt to identify the activity taking place on the plate surface. Distributive tactile sensing is a method of tactile sensing in which a small number of sensors are used to monitor the deformation of a continuous surface which is in contact with the object being sensed. The resulting deformation data is then used to infer the properties of the sensed object.

Distributive tactile sensing has been applied to several applications including, robotic grippers [17] and minimally invasive medical tools [18; 19]. Ellis *et al* [17] first suggested a distributive tactile sensing method to identify the shape and mass of an object being held by a robotic gripper. The surface, described as a skin, took the form of a pair of thin steel steel strips mounted on the gripper tips. Four strain gauge sensors were mounted on each strip. Using standard thin plate equations, Ellis derived the required formulas to determine the strain at any point on the surface for a given force distribution. Through the use of an inverse function, it was then possible to determine the force distribution from the measured strain values. High accuracies were achieved, with a 1.6% mean mass error and 3.8% length error.

34

Brett and Stone [18] extended this research to the medical field, investigating the use of distributive tactile sensing for providing force feedback in tele-surgery applications. In a similar set up to Ellis *et al* , Brett and Stone measure the force distribution and movement of an object through the measurement of deformation and slip occurring on a thin, 0.5mm thick aluminium plate. In this experiment, the plate was fixed at one end with the other end supported by a spring to form a cantilever. Eight strain gauges were placed equi-distant along the plate to measure the deformation. Three methods of analysis were investigated: closed form (as used by Ellis *et al*), interpretive and the use of a neural network.

Both the interpretive and neural network methods produced an accuracy to within 0.1N, with reasonable force distribution profiles. However, the neural network method was identified as the only viable option when non-linear measurements are required. This is demonstrated through a further experiment (in the same paper) using a flexible digit. Fibre Bragg Gratings are used to measure the bend of the digit, producing a non-linear output. A two hidden-layer back propagation neural network was used. It is claimed that accurate results were achieved in detecting the position and magnitude of the load applied along the digit after applying 100 training data samples.

Brett and Li go on to further extend the distributive tactile sensing method to two dimensions [20] by creating a membrane based keyboard. In this application a polymer plate is used with dimensions of 332mm x 224mm. The plate surface was segmented into 35 separate zones, each zone measuring 42mm x 38mm. The strain gauges used in previous experiments [17; 18] are replaced with non-contact infrared sensors. These sensors measure the intensity of the infrared light reflected off the underside of the plate surface and hence give an analogue voltage output which is proportional to the distance between the plate surface and the sensor. Five sensors were used, four near each corner and one in the centre. The experiment investigated whether it was possible to discriminate which zone a load was applied to using just the five sensors. As in previous experiments, a neural network is used to predict the location. Very high accuracies were achieved, with the exception of the presence of a dead zone between each of the identified zones,

where the neural network produced inaccurate predictions. Unfortunately, Brett and Li only state the accuracy of the given set up and do not extend the experiment to show how the accuracy varies with smaller zone areas or an increased number of zones to identify a spatial resolution of this application.

Tongpadungrod et al [21] added a further aspect to the distributive tactile sensing method, through the use of optimisation techniques . In their experiment, a one dimensional beam, supported at both ends was used. Again, the application was to identify the location of an applied force. However, their work proceeds further by attempting to optimise the number of sensors used and their location along the beam. Principal component analysis (PCA) was used to determine the optimum number of sensors required. Starting with eight sensors originally, it was found that only four were required to provide a significant contribution. A Genetic Algorithm (GA) was then used to find the optimum locations using a cost function that gave higher preference to those locations that equalised the eigenvalues between the four eigenvectors.

Interesting results were achieved, indicating that when only a small number of sensors are used (e.g. two), then optimisation of sensor location plays an important role in increasing the accuracy (compared to an equi-spaced set up). This difference in accuracy decreases rapidly as the number of sensors is increased, with five sensors providing virtually no difference in accuracy between optimised and equally spaced positions. However, it could be inferred in this instance, that this decrease is related to the decrease in the space available between the sensors as the number of sensors increases.

Using Tongpadungrod's techniques, Ma et al [19] revisited the flexible digit application first suggested by Brett et al [18]. Using sensor location optimisation and cascaded neural networks, they were able to deduce many features of the object applying the force, with an accuracy of 93% or greater.

2.4 Moving Force Identification

So far, the distributive tactile sensing method has only been applied to identifying the properties of a static object. In this thesis, it will be attempted to apply the distributive tactile sensing method to identify the properties of an object moving across the surface of a plate. To theoretically prove this concept is viable, a mathematical model is developed and discussed in Chapter 3, that is able to track the position of a moving force as it traverses a plate.

There has been large amounts of research into the dynamic response of plates due to a moving force. The outcomes have important applications, particularly in the form of bridge responses to vehicles traversing at speed. The literature can be divided into three areas: Plate response due to a moving load, identification of the applied moving load and the location of an impacting load. The most fundamental research is into the dynamic responses of a plate to a moving load. Plate dynamics are then used to identify and locate the applied force.

In some scenarios, the problem can be simplified to a one dimensional beam. Hilal and Zibdeh [22] investigate the response of an Euler-Bernoulli beam with general boundary conditions. They apply an analytical solution to determine the response when a load of constant amplitude traverses the beam in an accelerating, constant velocity and decelerating form. Similarly, Pesterev *et al* [23] looked at the response-velocity dependence of a simply supported and clamped beam. Gbadeyan and Oni [24] investigate both beams and plates when subjected to an arbitrary number of moving loads. Using analytical methods, they claim to provide a very generalised solution for forces moving at varying speeds and amplitudes for plates supported by any of the classic boundary conditions. Further to this, they compare the results of a moving force problem to that of a moving mass problem. However, Lin [25] argues that the latter part of the paper is inconclusive and may be misleading.

Various methods are used to determine the plate response. For example, Wu *et al* [26] use finite element analysis to determine the dynamic response of a plate

subjected to various moving loads, with variations in eccentricity, acceleration and initial velocity investigated. However, most papers use some form of analytical method. Zhu and Law [27] use the Lagrange equation along with modal superposition. Sun [28] uses a method based on Green's function to determine the response of an infinite plate on an elastic foundation. Sun claims that this model provides a suitable representation for use in analysis of vehicle-pavement interaction. In another application based paper, Kwon *et al* [29] use analytical methods to determine the vibration of bridges when subjected to moving loads and then go on to investigate the effects of a tuned mass damper to suppress this vibration.

Fryba [30] presents a comprehensive set of methods to analyse various forms of beams and plates subjected to moving loads in his book. However, the plate response equations derived require the use of the Laplace-Carson transform method and includes an integral in the solution creating a computationally expensive calculation. Szilard [31] provides an equally comprehensive but more generalised approach to various plate analysis methods in his book. Due to the general and hence extensible approach, the methods described in this book are used in the model defined in Chapter 3.

The ability to accurately determine the plate response to a given moving load, naturally leads to inverse methods being applied to identify the magnitude and/or location of the applied force. The application of various methods of force identification has been heavily researched by Law *et al* in the form of vehicle-bridge interactions. Initially, developing an interpretive method [32] using a beam model acting as a bridge, they attempted to identify the axle loads of a two axle vehicle. They found that errors of less than 5% were achievable, with the accuracy dependent on factors such as axle separation. A similar experiment is also undertaken using time-frequency domain methods [33]. Here they compare the use of Singular Value Decomposition (SVD) with the pseudo-inverse (PI) method, with results showing that while the PI method produces erratic results, SVD can be successfully used to identify the moving forces. However, it is concluded that due to the computational overhead, a real-time implementation is unrealistic.

Finally, the model is extended to a two dimensional plate, [34] where accurate results are achieved in a similar attempt to identify the individual forces applied by each wheel of a four-wheeled vehicle traversing the surface. Chan *et al* helpfully summarise the moving force identification findings in two papers [35; 36].

Research into damage detection of panels in aircraft have led to another area of research to identify both the magnitude and location of an impacting force. Wang [37] creates a theoretical model to predict the location and magnitude of both impact and harmonically applied forces. Wang presents examples using both the time and frequency domain. However, due to the computational overhead, it would not be possible to use this method to track the location of a force that moves along the surface. Choi and Changf [38] create a comparative model using piezoelectric sensors distributed over the surface to predict the location and magnitude of an impact force. However, again, this system only works for an impact force, rather than one that traverses the surface.

High data sampling rates combined with multiple sensors to monitor the deflection of the plate surface can result in impractically large amounts of time series data to be analysed. In these situations a method of dimension reduction is required. This is particularly important when using neural networks (NN) as a large number of input nodes can considerably increase the complexity of the network, reduce efficiency and in some cases reduce the performance due to the extra 'noise' in the system. Karhunen Loeve Decomposition (KLD, also referred to as Principal Component Analysis; PCA) is a well used method of dimension reduction. KLD can be used to reduce the spatiotemporal data into a set of optimal orthogonal basis functions along with a numerical value indicating how much each function contributes to the total energy of the system. This is optimal in the sense that the truncated series representation of the data has a smaller mean square error than a representation by any other basis of the same dimension [39]. A mathematical description of KLD is provided in Chapter 3.

Examples of KLD used as dimension reduction technique in order to transform the data into an efficient form, suitable for input to a neural network can be found

in the literature. For example, Gallina [40] uses a neural network to classify the quality of a painted surface using speckle interferometry as the input data. KLD is used to reduce the high dimensionality of the data so it is suitable for input to the NN. Both, Smaoui and Al-Enezi [41] and Ondimu and Murase [42] use KLD to again optimise their data for use in a predictive neural network. Smaoui found that using just a single eigenvector from two previous time samples gave the best result when predicting the next time series value of the Kuramoto-Sivashinsky equation. Ondimu concluded that reducing the dimensionality using KLD 'greatly increased the forecasting ability' of the neural network. However, it is also noted that overcompression can undermine the increase in the network efficiency. O'Farrell *et al* [43] give a description of how they apply KLD in order to reduce their large spectral dataset into just a three scalar value input to the neural network. Although, this was an unrelated application their methodology was very similar to that used in this thesis.

2.5   Balance and Sway

Measurement of postural stability is an important area of medical research, particularly in the elderly. For example, postural instability is a key characteristic of Parkinsons disease [44] and can increase the frequency of falls. Adkin *et al* . [45] produced results showing that trunk sway can be used to detect pathological balance control problems in patients with Parkinsons Disease, with the possibility of determining those at high risk of regular falls. Lord [46] has compiled evidence from several studies showing that the common occurance of impaired vision in the elderly can be a predictor of increased sway and hence an increased likelihood of falling.

Research into instruments to measure a person's balance and posture appears to be less active than that into gait analysis. Due to the nature of the measurements, the force plate, as used for gait analysis (see section 2.2) can also be effectively used to determine the variability of balance and posture in a person. Paillex

and So [47] use a 0.6m^2 force plate to investigate the changes in centre of pressure (COP) of stroke patients at the beginning and end of their rehabilitation. Similarly, Freitas *et al* [48] use a force plate to undertake a comparative test to determine how prolonged standing affects healthy adults and older adults. Using a force plate requires various algorithms to be introduced in order to convert the force plate data into a centre of mass (COM) value. Therefore, various commercial products are available such as the Biodex Balance System (Biodex Medical Systems, Inc, NY, US) or the PRO Balance Master (NeuroCom International, Inc., OR, US). These are based on a force plate, but are usually built around a periphery of accessories, such as hand rails and more importantly are provided with software that gives immediate balance related measurements.

Early testing of the reliability of force plates when used to measure balance, indicated that force measures, rather than COP measures were more reliable and sensitive in discriminating and measuring changes in steadiness [49]. Moe-Nilssen and Helbostad [50] claim that the 'ability of force plates to discriminate between test conditions' has been thoroughly studied but 'results are inconsistent'. Betker *et al* [51] also point out that force plates are expensive and not portable. Moe-Nilssen [50] and Betker [51] both then go on to investigate an accelerometer based solution. Accelerometers can provide an extremely compact solution. The instrumentation usually consists of a single, triaxial accelerometer housed in a small box and attached to the lower back area of the subject using a belt [50; 52]. Betker *et al* used two accelerometers, one placed at T2 on the spine and the other on the shank below the knee joint. Mayagoitia *et al* [52] make an attempt to compare the use of accelerometers against force plates to measure balance. However, as they point out, the numerical outputs of the force plate and accelerometer are different and therefore, they are only able to produce a relatively inconclusive qualitative comparison.

As with force plates, algorithms must be developed to determine the COM when using accelerometers. Betker *et al* [51] investigate the use of neural networks, an adaptive fuzzy system and a sum-of-sines model to determine the COM. When compared to the COM calculation generated by a motion capture system, all

three methods gave similar results, with both the neural network and sum-of-sines model achieving a normalised error of less than 10%.

For accelerometers to provide accurate data in relation to a subject's balance and posture, some fundamental issues need to be addressed. The main issue identified with piezoresisitive accelerometers relates to the inherent measurement of gravity and how to determine this component from an unknown or varying tilt in the accelerometer axes. Mayagoitia et al [52] offer a solution that makes the accelerometer calculations independent of inclination. However, this solution relies on the accelerometer's distance to ground remaining constant - a difficult situation to achieve in reality. Moe-Nilssen produces a more robust solution using trigonometric calculations based on time averaged sample values [53] to estimate the tilt and remove it from the data. In a further paper, Moe-Nilssen and So [50] use signal processing techniques to transform the raw accelerometer signal. They identify that a secondary problem with accelerometer usage is the low and medium frequency drift present in the data. Using quadratic curve fitting to remove the low frequency drift and a moving average filter to remove the medium frequency drift, they report that the transformed (high frequency) data can be used to consistently discriminate between different balance control challenges. On the other hand the non-transformed data was unable to differentiate between the tasks.

In this thesis, Chapter 4 details the implementation and results of an experiment that investigates the use of the platform along with distributive tactile sensing techniques to track the position of a pendulum attached to an A-frame construction. The accurate real-time, three-dimensional tracking achieved indicates the system could be applied to the measurement of postural stability and balance during quiet standing. It is not proposed that the system developed provides substantial advantages over the systems discussed above. However, the experiment is used to demonstrate the flexibility and accuracy of the system developed, in both the measurement and discrimination of motion.

2.6 Gait Discrimination

Gait classification is currently an active area of research. A review of the literature indicates that gait classification is divided into two main areas of research: person identification and the discrimination between 'normal' gait and some form of walking disorder.

Although there are many papers discussing discrimination between normal and pathological gait, very few rely solely on kinetic, force plate data. Therefore, the remaining literature relies on the more expensive and complex motion capture video based equipment. The use of motion capture systems enables the capture of many more gait variables than that provided by a force platform and therefore it can be seen why many researchers use the system to get robust classification results. However, the ability to classify data using a platform based system (i.e. the force plate, or the system described in this thesis) would provide a much more accessible method for gait diagnosis.

A useful review into current gait classification research is provided by Schollhorn [54], who dedicates a section of the review to the use of neural networks for the classification of gait and running data. Neural networks are a key tool for classification and Schollhorn's review reveals that neural networks consistently outperform other statistical based methods when used in comparative experiments. This also agrees with the results achieved in this research. Overall, the results presented in the papers under review vary greatly, from approximately, 50% discrimination accuracy right up to 100% accuracy.

The review is heavily dominated by Kohle *et al* . They have investigated several methods to discriminate between normal gait and various walking disorders. In their most recent publication, Kohle and Merkl [55] present a promising paper in which they use force plate ground reaction forces (GRF) along with a neural network to try and identify different 'gait malfunctions'. Unfortunately, much of the presented information is either limited in scope or ambiguous. Using a gait analysis laboratory database, data from 487 patients was extracted. Data from

'healthy persons' was also included but it is not stated how many were added to the sample, nor is there any further breakdown of the sample with regard to the number of subjects in each class.

The authors use a radial basis function (RBF) network with 100 centres (and later 500 centres) to predict the class the input GRF should be assigned to. The output is a 15 digit, three-state code, the three states being; 'okay', 'injured', 'prosthesis'. Each of the 15 digits represents a body region. Of the possible combinations, there are 55 valid classes representing various 'malfunctions'. However, as stated above, it is not known what proportion of the test data belongs to each class. The GRF data is fast fourier transformed and normalised to reduce it into a suitable format for input into the RBF. It is claimed the 'first few coefficients contain most of the information' to reproduce the GRF, however, again it is not stated how many coefficients are used as an input to the RBF.

The authors present results showing the recognition accuracy for different GRF component inputs using the test dataset and the training dataset (the latter being superfluous, as the training dataset will always produce over-optimistic results when used for testing). These results show a reasonable classification accuracy, particularly when using 500 centers. What is not clear is whether these results represent the overall classification accuracy of all the classes or are from a specific class or group of classes. This ambiguity is raised by the concluding statement that 'some malfunction classes still show rather poor recognition accuracy' and only 15% 'show a clear dislocation'. It would therefore have been useful to accompany the given results with a confusion matrix showing how the data was being mis-classified.

Lafuente et al [56] provide a very indepth statistical analysis of gait classification. They investigate the ability GRF data to classify between two groups of subjects, one group with pathological gait problems, namely lower limb arthrosis and a control group with no known problems. The research also investigates the comparative performance of neural networks and Quadratic Discrimination Analysis (see Chapter 5). Using feature extraction techniques they produce an

optimised feature vector for use in both the neural network and QDA algorithms. Comprehensive results show that an overall classification accuracy of 80% and 75% is achieved using the neural network and QDA methods respectively. However, both classifiers appear to be considerably unbalanced. For example, the neural network correctly classified the control group 87% of the time, but the Arthrosis group was classified correctly 73% of the time. A similar difference was found in the QDA results. The work presented by the authors is similar to that discussed in Chapter 6. Although, differences in the work do not allow direct comparison, it is interesting to note that similar results are achieved in this thesis when using feature extraction and linear/quadratic discrimination analysis. However, as discussed in Chapter 6, it was found that using a shape matching algorithm provided better results than feature extraction when looking for small changes in gait. This is due to the presence of certain features in one class not being present in another - feature analysis relies on the features being present in both classes. Also, the classifier discussed in Chapter 6, was found to be well balanced, with fairly equal accuracies in each class.

A key area of research is into the identification and classification of various neurological gait disorders. In particular, cerebral palsy (CP) classification is investigated by many publications as indicated by the review undertaken by Dobson *et al* [57]. They state that this area is of interest due to the 'diversity of gait deviations observed in children with CP' and that 'gait classifications may enable clinicians to differentiate gait patterns into clinically significant categories that assist with clinical decision-making'. In their paper, eighteen studies are identified and systematically reviewed, specifically investigating the reliability and validity of the studies. Interestingly, of the studies identified, fifteen used kinematic data for classification, with kinetic data used as a supplementary data source in five rather than for exclusive capture. This, as discussed previously, shows the current reliance on the more expensive motion capture systems to classify gait rather than the use of a platform based (i.e. force plate) device. Dobson *et al* go on to conclude that none of the studies reviewed were able to 'reliably and validly describe the full range of gait deviations' found in children with CP.

Armand *et al* [58] also investigate neurological disorders to identify different pattern classes within groups of people who are 'toe-walkers'. They use data-mining of a large gait analysis database to carry out their research and identified three groups of different sagittal ankle kinematic patterns using a fuzzy c-means algorithm. This differs from other gait classification methods discussed as it uses an unsupervised classification method. Here the data is presented to the fuzzy algorithm and clustering is identified. The authors then relate the three identified groups to various neurological disorders present in the patients. Their findings showed a strong relation between a single group and the presence of particular conditions, although some conditions such as cerebral palsy were distributed evenly across the three groups. In comparison, able-bodied subjects walking on their toes were mostly unclassified, therefore providing some confirmation that the classes were related to some change in gait due to the neurological disorders.

A possible area of future research is to extend the platform in this thesis to an 'active floor'. Alwan *et al* have carried out research along similar lines, by determining human gait characteristics from floor vibrations [59]. In this paper, they describe the use of optical fibre sensors to detect foot strikes along a floor. Using fairly simple signal processing techniques, impulse like datastreams are produced as a person ambulates over the floor. The authors claim that through the analysis of the pulses, various gait characteristics can be derived such as step count and cadence. They also classify types of gait into walking, limping and shuffling classes, using the periodicity and amplitude of the captured pulses. Finally, a fall detection method is also described, with a focus on the system being used as a method of remote monitoring for the elderly at home. Unfortunately, the paper appears to be more of a conceptual approach, with no details on the methods used for identifying the different characteristics and no reporting of the classification accuracy. No further literature has been identified to suggest that this research has progressed further.

A more ambitious attempt is made by Addlesee *et al* . in the form of the 'ORL Active Floor' [60]. They developed a floor consisting of nine steel tiles (arranged as 3×3) supported by a 4×4 array of load cells. Using the load cell data it was

possible to calculate the total weight of objects supported by the floor, positions of particular statically located objects and the detection of object removal or addition (from the change in supported weight). The authors then investigate the use of the active floor for person identification. Using Hidden Markov Models (HMM) they analyse the time series data in an attempt to correctly identify a sample of fifteen people as they walk over the active floor (one at a time). Optimising the HMM resulted in a claimed accuracy of over 90% when tested on 150 samples. However, once the data had been normalised such that weight was no longer a factor, the accuracy dropped to just 50%. The research in this thesis identifies both weight and shoe type as possible artificial factors that could falsely improve recognition rates when small samples are used. Therefore, normalisation methods are used to ensure weight is not a factor and subjects walked in stocking feet to ensure no dominating artificial factors were present.

The latter paper, is one of very few papers that investigates person identification using a platform based measurement system. The majority of the literature uses video based methods to identify individuals based on their gait kinematics. There is vast array of literature in this area, however, the subject of video based person identification is not related to the research in this thesis and therefore will not be reviewed in detail. For the interested reader, two recent publications are suggested to provide an indication to the progression of this area of research. Zhang *et al* [61] investigate the general identification of people in the sagittal plane against a noisy background, while Bauckage *et al* [62] use the methods developed to identify people using video to discriminate between normal and abnormal gait.

Classification of gait data rather than just measurement required various pattern recognition algorithms to be investigated such that they could be applied to the sensor data. As the output from each sensor was effectively one-dimensional time series data, classification algorithms that had been developed for similar applications were investigated. Hand writing or signature recognition is a well researched area using various classification methods. The data used in the recognition of hand writing was identified to have close similarities to that of the sensor outputs used in this research. The literature indicated that a popular

method used in this area is Dynamic Time Warping (DTW). Chapter 5 gives a full derivation and description of DTW, based on two very good overviews written by Ratanamahatana and Keogh [63; 64]. Niels [65] presents an in-depth study of DTW for hand writing recognition, claiming between 88% and 97% accuracy during tests. Kholmatov and Yanikoglu present an award winning (SVC 2004: First International Signature Verification Competition) method using DTW to identify between genuine and forged signatures. Their approach uses DTW to compare the test signature to the nearest, farthest and template reference signatures. Bayes classifier and Principal Component Analysis methods are then used to infer the resulting vector as an identification of a geniune or forged signature. In a more closely related area, Boulgouris *et al* use DTW for gait recognition. They describe, in a relatively vague sense, the use of DTW to compare the gait cycles of people captured using a video based system. The algorithm is tested using the Gait Challenge database (University of South Florida) and compared against a baseline algorithm also developed by the University of South Florida. Results showed that it outperformed the baseline algorithm in the majority of cases, but the authors conclude that the method 'might not be used on its own for the purpose of authentication without the use of additional biometrics or access control mechanisms'.

In Chapter 5, feature extraction methods are investigated along with the use of discrimination analysis techniques to classify those features. The well known GRF shape resulting from a human walking over a force plate lends itself to easy extraction of the main features. Su and Wu [66] extract nine force parameters and their corresponding temporal occurances from the three force plate components, resulting in an eighteen feature vector. Using a genetic algorithm neural network, the features were used to discriminate between normal walking and that caused by ankle arthrodesis. The use of the genetic algorithm enabled the authors to determine the features that contributed most to the discrimination of the two classes. This optimised the original eighteen feature vector down to three essential features.

Hsiang and Chang [67] use GRF features, not for gait recognition, but to inves-

tigate the variability and reliability of a gait pattern when subjected to various speed and loading conditions. Using the vertical GRF component only, they investigate the peak amplitudes at heel-strike, mid-stance and toe-off, gradients of heel-strike and toe-off and also centre of pressure velocity. Volunteers used an instrumented treadmill, walking at three different speeds. They were asked to carry loads which were either held in both hands or attached to the front, back or both front and back. They also walked without carrying any load. The research investigated whether the load-speed combinations affected the variability of the person's gait pattern in comparison to their natural walking. Results showed that the mean value of the selected features differed significantly for each of the loading positions. However, only the gradient measures had standard deviations that differed significantly. Two hand carrying in particular produced large amounts of variation in the gait pattern in comparison to other load positions. As suggested by the authors, this is likely to be due to the body's inability to 'swing the arms to produce necessary counter forces' when carrying the load in this way. It will be seen in Chapter 6, that the results from this paper help define the classification experiment undertaken in this thesis. The results in this paper suggest that natural walking can be subtly perturbed through the use of various load carrying tasks. This provided a suitable alternative in the gait classification experiments, where volunteers with specific gait disorders were unavailable.

2.7   Summary

The review has investigated five key areas of research related to the development of the system described in this thesis. It has been shown that there are some well established instruments being used in the majority of gait analysis laboratories. However, these instruments are not without their shortcomings and therefore, much research has been carried out into improving current instruments or implementing novel solutions. Probably the most effective solution so far has been the instrumented treadmill, which enables repeated gait measurements in a

small area without the need for the subject to 'aim' for the force plate. Unfortunately, the use of treadmills bring their own issues, particularly the suggestion that treadmill locomotion is different to natural, overground gait and therefore cannot provide valid data. The contradictory results presented in the literature suggests that there is still further work to be done before a conclusive result can be demonstrated. Other methods, such as the FSCAN in-shoe pressure measurement system provide a useful solution in certain circumstances, but has serious reliability issues.

The Distributive Tactile Sensing (DTS) method was then discussed. This is an interesting and recent development whereby a small number of sensors are used to measure the deformation of a continuous surface. Through the use of neural networks, the data from the sensor outputs can be used to infer characteristics of the object causing the surface deflection. The method has been used to determine object dimensions and force position and amplitude, on both one and two dimensional surfaces. However, the method has only been applied to a small-scale, static problems. In this thesis, the DTS method is used on a relatively large surface to infer the characteristics of an object moving across that surface, namely an ambulating person.

To ensure that DTS was a viable method for this application, Chapter 3 discusses the development of a mathematical model that uses the DTS method to track a moving load as it traverses a plate. A review of the literature found many publications detailing the dynamic plate response due to a load moving across it. Several papers then go on to use inverse methods to determine the amplitude of the applied force as it passes over the surface. A few papers also used methods to determine the location of an impacting force. However, no publications were found that enable the tracking (in near real-time) of the load position as it passes over the surface with varying amplitude. A key method used for reducing the dimensionality of the data in the model developed is Karhunen Loeve decomposition (KLD). Several papers were discussed to show how KLD is used to reduce large time series datasets.

The measurement of balance and postural instability is another potential application of the platform developed. The review of the literature indicated that research into devices for balance measurement is fairly limited and is generally based around the use of a force plate or more recently accelerometers. The lack of research suggests that these instruments provide a suitable means of measurement, although various signal processing algorithms are needed to be applied to accelerometers to avoid various inherent measurement problems.

Finally, the area of gait discrimination is investigated. The platform developed in this thesis has been developed to aid with analysis of gait by being able to discriminate between different gait patterns. Several authors have investigated the classification of gait patterns, however, only a few have used an exclusively platform based approach. The remaining authors use video based methods. The results produced from the platform based approach are mixed with some being presented in an ambiguous way. Only those that discriminate between normal walking some specific gait disorder appear to have had some success.

In this thesis, a platform based walkway is designed and implemented. Taking into account the limitations of the force plate, the platform has been designed to accommodate a full gait cycle, i.e. one left foot and one right foot strike and therefore does not require the subject to aim for such a small area, as is the case for force plates. The platform is not designed to improve the accurate measurements provided by the force plate, but instead aims to take analysis a stage further by being able to discriminate between different gait patterns. To do this the Distributive Sensing Method is used to measure the surface deflection of the platform using a small number of sensors. The research in this thesis develops both a novel design and also a discrimination algorithm that produces results that are more robust and accurate than the majority of the platform based classification attempts currently published.

Chapter 3

Tracking the position of a moving load

3.1 Introduction

So far, the distributive tactile sensing (DTS) method has been used on static applications [17; 18; 19]. In this thesis, DTS is used on a relatively large scale platform and used to infer the dynamic characteristics of a person's gait pattern through the measurement of platform deformation. As this was a novel application, an investigation into the viability of using this method was required before equipment and prototypes were designed and manufactured. Therefore, a mathematical model was developed to investigate whether DTS could successfully be used to track the location of an object as it traversed the surface of a plate. As the process of walking causes a variation in the force applied to the surface, the force applied in the model is designed to vary harmonically.

The model was implemented in Matlab and developed in two stages. First, a mathematical simulation of dynamic plate response when subjected to a moving

load was developed. As discussed in section 2.4, there are various solutions published on this area. However, the solution provided by Szilard [31] was found to be the neatest solution for the required application. The solution developed by Szilard was implemented and extended to the application of a moving load varying harmonically with damping taken into account. This enabled the deflection of the plate to be measured at any point as the load traversed the surface.

Secondly, a method was developed, based around the DTS technique, that enabled the load's position to be tracked as it traversed the surface. The method developed only had the plate deformation data available to infer this position. The solution consisted of several steps as shown in Figure 3.1, each stage reducing the dimensionality of the data towards a single value indicating the location of the load. The first stage investigated the use of genetic algorithms to optimise the sensor locations and the number of sensors required. This immediately reduces a very large three dimensional matrix containing the time-series plate deflection data at every point on the plate, to just a small set of time series for each of the required sensors. Next a moving-window method is combined with Karhunen-Loeve decomposition to reduce the time series datasets into a single vector containing a single value for each sensor. The vector relates to the position of the load at a particular point in time. Finally, the vectors are used to train and test a back propagation, multilayer perceptron neural network. The output from the neural network provided a normalised, predicted position of the load at that moment in time.

The results achieved show that a load can be accurately tracked with just a 2% tracking error, with the accuracy dependent on the window size. The remainder of this chapter discusses the development of the model and the results in more detail.

The experiment described in this chapter has recently been published by Elliott *et al* [68].

Figure 3.1: *Operations required to reduce and format data to perform location tracking using an artificial neural network*

3.2 Plate Dynamics of a Moving Force

In this section, an analytical solution is developed that describes the dynamic response of a plate as a load traverses the surface. The model developed below is based on the solution developed by Szilard [31]. First, a solution is developed for a load who's applied force varies in a simple harmonic way. It is then extended to more complex harmonically varying loads described using the Fourier series.

3.2.1 Simple Harmonic Moving Force

Figure 3.2 shows the theoretical set up and notations used, for a damped plate traversed by a harmonically varying moving force at a fixed velocity. The equation of motion for the plate is defined as:

$$D\nabla^2\nabla^2 w(x,y,t) + d\frac{\partial w(x,y,t)}{\partial t} + \overline{m}\frac{\partial^2 w(x,y,t)}{\partial t^2} = p(x,y,t) \qquad (3.1)$$

where: D is the flexural rigidity, $\overline{m}$ is the mass per unit area, d is the damping coefficient and $p(x,y,t)$ is the external load function applied to the plate. The plate under investigation is simply supported all round and has length, a, in the direction of the x-axis and width, b, in the direction of the y-axis. The initial conditions are:

$$w(x,y,t)|_{t=0} = 0, \quad \frac{\partial w(x,y,t)}{\partial t}\bigg|_{t=0} = 0 \qquad (3.2)$$
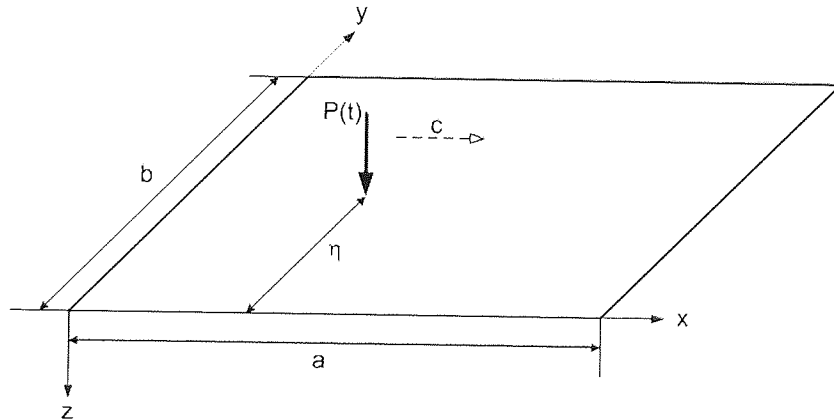
Figure 3.2: *Plate model with moving force*

Assuming the applied force is simple harmonic with angular frequency, ω_p, the right hand side side of equation (3.1), i.e. the forcing function, can be represented

as a double Fourier series in the form:

$$p(x, y, t) = \sin(\omega_p t) \sum_{m=1}^{\infty} \sum_{n=1}^{\infty} P_{mn} \sin\left(\frac{m\pi x}{a}\right) \sin\left(\frac{n\pi y}{b}\right) \tag{3.3}$$

A possible solution to equation (3.1) is a double Fourier series in the form:

$$w(x, y, t) = \sum_{m=1}^{\infty} \sum_{n=1}^{\infty} W_{mn} \sin(\omega_p t - \phi_{mn}) \sin\left(\frac{m\pi x}{a}\right) \sin\left(\frac{n\pi y}{b}\right) \tag{3.4}$$

The natural angular frequency for mode (m, n), ω_{mn} can be found by substituting, equation (3.4) into the time invariant part of equation (3.1) and dividing by the mass per unit area, $\overline{m}$:

$$\omega_{mn} = \frac{D}{\overline{m}} \nabla^2 \nabla^2 w(x, y, t) = \sqrt{\frac{D\pi^4}{\overline{m}}} \left[\frac{m^2}{a^2} + \frac{n^2}{b^2}\right] \tag{3.5}$$

For a particular value of m and n, the equation of motion is rearranged in terms of ω_{mn} and reduced to a time dependent function:

$$\frac{\partial^2 w(t)}{\partial t^2} + 2\zeta\omega_{mn}\frac{\partial w(t)}{\partial t} + \omega_{mn}w(t) = \frac{p(t)}{\overline{m}} \tag{3.6}$$

where ζ is the damping ratio and is given by:

$$\zeta = \frac{d}{2\overline{m}\omega_{mn}} \tag{3.7}$$

The value of d in the model was estimated through experimental measurement of a real plate.

Now assume a solution to equation (3.6) where

$$w(t) = A_{mn}\sin(\omega_p t) + B_{mn}\cos(\omega_p t) \tag{3.8}$$

and

$$p(t) = P_{mn}\sin(\omega_p t) \tag{3.9}$$

Substituting into equation (3.6) and using Cramer's Rule gives solutions for A_{mn} and B_{mn} as

$$A_{mn} = \frac{\left(P_{mn}/\overline{m}\right)\left(\omega_{mn}^2 - \omega_p^2\right)}{\left(\omega_{mn}^2 - \omega_p^2\right)^2 + \left(2\zeta\omega_{mn}\omega_p\right)^2} \tag{3.10}$$

$$B_{mn} = \frac{-\left(P_{mn}/\overline{m}\right)\left(2\zeta\omega_{mn}\omega_p\right)}{\left(\omega_{mn}^2 - \omega_p^2\right)^2 + \left(2\zeta\omega_{mn}\omega_p\right)^2} \tag{3.11}$$

Equation (3.8) is now condensed to the form $W_{mn}\sin(\omega_p t + \phi)$ where

$$W_{mn} = \frac{P_{mn}}{\overline{m}\omega_{mn}^2\sqrt{\left[1 - (\omega_p/\omega_{mn})^2\right]^2 + \left[2\zeta\omega_p/\omega_{mn}\right]^2}} \tag{3.12}$$

is the magnitude given by $\sqrt{A_{mn}^2 + B_{mn}^2}$ and

$$\phi_{mn} = \tan^{-1}\left[\frac{2\zeta\omega_p/\omega_{mn}}{1 - (\omega_p/\omega_{mn})^2}\right] \tag{3.13}$$

is the phase shift.

Finally, to complete the solution, P_{mn} must be calculated. To find P_{mn}, the forcing function, $p(x, y, t)$ needs to be defined. For this model a point force is considered with a time related magnitude, $P(t)$, moving in a straight line $y = \eta$, parallel to the x-axis with speed c:

$$p(x, y, t) = \delta (x - ct) \, \delta (y - \eta) \, P(t) \tag{3.14}$$

where δ is the Dirac delta function. Assuming $P(t) = P_0 \sin(\omega_p t)$, P_{mn} can now be found using the following double integral

$$
\begin{aligned}
P_{mn} &= \frac{4P_0}{ab} \int_0^a \int_0^b \delta (x - ct) \, \delta (y - \eta) \sin \frac{m\pi x}{a} \sin \frac{n\pi y}{b} \, dx \, dy \\
&= \frac{4P_0}{ab} \sin \frac{m\pi ct}{a} \sin \frac{n\pi \eta}{b}
\end{aligned}
\tag{3.15}
$$

The deflection of the plate, $w(x, y, t)$, due to the defined moving force can now be shown by:

$$w(x, y, t) = \frac{4P_0}{ab} \sum_{m=1}^{\infty} \sum_{n=1}^{\infty} W_{mn} \sin(\omega_p t - \phi_{mn}) \sin \left(\frac{m\pi x}{a} \right) \sin \left(\frac{n\pi y}{b} \right) \tag{3.16}$$

where

$$W_{mn} = \frac{\sin \left(m\pi ct/a \right) \sin \left(n\pi \eta/b \right)}{\overline{m}\omega_{mn}^2 \sqrt{\left[1 - \omega_p/\omega_{mn} \right]^2 + \left[2\zeta \omega_p/\omega_{mn} \right]^2}} \tag{3.17}$$

3.2.2   Non-Trivial Harmonic Forces

When the applied force is not simple harmonic it can be represented by a Fourier series. This creates an additional summation term to the deflection equation (3.3)

such that it is now defined as:

$$w(x,y,t) = \sum_{r=1}^{\infty} \theta_r(t) \sum_{m=1}^{\infty} \sum_{n=1}^{\infty} W_{mnr} \sin\left(\frac{m\pi x}{a}\right) \sin\left(\frac{n\pi y}{b}\right) \qquad (3.18)$$

where $\theta_r(t)$ are the individual terms of the Fourier series of the force. For the remainder of the model, the load is assumed to vary in amplitude in the form of a square wave with period, T and pulse width, τ (Figure 3.3). $\theta_r(t)$ is therefore defined as:

$$\theta_r(t) = \frac{2P_0}{\pi r} \sin\left(\frac{\pi r}{T/\tau}\right) \cos\left(\frac{2\pi r t}{T}\right) = P_r \cos(\omega_{p_r} t) \qquad (3.19)$$
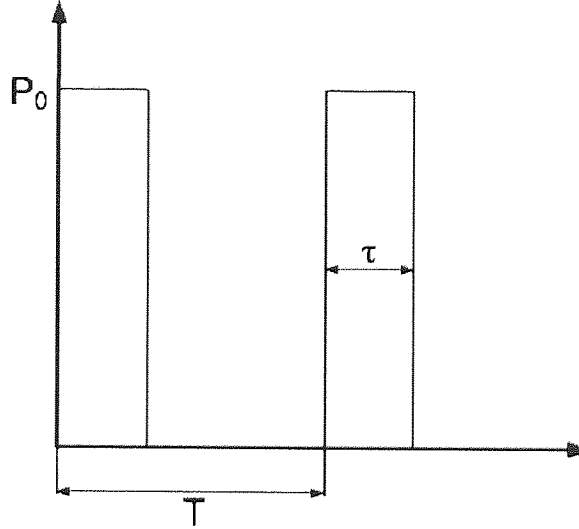
Figure 3.3: *Square wave definition.*

W_{mnr} is the amplitude of the mode(m,n), excited by the rth harmonic and is simply an extension of equation (3.12):

$$W_{mnr} = \frac{P_{mnr}}{\overline{m}\omega_{mn}^2 \sqrt{\left[1 - (\omega_{p_r}/\omega_{mn})^2\right]^2 + \left[2\zeta\omega_{p_r}/\omega_{mn}\right]^2}} \qquad (3.20)$$

where

$$P_{mnr} = P_{mn} \cdot P_r \tag{3.21}$$

Similarly for the phase,

$$\phi_{mnr} = \tan^{-1}\left[\frac{2\zeta_{mn}\omega_{p_r}/\omega_{mn}}{1 - (\omega_{p_r}/\omega_{mn})^2}\right] \tag{3.22}$$

The result is equation (3.23) which defines the dynamic response of a simply supported plate, subjected to a moving load, whose contact force is non-trivial harmonic.

$$w(x,y,t) = \sum_{r=1}^{\infty}\sum_{m=1}^{\infty}\sum_{n=1}^{\infty} W_{mnr} \cos\left(\omega_{p_r}t - \phi_{mnr}\right)\sin\left(\frac{m\pi x}{a}\right)\sin\left(\frac{n\pi y}{b}\right) \tag{3.23}$$

In the following sections, the model developed is tested using a square wave periodic force as shown in Figure 3.3.

3.3 Methodology of Position Tracking

To test the model developed, a steel plate is defined that is simply supported on all sides and has the following mechanical properties:

- Young's Modulus: 200GPa.

- Poisson's Ratio: 0.3.

- Length: 0.90m.

- Width: 0.53m.

- Thickness: 0.003m.

- Mass per Unit Area: 23.6kg m^{-2}.

With the dynamic plate deflection model fully defined, a novel method of tracking the position of a moving load is defined using the plate response. The applied square wave force has a peak amplitude of $P_0 = 500N$, a period $T = 0.1s$ and pulse width $\tau = 0.05s$. The force traverses along the centre of the plate at a range of speeds varying from 2.4ms^{-1} to 3.4ms^{-1}. Plate deflection is measured at $N = 6$ chosen locations using data generated by the model. The resulting time series data is formatted and reduced using the Karhunen-Loeve Decomposition (KLD) method and the derived K-L modes are used to train a neural network to determine the location of the force as it moves along the plate without knowing the force characteristics. A genetic algorithm is developed in an attempt to optimise the sensor locations and various parameters are modified to improve the tracking capability of the system.

The mathematical model of the plate derived in section 3.2 was implemented using the MATLAB suite of software (see Appendix B). The summations for the two sine function terms of equation (3.23) were found to successfully converge for $m = n = 10$, while the square wave force was formed by creating a Fourier series with $r = 30$ terms. The deflection was measured over the area of the plate using a 0.05m grid. A sampling rate of ten thousand samples per second (10kS/s) was used.

3.3.1 Windowing

To be able to track the force as it moves along the simulated plate, a windowing method is used. By using a windowing method a time history of samples can be examined. In contrast to capturing just the current sample from each of the

six sensors, this provides a larger amount of information to the neural network regarding the plate response and object location. The window technique uses a shifting method whereby a fixed width window, containing γ samples, is progressed along a time series dataset by Δ samples each time. Figure 3.4 shows a windowing method with a window size, $\gamma = 3$ and a shift of $\Delta = 1$, such that the first window captures data samples, s_1, s_2, s_3, the second captures data samples, s_2, s_3, s_4 and so on.

$$s_1 \quad s_2 \quad s_3 \quad s_4 \quad s_5 \quad s_6 \quad s_7 \quad s_8 \quad s_9 \quad s_{10} \quad s_{11} \quad s_{12} \quad s_{13} \quad \cdots \quad s_j$$

$$s_1 \quad s_2 \quad s_3$$

$$s_2 \quad s_3 \quad s_4$$

$$s_3 \quad s_4 \quad s_5$$
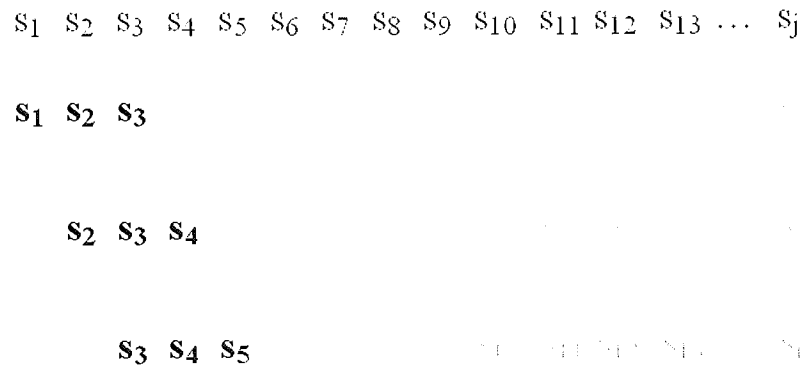
Figure 3.4: *Illustration of the moving window method, with a window size of 3 and shift size of 1.*

3.3.2 Karhunen Loeve Decomposition

The high dimensionality of the data makes it inappropriate for input to a neural network. Therefore, Karhunen Loeve Decomposition (KLD) was performed on each window of data. KLD can be used to reduce a set of high dimensional data down to a small set of orthogonal eigenfunctions known as KL Modes or Proper Orthogonal Modes (POMs). The small number of resulting POMs are known to account for more energy than any other set of orthogonal modes, with the associated eigenvalues or Proper Orthogonal Values (POVs) providing a numerical estimate of the amount of energy captured by each POM.

There are two methods of applying KLD; Direct and Snapshot. The Direct method is used for data consisting of large time series and a low spatial resolution, while the Snapshot method is useful for data sets with a high spatial resolution [69]. In this application, large time series datasets are generated by a small number of sensors. Therefore, the Direct method is the most appropriate choice.

Taking a general case and using the Direct method, Wolter *et al* [69] demonstrate KLD applied to a dynamical system with the displacements being sampled at N locations and labeled, $w_1(t), w_2(t), ..., w_N(t)$. Taking M samples over time results in an M x N matrix:

$$\mathbf{W} = [\ \mathbf{w_1}\quad \mathbf{w_2}\quad \cdots \quad \mathbf{w_N}\ ] = \begin{bmatrix} w_1(t_1) & w_2(t_1) & \cdots & w_N(t_1) \\ w_1(t_2) & w_2(t_2) & \cdots & w_N(t_2) \\ \vdots & \vdots & \ddots & \vdots \\ w_1(t_M) & w_2(t_M) & \cdots & w_N(t_M) \end{bmatrix} \tag{3.24}$$

The resulting data in the $M \times N$ ensemble matrix needs to be both strict-sense time stationary and ergodic. This requirement is satisfied by taking equation (3.24) and subtracting the column mean from each element in that column as follows:

$$\mathbf{V} = \mathbf{W} - \frac{1}{M}\begin{bmatrix} \sum_{i=1}^{M} w_1(t_i) & \sum_{i=1}^{M} w_2(t_i) & \cdots & \sum_{i=1}^{M} w_N(t_i) \\ \vdots & \vdots & \ddots & \vdots \\ \sum_{i=1}^{M} w_1(t_M) & \sum_{i=1}^{M} w_2(t_M) & \cdots & \sum_{i=1}^{M} w_N(t_M) \end{bmatrix} \tag{3.25}$$

A spatial correlation matrix, $\mathbf{R}$, can now be formed as

$$\mathbf{R} = \frac{1}{M}\mathbf{V}^T\mathbf{V} \tag{3.26}$$

where $\mathbf{V}^T$ is the transpose of $\mathbf{V}$, defined in equation (3.25).

The POMs are now given by the eigenvectors of $\mathbf{R}$ which are orthogonal due to $\mathbf{R}$ being real and symmetrical, while the eigenvalues are the proper orthogonal values.

3.3.3 Optimisation of sensing positions

Tongpadungrod et. al. [21] have successfully used genetic algorithms to find the optimum sensor locations along a beam for tactile sensing purposes. In this experiment, genetic algorithms were used in an attempt to determine the optimum sensor locations on the plate to ensure there was a minimum level of redundancy in the data. Genetic Algorithms operate using the theory of evolution. By breeding and mutating a set of chromosomes (the coordinates of the sensor positions in this case) the chromosomes are evolved through several generations resulting in a set of optimum coordinates.

The algorithm starts with a random set of coordinates, and converts the values to binary strings (the chromosomes). A population is generated, initially consisting of many sets of different chromosomes. A cost function (see section 3.3.3.1) is used to assess each of the chromosomes with a lower score indicating a better suited chromosome for the job. Each chromosome is tested against the cost function and the best chromosome from the population is stored.

A 'wheel of fortune' is then constructed. Each chromosome in the population has a segment on the wheel. The size of the segment is inversely proportional to the score, so the lowest score has the largest segment and hence is most likely to be chosen. The wheel is then 'spun' a number of times to select a chromosome. Whichever segment is landed on results in that chromosome being added to the new population. The resulting new population is most likely to be made up of only the best fitting chromosomes (i.e. those with the lowest scores).

The new population is then 'bred'. A proportion of the chromosomes are selected at random. The breeding process involves splitting pairs of chromosomes at a random point into two parts. The first part of the first chromosome is joined to the second part of the following chromosome, whilst the second part of the first chromosome is joined to the first part of the second chromosome. Finally, mutations are carried out. This involves inverting random bits of some chromosomes in the population. Only a small proportion of chromosomes are mutated.

The new population is now complete, with the process repeating, starting with a new set of scores being calculated. After the final generation has been created, the resulting chromosomes are converted back into coordinate values, indicating the optimum sensor locations.

3.3.3.1 Cost function

A cost function is used to assess the fitness of the resulting population. Each chromosome is assessed by evaluating a cost function against it. The lower the cost, the better the chromosome is in achieving the required goal. Using the 'survival of the fittest' theory, the chromosomes with the lowest costs are then given the highest chance of breeding, hopefully improving the fitness of the next generation of populations.

In this case, the aim is to find the optimal sensor locations that will minimise the error in predicting the force position by the neural network. Two cost functions were devised, the first uses correlation of the time series data, the second uses the variance of the eigenvectors. Each is discussed below.

Correlation Method

The initial idea was to use correlation as a cost function. Distributive tactile sensing relies on each sensor providing time series data which is as different as possible to that of the other sensors. Achieving this will provide the optimum
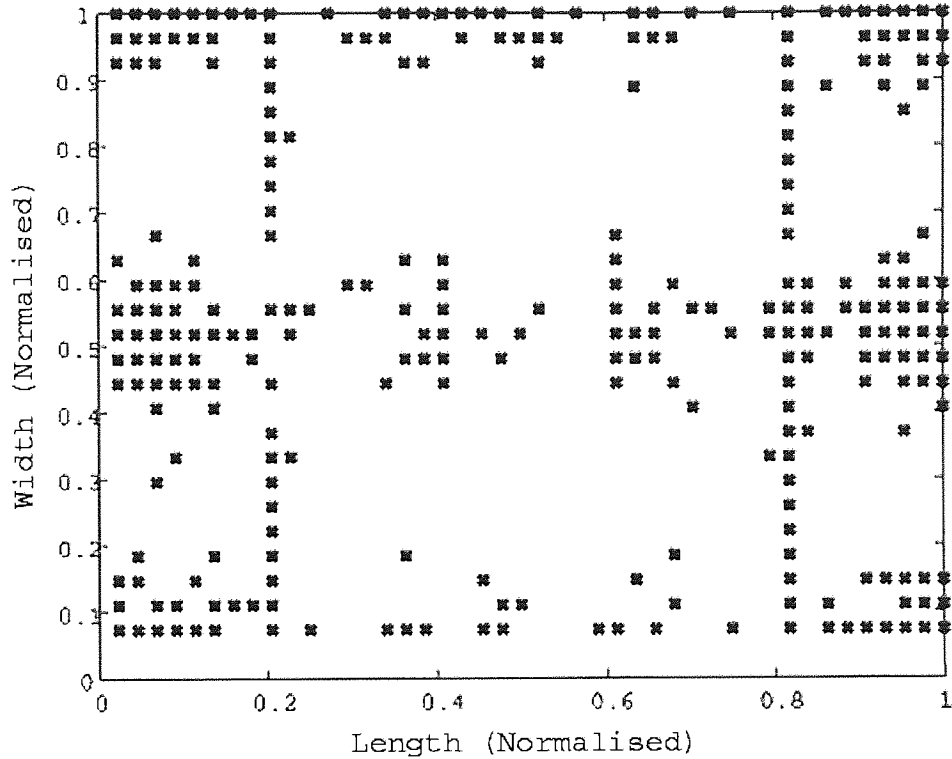
Figure 3.5: *Distribution of sensor locations using genetic algorithm*

amount of information about the plate surface to the neural network. A cost function was therefore derived that measured the correlation of each set of time series data. Those populations with the lowest correlation between all the sensors were deemed to be the 'fittest' and assigned the lowest cost. A high correlation indicates the time series data was similar between sensors, therefore, providing redundant data.

The algorithm was run for eighty generations (i.e eighty breeding events occurred) using plate deflection data generated from a moving load passing over the surface at 3.2ms^{-1} (the load had the same properties as those described at the beginning of section 3.3). The fittest population of the eightieth generation was stored. This was then repeated two hundred and fifty times, generating 250 optimum populations. Each optimum sensor location is plotted in Figure 3.5. As can be

seen, the populations cluster around various areas on the plate.
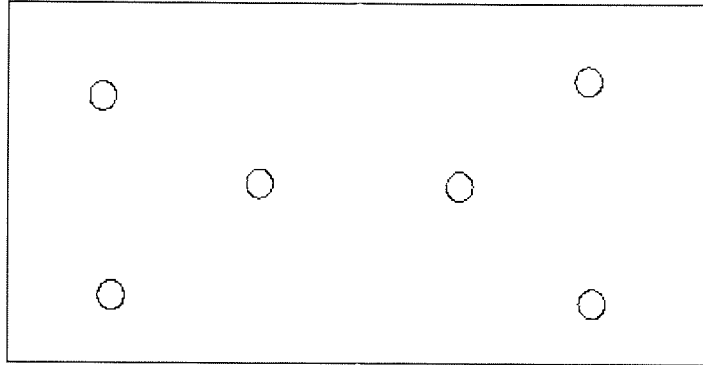
Figure 3.6: *Chosen sensor locations, determined from GA results.*

Eigenvalue Distribution Method

Another hypothesis was that the best tracking accuracy could be achieved when there was a large variation in the eigenvectors between each sampling window representing a different load position. To quantify this, the variance of each of the six components of the first eigenvector were measured from the set of eigenvectors resulting from a load fully traversing the plate at $3.2ms^{-1}$. The 'cost' was then based on the resulting variance of the vectors, the aim being to achieve the highest variance and therefore hopefully achieve the greatest spread with easily distinguishable vectors. The cost function for each set of sensor locations is therefore calculated as the mean of the variance of each of the eigenvector values.

The algorithm was run for 200 generations, with a population of 100 sets of locations, each set containing ten possible sensor locations. Although no grouping was found with this method, the ten sensors locations tended to converge to six valid sensor positions. Therefore, using the clustering identified from the first method and the optimum number of sensors suggested by this method, a sensor layout was devised as shown in Figure (3.6)

3.3.3.2 Comments

Genetic algorithms have been found to be very successful for various applications, where a clear cost function can be defined. However, their performance is questionable in some applications such as this one, where a large number of possible combinations are possible, along with an unclear definition of what the cost function should be. It is suggested for this application, a logical distribution of the sensors will yield equally as good results, but with a lower computational overhead. However, on the otherhand by using the genetic algorithm, a gauge of how many sensors are likely to be required for this application has been identified.

3.3.4 Neural Network Implementation

The neural network was generated using the MATLAB Neural Network Toolbox (v4.0). The network used was a multi-layer perceptron (MLP) with an error back propagation training algorithm. The input data was in the form of the resulting eigenvectors generated using the KLD method. Therefore, six input nodes were implemented, one for each of the values in the vector.

The network was trained and tested using 4, 8, 12, 20 and 40 hidden nodes, to see which gave the best performance. It was found that the number of hidden nodes had very little effect on the network error. However, twenty hidden nodes were chosen as it produced the overall lowest mean error.

A single output node was used to provide the location prediction. The output value was a normalised location along the length of the plate in the range [0,1] (note, the position of the load along the width of the plate remained fixed as the load moved across the length of the plate).

The hidden-node transfer function was a tan-sigmoid function, with a pure-linear function applied to the output node, which is the standard architecture for regression (as opposed to classification) networks such as this one.

3.3.4.1 Training

In an attempt to make the model resilient to speed variation, datasets were generated for loads traversing the plate at speeds between 2.4ms^{-1} and 3.4ms^{-1}, going up in steps of 0.2ms^{-1}. The resulting plate deflection matrices were then split into two groups. The first group was used for training the neural network and contained the plate deflection matrices for speeds of 2.6, 3.0 and 3.4ms^{-1}. The second group was used for testing the neural network and contained the plate deflection matrices for speeds of 2.4, 2.8 and 3.2ms^{-1}. Each dataset was compiled into windows of data using the method described in section 3.3.1. Gaussian noise

was added to each window of data with a mean amplitude of 0.3 times the mean data amplitude, which was found to provide a realistic level of distortion to the signal. Ten separate noisy data windows were generated for each window position within the time series, resulting in ten slightly different sets of data for the same output value.

A KLD was then carried out on the data window, resulting in corresponding POMs and POVs. Ordered by the magnitude of the corresponding POV, the first, most significant POM resulting from each window was used and normalised. Training data therefore consisted of three (number of different speeds) by ten (number of noisy variations of the sensor data) eigenvectors for each corresponding location on the plate. The expected output vector had to be a location corresponding to the input vector. The position of the load is defined to be its location when the last window sample is captured. To make it dimensionless it is divided by the plate length to give a relative position between zero and one. For the model, the position, $Y(i)$ is calculated using:

$$Y(i) = \frac{(i\Delta + \gamma)Tc}{a} \tag{3.27}$$

where: i is the ith data window, γ is the window size, Δ is the shift size, c represents the speed of the moving force, T is the sample period and a is the length of the plate.

This equation also makes it clear that the tracking resolution is dependent on the window shift size, δ. Therefore, for a given shift size, the delay between calculated position readings is simply $\Delta \cdot T$ seconds.

When training the neural network, it is important that the resulting architecture fits the generalised underlying model of the data and is not overfitted, such that it also follows the noise in the training data. Therefore, the Bayesian regularisation method was used to train the network. Bayesian regularisation [70] uses the assumption that the weights and biases of the neural network are random variables with specified distributions. The regularisation performance parameters

are related to these distributions, and can then be estimated through statistical techniques. The main advantage of the Bayesian regularisation method is that it does not require a separate set of validation data. The Bayesian method can achieve a successful generalised result using a single set of data, thereby reducing the quantity of training data required.

A summary of the neural network implementation is shown in Table 3.1.

Network type	Multi-Layer Perceptron (MLP)
Training method	Back Propagation with Bayesian Regularisation
Hidden node $f(x)$	Tan-sigmoid
Output node $f(x)$	Pure linear
No. of input nodes	6
No. of hidden nodes	20
No. of output nodes	1
Input data	Single, six value eigenvector (see 3.3.1 and 3.3.2)
Output data	Continuous value in the range [0,1], representing a location along the length of the plate (see 3.3.4.1)

Table 3.1: *Summary of the neural network implementation*

3.4 Results

3.4.1 Model Verification

A verification of the devised model was implemented using a transient test in which the response of the real and theoretical plate was compared. A simply supported steel plate with physical properties matching those described in section 3.3 was struck with a plastic tipped force hammer (location $(0.14m, 0.34m)$). The response of the plate was recorded using a scanning laser vibrometer (Polytec PSV-400) to measure the vibration at a single location $(0.26m, 0.26m)$.

The force created by the force hammer represented an impulse of approximate duration of 1.2ms and a peak force of 90N. The velocity of the plate deflection was measured by the scanning laser vibrometer. To simulate this scenario, the model was run with a statically located force whose profile was generated using a fourier series with a long duty cycle such that the impulse was just 1.2ms in duration but had a period of 100ms. This enabled the simulated response due to the single impact to be analysed for a duration of 100ms.

After substitution of an appropriate damping factor and differentiating the simulated displacement to obtain the response velocity, the resulting comparison of the experimental response against the simulated response shows a good resemblance in both the time and frequency domains as shown in figures 3.7 and 3.8.

3.4.2 Optimum Window Dimensions

The window size and shift values can affect the resolution and accuracy of the resulting predicted values. Three different window sizes and three different shift sizes were tested in combination. The windows contained 500, 1000, and 1500 data samples, relating to a duration that was 0.5x, 1.0x and 1.5x the applied force period, respectively. The window shifts were 20, 50 and 100 samples. Table 3.2

72
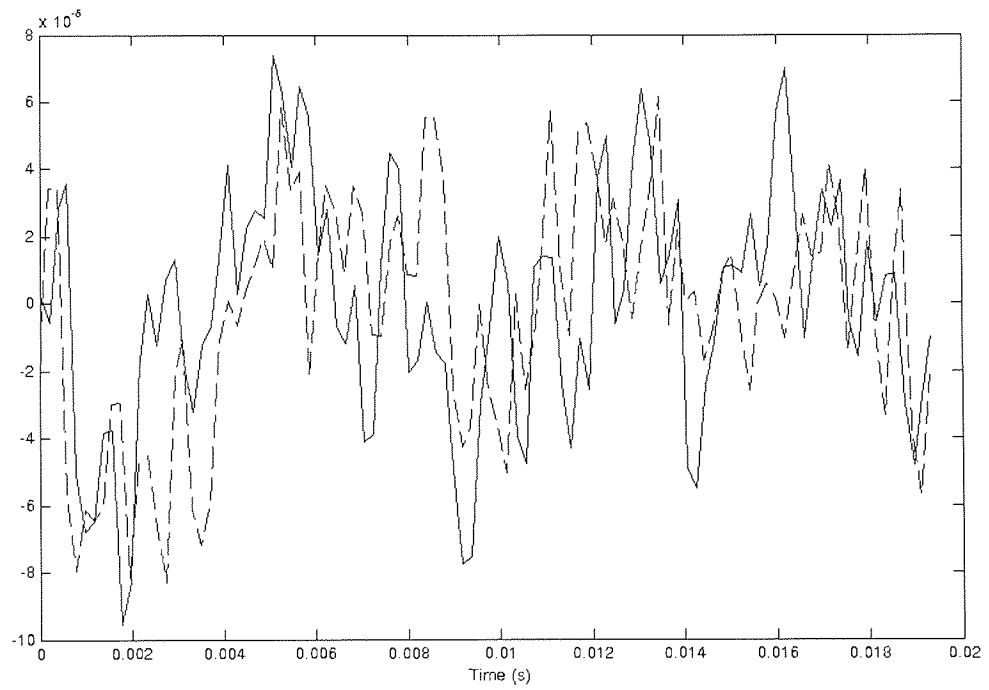
Figure 3.7: *Comparison of time domain transient response (–) of a real plate compared to the simulated response (- -) of a plate with similar properties.*
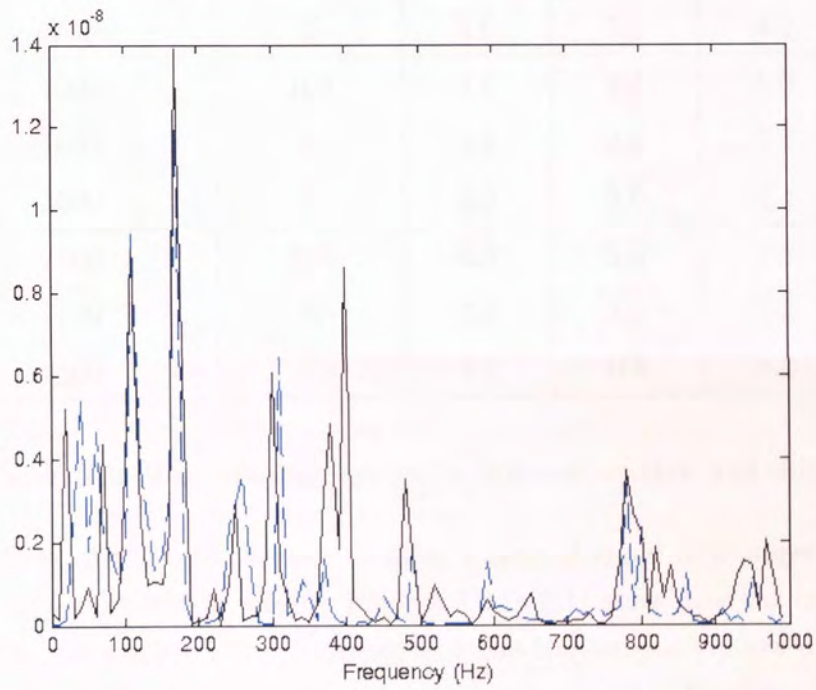
Figure 3.8: *Comparison of frequency domain transient response (–) of a real plate compared to the simulated response (- -) of a plate with similar properties.*

shows the resulting errors for the different window size-shift combinations over a range of speeds.

Window Size (n)	Shift (m)	Error (%)			
		2.4ms^{-1}	2.8ms^{-1}	3.2ms^{-1}	Mean
500	100	6.2	3.8	3.4	4.5
500	50	11.8	3.6	3.5	6.3
500	20	5.8	3.6	4.9	4.8
1000	100	4.6	4.4	5.6	4.9
1000	50	4.8	4.6	5.4	4.9
1000	20	3.6	3.6	4.4	3.9
1500	100	5.5	1.5	1.8	2.9
1500	50	2.6	1.4	1.3	1.8
1500	20	1.5	0.9	1.2	1.2

Table 3.2: *Mean tracking errors for different window and shift sizes.*

The results in the table appear to show a general trend of a larger window size giving better prediction results. Figures 3.9 to 3.11 show how the tracking varies with different window sizes. Starting with the 500 sample window, it can be seen that for the majority of the time the tracking is accurate. However, large glitches in the prediction occur along the way, causing the overall mean error to be high. The 1000 sample window appears to have the worst tracking performance, with a periodic variation in its tracking. Finally, the 1500 sample window manages to track the actual location very accurately, with less than two percent error, when a fifty or twenty sample shift is used.

Further investigation indicates that the optimum window size is related to the period of the harmonically varying amplitude of the applied load. Specifically, results show the optimum window size (duration) is 1.5 times the period of the applied load. Whilst the window size has a considerable effect on the accuracy,

it was found that the shift size has very little effect. Ideally, the shift size should be as small as possible however, to maximise the data resolution. In reality, this will be limited by how fast the PC can process the data between captures.

3.4.3 Noise Tolerance

The overall system was tested to see how tolerant it was to noise present on the input signal. The results of the test gave an indication of whether the algorithm would still produce acceptable tracking results when real data is presented to the system rather than simulated data.

The neural network was trained as defined in the previous sections, with Gaussian noise added to the time series data from the six sensors. The neural network was then tested using simulation data with increasing levels of noise added. The input data was taken from the simulated response of the plate subjected to the square wave moving force traversing the plate at 3.2ms^{-1}. Noise was added with an amplitude of between 0.3 and 2.0 times that of the mean time series data amplitude. The resulting percentage error, calculated as the difference between the actual and predicted location, divided by the plate length, is shown in Figure 3.12. The tracking algorithm continues to give robust results until the mean noise magnitude is equal or greater than the mean data signal amplitude, after which the error increases substantially.

3.5   Conclusion

In this section it has been shown that, using a mathematical model, the location of a moving load with an unknown, harmonically varying amplitude can be tracked along the length of a plate. Based on the Distributive Tactile Sensing method, it was possible to track the location of the force over a range of speeds

76

with an error of less than two percent. Initially, a model of the dynamic plate response was implemented based on that developed by Szilard [31] and extended to a damped response due to a moving force. The time series data was dimensionally reduced using a windowing method along with the Karhunen-Loeve decomposition method. The method developed enabled tracking of the load position to a high accuracy at a reasonable time resolution. Gaussian noise was applied to the simulated sensor outputs in an attempt to recreate real operating imperfections. The algorithm developed was found to be tolerant to the added Guassian noise up to an amplitude equal to that of the mean signal amplitude.

Although it was found that the optimum window size is related to the frequency of the amplitude of the applied load, having a 'mismatched' window only introduces a small increase in error. This area would however, benefit from further investigation when working with randomly varying loads. The results from this section can also be used as an indicator of how to manage large amounts of time series data from practical vibration related experiments. Karhunen-Loeve decomposition along with a moving window method has been shown to be an effective technique in formatting and reducing data dimensionality for real-time processing.
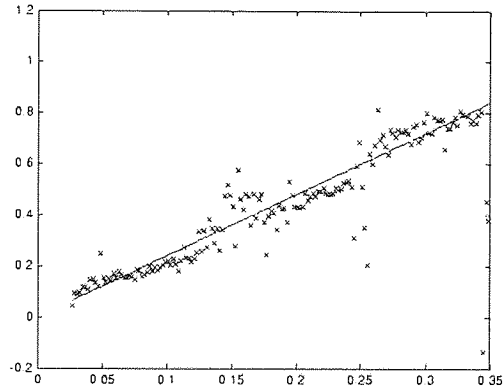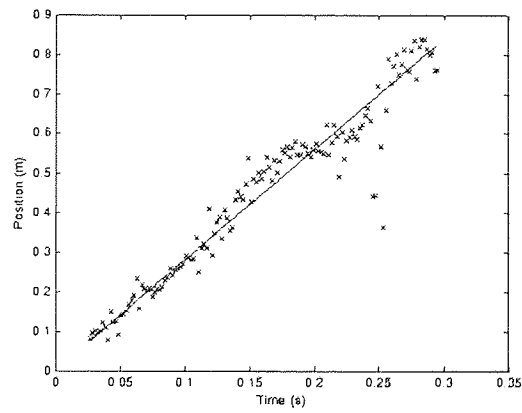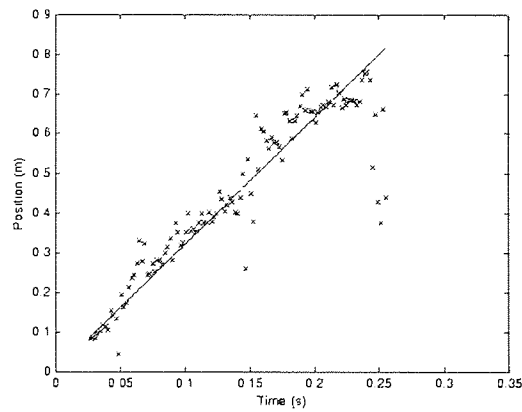
(a) 2.4m/s

(b) 2.8m/s

(c) 3.2m/s

Figure 3.9: *Actual force location against predicted force location using a 500 sample window and a shift of 20 samples*
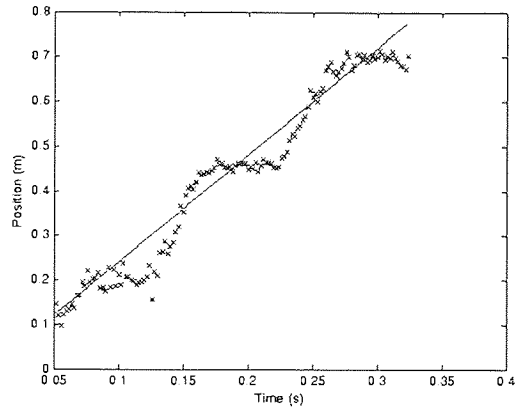
(a) 2.4m/s
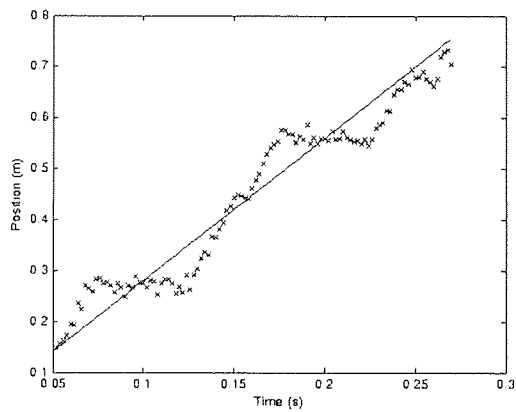
(b) 2.8m/s
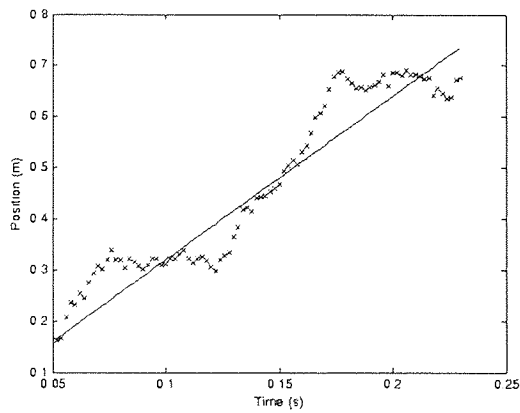
(c) 3.2m/s

Figure 3.10: *Actual force location against predicted force location using a 1000 sample window and a shift of 20 samples*

79
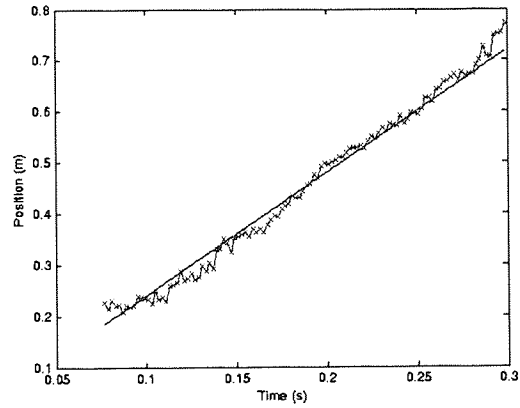
(a) 2.4m/s
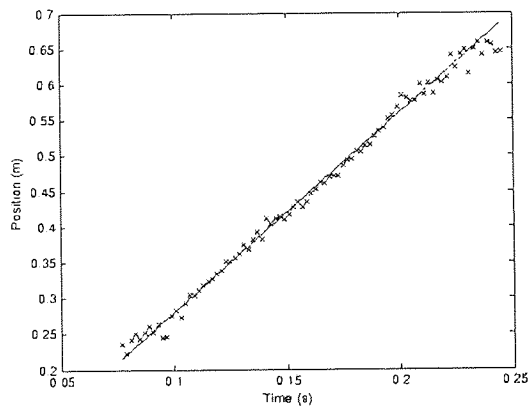
(b) 2.8m/s
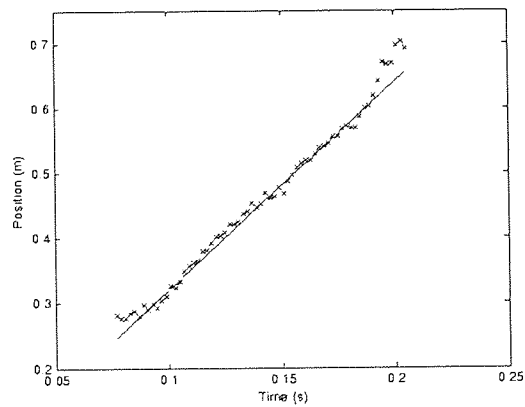
(c) 3.2m/s

Figure 3.11: *Actual force location against predicted force location using a 1500 sample window and a shift of 20 samples*
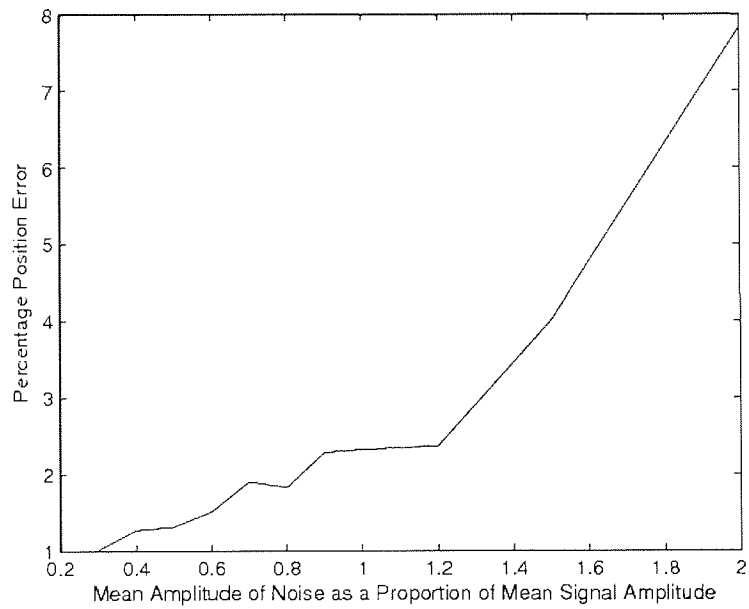
Figure 3.12: *Position tracking error as a function of noise amplitude*

Chapter 4

Tracking the position of a pendulum in real-time

4.1 Introduction

In this section, the distributive tactile sensing method is applied in an experiment that simulates the measurement of sway. The experiment was designed to examine the viability of using distributive tactile sensing for a relatively large scale, dynamic, platform based application. As this was one of the initial experiments, it was designed to be controllable with only a small number of variables such that the required platform and signal processing circuits could be developed and tested. To do this the experiment investigated the use of a platform along with distributive tactile sensing methods to track the position of a swinging pendulum supported by a frame mounted on the platform. This has relevant applications in the area of balance and sway measurement of people during quiet standing and also provided a practical proof of concept, where the techniques were able to be further developed for the application of gait classification (Chapter 5).

Postural stability is a key indicator of an increased risk of falls in the elderly [44; 45; 46] and therefore is an important area of research. Common instruments currently used in the measurement of balance during quiet standing are the force plate [47; 48] and commercial products based around the force plate such as the Biodex Balance System (Biodex Medical Systems, NY, US). However, these are expensive devices that tend to be found only in professional gait analysis laboratories [51]. Recently, much research has gone into the development of accelerometer based balance measurement devices [50; 51]. However, these require various corrective algorithms to overcome fundamental issues such as the presence of an unknown gravity component and inherent drift [50]. Furthermore, the use of accelerometers commonly requires a large belt [50; 52] that must be tightly fitted. This could cause discomfort and tension in a person who is already unsteady in long standing periods. The DTS method developed can provide a low cost solution to the measurement of balance and sway, whilst causing a little restriction to the subject in comparison to current methods.

4.2 Collaboration

The experiment described in this chapter was carried out jointly with Iskander Petra, a PhD research student at Aston University, investigating the implementation of neural networks on electronic embedded devices (e.g. Field Programmable Gate Arrays). Collaboration provided benefits to both parties, using the combined skills and knowledge to produce an accurate method of tracking the pendulum position in three dimensions and in real-time. Table 4.1 has been provided to give an indication of the distribution of the work in this experiment.

MTE	IP	Joint
Sensor evaluation (4.3.3)	Neural network	Data analysis (4.5)
Platform and	evaluation (4.3.6)	Swing design (4.3.2)
base-plate design (4.3.1)	Neural network	Amplifier circuit (4.3.4)
Offset circuit evaluation	implementation (4.3.6)	Capture of results (4.4)
and design (4.3.4)	Clipping circuit design (4.3.4)	
Motion capture operation (4.3.5)	FPGA programming (4.3.6)	
Plate deflection model (4.4.1)		

Table 4.1: *Breakdown of work distribution for this experiment*

4.3   Experimental Setup

In this experiment, a supported steel plate is used as the contacting surface. The motion of a pendulum mounted on the plate causes the surface to deform in response. Three infra-red deflection sensors are located underneath the plate to measure the corresponding plate deflection. The outputs from these sensors along with the measured swing position captured by a motion capture system are used to train a neural network to relate the sensory data to corresponding swing positions. The trained neural network is then implemented onto an embedded system and used to predict the pendulum position in three dimensions, in real time.

A detailed description of the experimental setup is given in the following section.

4.3.1   Platform Design

A supported steel plate was designed which acted as the measurement platform. The plate dimensions were 900mm x 530mm, with a thickness of 3mm. The plate

was supported by a frame made of hollow rectangular steel tubing and could be clamped on the long sides if required. The frame was used to support the plate and raise it up to a suitable height to enable the sensors to be positioned underneath. As shown in Figure 4.1, the coordinate system of the set up was orientated such that the X-axis ran parallel to the short side of the plate, the Y-axis ran parallel to the long side of the plate and the Z-axis pointed vertically upwards. The origin of the coordinate system used was positioned at a corner of the plate.
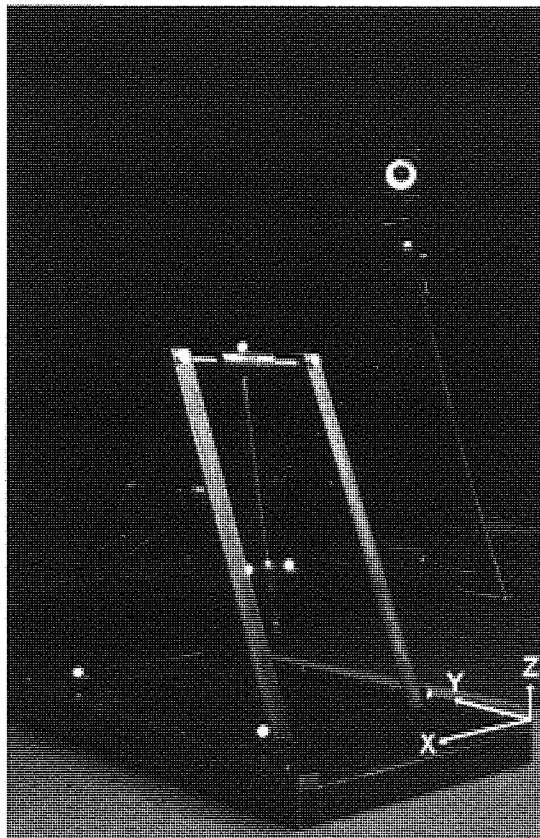
Figure 4.1: *Photograph of the experimental setup.*

4.3.2   Swing Design

The swing consisted of a four legged 'A' frame which supported a centrally located pendulum. The frame was a steel construction with legs of length 720mm. The angle between the A-frame legs was adjustable if required. The feet were free to rotate so that if the frame angle was altered the feet remained flush to the surface of the plate. The width of the frame was fixed such that the feet of the frame were set 45mm in from the inner edge of the plate clamps. The pendulum consisted of a 500mm long, 9mm diameter threaded bar attached to a hub which rotated around the top horizontal bar. The pendulum was able to hold standard, stackable metric weights of 5kg or 10kg. A nut and large washer positioned above and below the weights were used to hold them in position. A mechanical drawing of the swing is shown in Figure 4.2. A photograph of the experimental setup is shown in Figure 4.1.
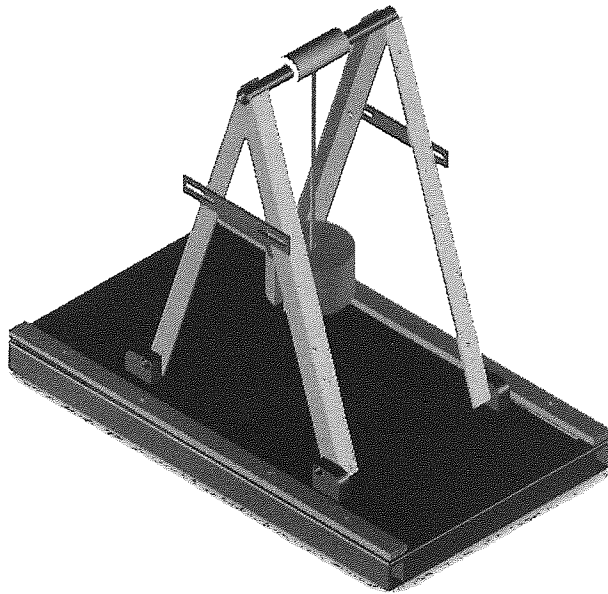
Figure 4.2: *Mechanical drawing of swing and platform*

4.3.3 Sensor Design

4.3.3.1 Sensor Types

Sensing devices were used to measure the response of the platform surface and output a signal in an electrical form. Various sensor types were investigated to find a device that was most appropriate for this application. Tests were carried out on three different sensor types:

a). Accelerometers. These devices are commonly used for vibration measurement experiments and have also been used as a measurement of sway [50; 51]. Two different accelerometer devices were tested for their suitability.

b). Fibre Bragg Gratings. Optical fibres with an etched grating have been successfully used by Cowie *et al* [71] in a static distributive tactile sensing application. In the experiment, the gratings were found to have a better accuracy than that provided by an electronic strain gauge.

c). Optical Displacement Sensors. Again, successfully used in previous static distributive tactile sensing experiments [20; 21], these are low cost devices that provide a sensitive analogue output related to the distance between the sensor and the reflecting surface.

The outcomes from the evaluation of each device are discussed below.

Accelerometers

Accelerometers can accurately measure the acceleration of the surface they are attached to. They are commonly used in vibration analysis experiments due to their high sensitivity and bandwidth. Accelerometers primarily contain one of two technologies: piezo-resistive or piezo-electric.

A piezo-resistive accelerometer works through the use of a wheatstone bridge network that changes resistance in proportion to the applied seismic force [72]. This

87

type of accelerometer can operate down to zero hertz and is therefore, commonly used for low frequency applications such as motion detection. However, this type of accelerometer has inherent issues when operated at low frequency, related to drift and the unknown contribution of gravity when the axes are offset from the normal.

A piezo-electric accelerometer does not have a frequency range down to zero hertz and therefore can only detect *changes* in acceleration (such as that occurring in vibration situations). The applied vibration causes the compression and expansion of a piezo-electric crystal inside the device [72]. Due to the very small signals produced, the device will usually include an internal amplifier (known as Integrated Electronics Piezo-Electric: IEPE) that converts the charge produced by the crystal into a voltage (in the millivolt range). Others will output the charge direct in units of pico-Coulombs.

Accelerometers are either packaged in a low cost integrated-circuit (IC) form or as a much more expensive, highly engineered form. Two accelerometer devices were evaluated to assess their viability for both the experiment described in this chapter and those in chapters 5 and 6. The first device was a Star APA300 triaxial piezo-ceramic accelerometer (piezo-ceramic uses a similar operating principle as piezo-electric). This was a low cost, IC based design and therefore required external electronic circuitry for correct operation. The device was passive and hence had no internal pre-amplifiers. Therefore, the output signal was extremely small, requiring a high impedance input to the external op-amps with a minimum amount of track distance between the amplifier and the device to minimise noise. A circuit was developed based on a recommended design described in the associated design guide [73]. The schematic design, layout design and photo of the final implementation can be seen in figures 4.3 to 4.5.

Unfortunately, testing presented very poor results. The output suffered severe drift problems and the sensitivity to vibration was very low. This could be due to the device being passive and therefore requiring strict tolerances on the external circuitry. Although the printed circuit board (PCB) developed followed the rec-
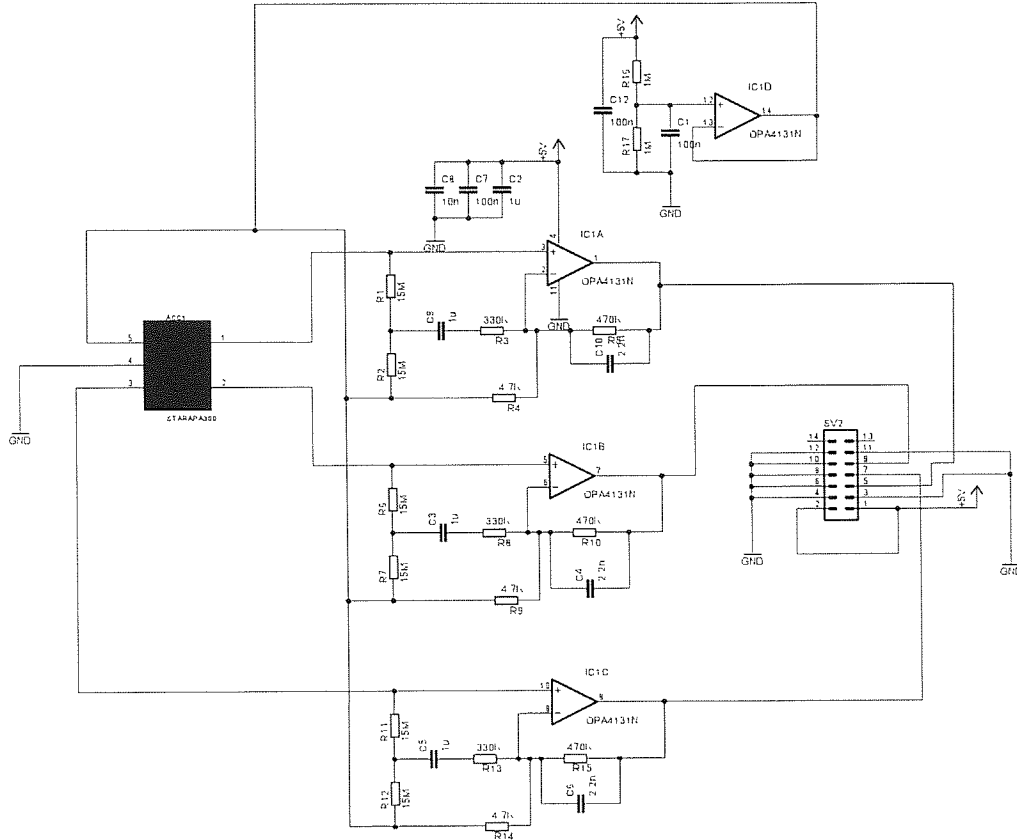
Figure 4.3: *Schematic design for APA300 accelerometer device*

ommended guidelines, high quality manufacturing equipment was not available and as such the tracking quality may not have been to the required standard. It's possible that a shielded box may also have reduced external noise, although the ideal solution would have been for the device to have had an internal amplifier. The Star ACB302 device was introduced to the market approximately two years after the evaluation of the APA300 took place. This was a new version of the APA300 with a built in amplifier and a frequency range that included zero hertz. Unfortunately, the project had progressed with a different sensor technology at this stage and hence the device was not evaluated for use in this project.

Due to the low cost device having a poor sensit
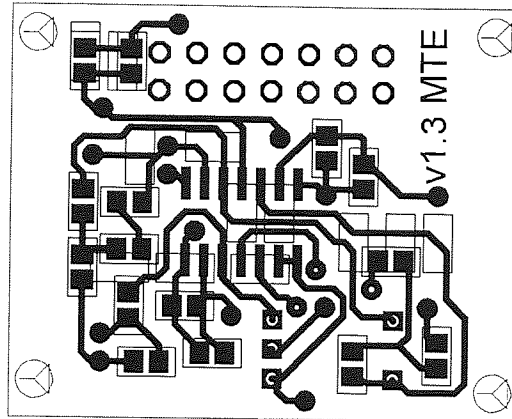
Figure 4.4: *PCB Layout of APA300 Accelerometer design*

Results from experimental tests of this accelerometer showed that although it was highly sensitive, the low frequency of the swing application described in this chapter and that of the walking experiments in chapters 5 and 6 meant that meaningful data could not be retrieved. It is suggested that accelerometers could be useful in applications where the subject is running over the surface due to the increased impact and hence vibration amplitudes generated. However, due to the low frequencies and small deflections involved in these experiments, it was concluded that both the low cost Star APA300 accelerometers and the much higher precision BK4506 accelerometers were not viable sensor devices for this application.

(a) Top   (b) Bottom
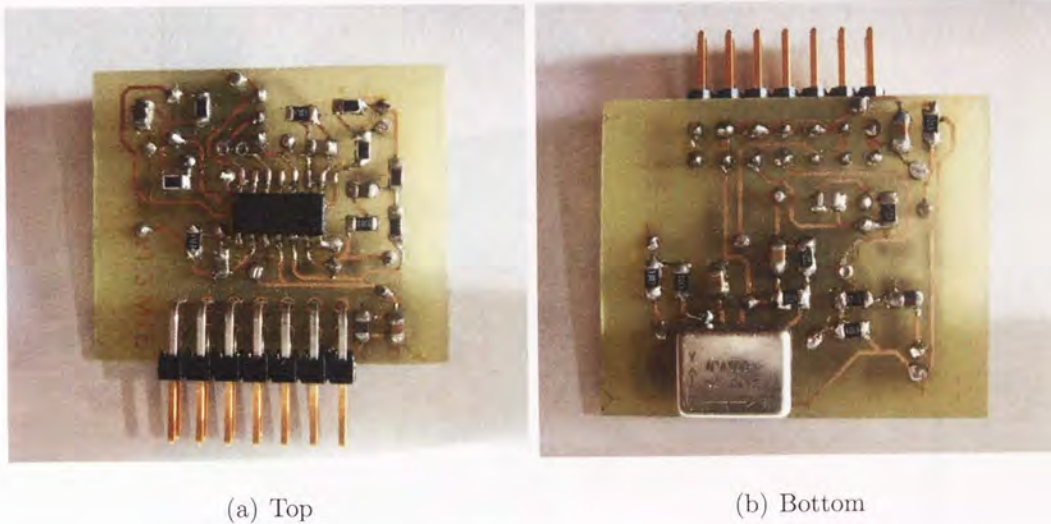
Figure 4.5: *Photographs of manufactured APA300 PCB*

Fibre Bragg Gratings

Fibre Bragg Gratings (henceforth referred to as 'gratings') consist of a single-mode optical fibre which has a fine grating etched on to the core. The grating consists of an axially, periodically varying, refractive index along the core of the fibre. The grating causes the fibre to become a highly wavelength selective mirror [71]. Therefore, by shining broadband light into the fibre only a narrow wavelength of light is reflected back. By subjecting the fibre to strain (or temperature variation), the dimensions of the grating are affected which causes a shift in the wavelength of light reflected back. Multiple gratings can be placed in a single fibre if the central wavelength of the reflections from each grating have significant separations from each other. Hence, multiple wavelengths and their corresponding shifts can be monitored to infer the strain at different points along the fibre.

Using this technique, it would be possible to embed several optical fibres parallel to each other along the length of the platform. With each fibre containing multiple gratings, the whole platform surface could be monitored using the distributive method. Cowie *et al* have previously applied the distributive tactile sensing method using fibre bragg gratings to a static two dimensional set up [71].
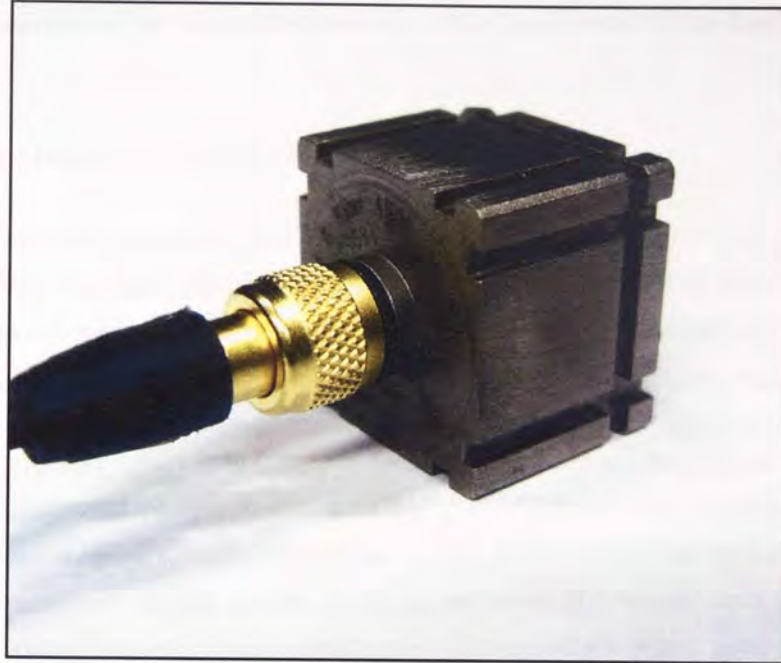
Figure 4.6: *The BK4506 Accelerometer*

In this experiment, they attempted to use the technique to determine the position and number of loads on the surface. The results showed a higher accuracy in comparison to using standard electrical strain gauges for the same application. However, temperature related effects were found to cause a significant issue, with a one degree celcius change in room temperature causing a 15 picometre (pm) wavelength shift which, in comparison to the applied loads causing between 20pm and 120pm shifts, was significant. Therefore, some form of temperature compensation technique would be required to remove this biasing effect.

Due to the larger deflection magnitudes likely to occur in the applications discussed in this thesis, it is unlikely that temperature drift would have a significant contribution when controlled for. However, although the fibre bragg grating method is a viable method for this application, the sensing equipment is relatively high cost and analysing the resulting outputs does require some knowledge of photonics, which wasn't readily available for the duration of the project. The advantage of using this method over the chosen method (see below) is that the

sensing elements can be embedded into the plate itself resulting in a self contained unit.

Infra Red Deflection Sensors

Infra-red deflection sensors have been successfully used in previous distributive tactile sensing applications [20; 21] and after weighing up the alternatives described above it was decided that the simple operation, sensitive output and low cost meant that these devices were the best sensor choice for this application.

The sensor devices (part number: SY-CR102, unbranded) consist of an infrared LED and integrated phototransistor. The LED is shone onto a surface with the reflection captured by the phototransistor. The intensity of the light captured by the phototransistor relates to the distance between the sensor and the surface. The sensor outputs a continuous analogue voltage, which when used with a high resolution analogue-digital converter is very sensitive to small changes in plate deflection. The output voltage is non-linear and is designed such that at very close range a binary output is given such that the device can be used as a counter or for measuring rotational speed. Between approximately 1mm and 5mm distance, the output increases non-linearly. After 5mm, the output continues to increase but asymptotically. A typical output characteristic is shown in Figure 4.7. The unshaded area indicates the optimum operating range as defined using the mathematical model discussed in section 4.4.1.

4.3.3.2 Sensor Mountings

The sensors themselves are very small with a dimension of just 2.5mm x 1.5mm and only require a small number of external passive components for correct operation. The schematic and PCB layout are shown in Figure 4.8 and Figure 4.9 respectively. Three connections were required to the PCB: 5V (power in), GND (ground connection) and VOUT (signal output).
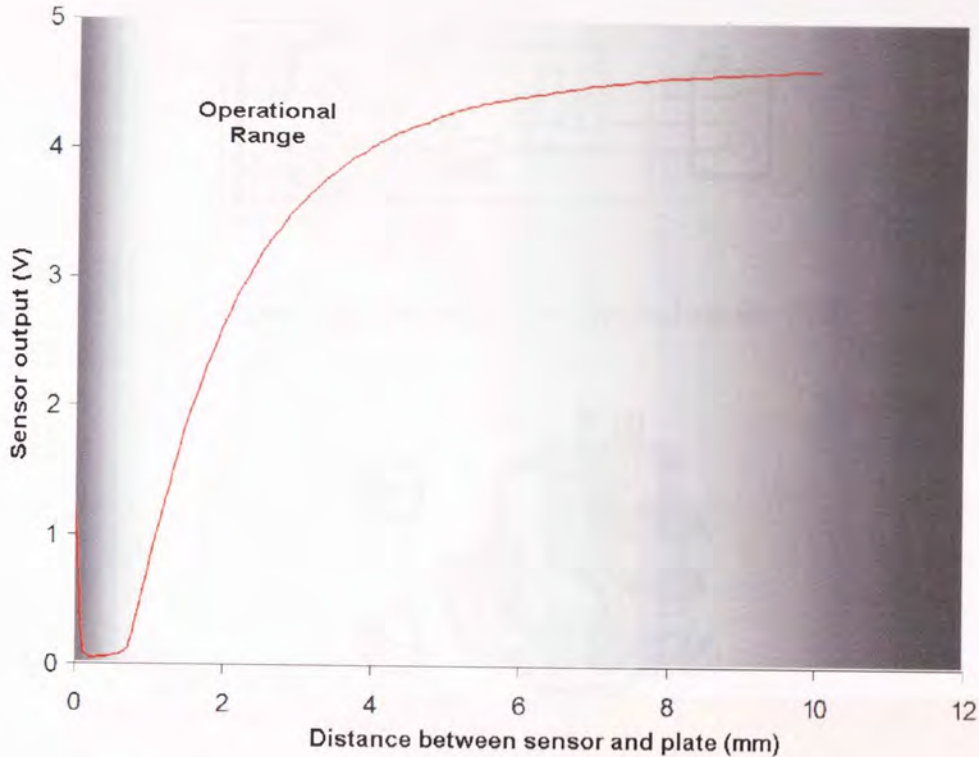
Figure 4.7: *Typical output characteristic of infra-red deflection sensor. Unshaded areas show valid operating distances for this experiment.*

To mount the sensor PCBs an appropriate distance from the plate surface a set of adjustable brackets were designed. The brackets were made up of two identical L shaped steel pieces, each with a slot cut out of the top of the long end. The two pieces were bolted together through the slot as shown in Figure 4.10. The length of the slots enabled the bracket height to be adjusted as required. The PCB was screwed onto the upper horizontal part of the bracket. A button magnet was fixed to the lower horizontal part of the bracket using adhesive tape.

A 'base-plate' was positioned under the mounted plate. The base-plate was flush to the floor and had dimensions of $0.4m \times 0.8m$, such that it fitted inside the frame supporting the plate. The base-plate had two uses, To enable flexible positioning of the sensors and to mount power and ground rails. The base plate was made
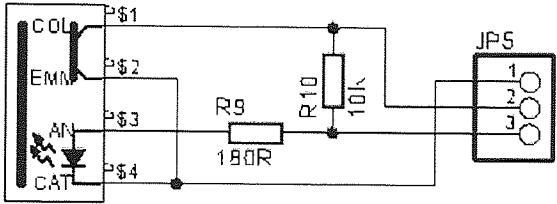
Figure 4.8: *Schematic for infra-red sensor PCB*
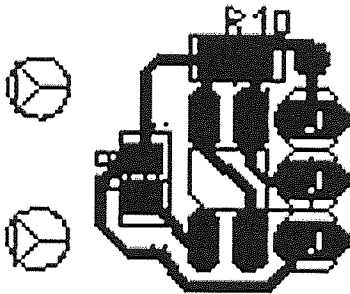
Figure 4.9: *Component layout of infra-red sensor PCB*

from steel, therefore enabling the magnets mounted to the sensor brackets to clamp the sensor into any position on the plate. This enabled the effectiveness of different sensor locations to be tested simply if required.

To ensure the sensor positions were fully flexible and to reduce the number of wires emerging from the plate, power and ground rails were placed along the long edges of the base plate. To construct the rails a bolt was positioned at each corner of the plate. Exposed twisted copper wire was then mounted between the bolts parallel to the long sides of the plate. A short length of wire terminated with a crocodile clip was then all that was required to connect the power and ground of each sensor regardless of its position on the plate. The sensors were located directly under the swing frame such that one was positioned between the two front feet, one between the two rear feet and the final one under the frame centre point (see Figure 4.11). Notice that the sensors are slightly offset from
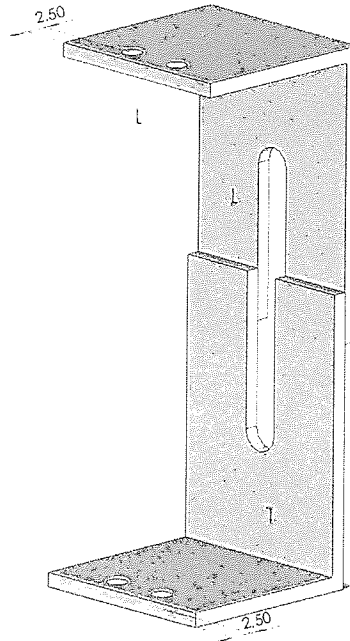
Figure 4.10: *Design drawing of the adjustable sensor bracket.*

each other to avoid symmetry. The output from each sensor was connected to a signal conditioning circuit, described in section 4.3.4.

4.3.4   Signal Conditioning

The output from the sensors when in a steady state, i.e with the swing mounted onto the plate but not moving, produced a stable (d.c) voltage of between approximately four and five volts. With the swing in motion, a small dynamic plate deflection was produced by the motion and detected by the sensors. This created a variation in the original d.c voltage of a few millivolts (a.c voltage). Therefore, the output signals consisted of two components: the d.c offset voltage, V, and the much smaller a.c voltage representing the movement of the swing ΔV, i.e. $V_{out} = V + \Delta V$. Therefore, the sensor signals were required to be conditioned using a circuit that removed the d.c component, V, such that the newly condi-
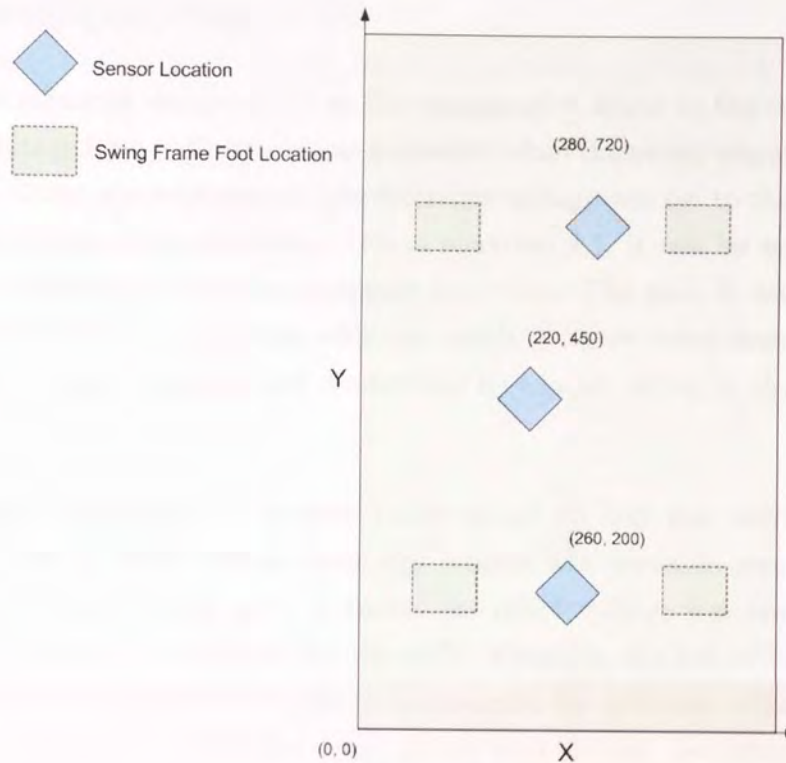
Figure 4.11: *Sensor locations under the platform (coordinates in mm).*

tioned signal only consisted of the dynamic component, ΔV, which could then be amplified to an appropriate level.

4.3.4.1 Manual Adjustment

The initial signal conditioning design made use of a differential amplifier. This worked by subtracting the signal input from a reference input and multiplying the resulting voltage by a set gain, as shown in equation 4.1.

$$V_{diff} = G(V_{in} - V_{ref}) \tag{4.1}$$

where: V_{diff} is the output voltage, G is the gain, V_{in} is the sensor output and

V_{ref} is a comparison voltage.

A voltage reference was supplied as the comparative input to the sensor signal. The d.c voltage from each sensor was measured when the swing was stationary on the plate. Using a potentiometer, the reference voltage was set to the same value as the d.c voltage from the sensor. From equation 4.1, it can be seen that this causes the differential amplifier to output zero volts. The gain, G was set to ten. By removing the d.c component only the small dynamic component caused by the swing movement remains and is amplified by a factor of ten by the differential amplifier.

This method turned out to be very fiddly to set up and was very susceptible to drift. The d.c offset voltage from the sensors was unstable over time, such that the reference voltage used to cancel the offset voltage was required to be readjusted regularly to account for the drift. Secondly, the use of low precision components in the system (i.e. the potentiometer for reference adjustment and op-amps used for the differential amp) meant that getting the reference voltage to exactly match the d.c offset voltage was very difficult. For example, due to the gain of ten amplification, a difference between the reference voltage and the offset voltage of just 0.1V resulted in a 1V d.c offset still being present on the output. This was unacceptable as the FPGA inputs had a maximum input voltage of 1V.

After several attempts it was decided that the circuit was unworkable and a new design had to be considered.

4.3.4.2 Filtering Method

A second design was investigated that was based on an ECG monitor amplifier and used a filter circuit to decouple the d.c voltage from the a.c component [74]. The design is shown in Figure 4.12 and uses two op-amps. The first in the upper left corner is a high accuracy instrumentation amplifier, which is used to reduce any inherent drift and offset voltages in the circuit. The second op-amp

is a standard device which is fitted with a resistor and capacitor to implement a low pass filter. Because this op-amp is connected in a feedback form to the instrumentation amplifier, it operates as a high pass filter on the input to the instrumentation amplifier.
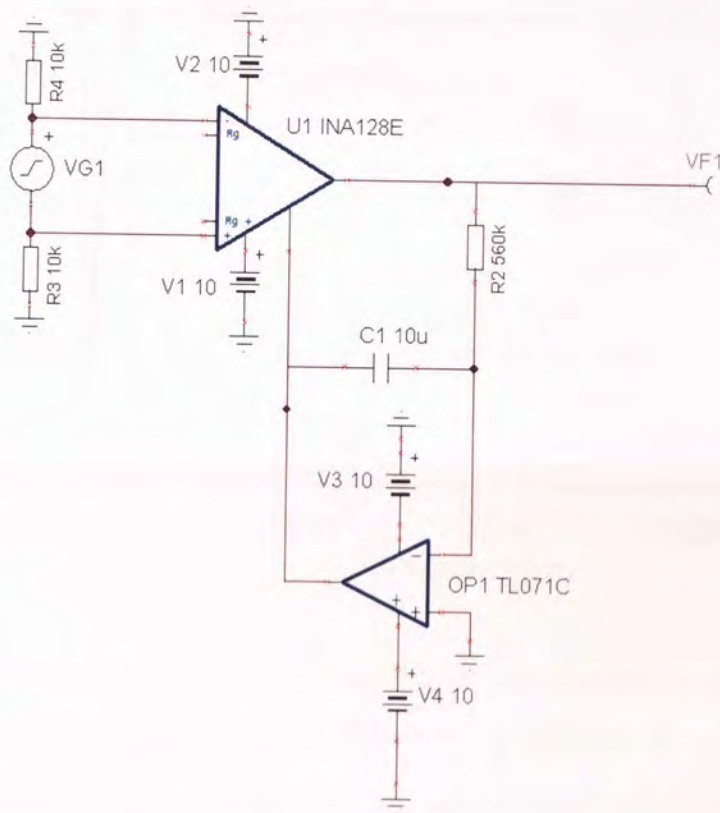
Figure 4.12: *Schematic for first stage of the signal conditioning circuit.*

The 3dB cut off frequency is given by:

$$f_{-3dB} = \frac{1}{2\pi RC} \qquad (4.2)$$

The natural frequency of the pendulum was measured to be 0.75Hz, so a cut-off frequency close to 0Hz as possible was required. A $4.7\mu F$ and $560k\Omega$ resistor provided a cut-off frequency of 0.06Hz. As shown in Figure 4.13, this attenuated

the d.c voltage by over 15dB whilst causing an insignificant attenuation of just 0.03dB at the pendulum frequency.
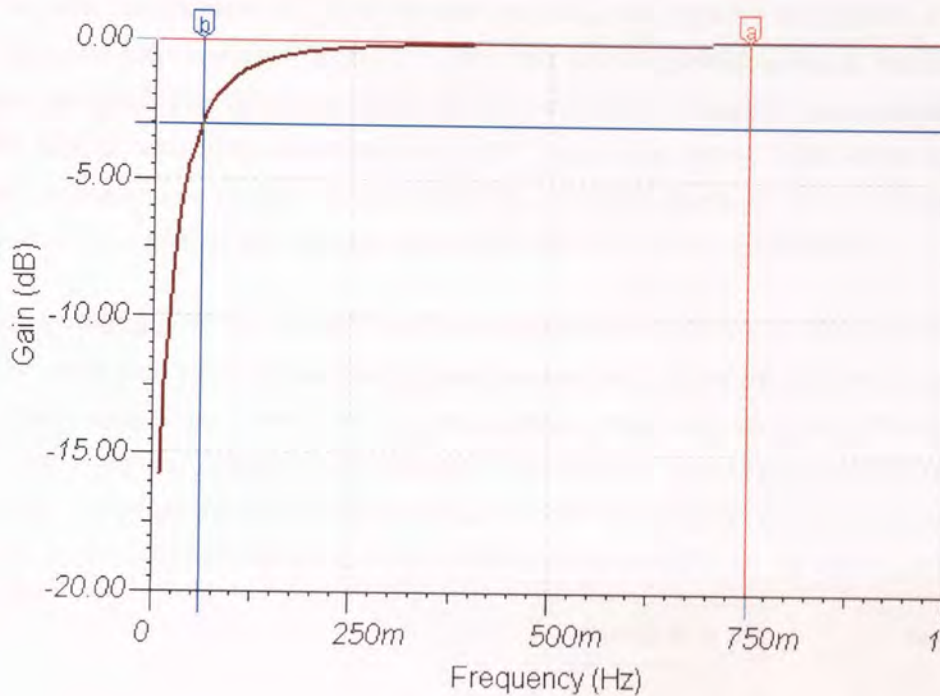
Figure 4.13: *Frequency response of the filter circuit. Marker (a) shows the natural frequency of the pendulum. Marker (b) shows the 3dB cut-off of the filter.*

A second op-amp stage was added to the output of the above circuit to provide a signal gain of ten. The resulting steady state output (swing stationary) after applying a gain stage of ten was found to be just $0.04V \pm 0.02V$. This was a much improved result in comparison to the original circuit with the offset becoming insignificant in relation to the amplified a.c output. In addition, the offset was found to suffer very little from drift, even when the swing frame was moved to a different position on the platform. This made the repeatability of the captures much more stable, an essential requirement for the neural network to accurately calculate the location.

The Analogue-Digital Converter (ADC) device used by the FPGA had an input limit of ± 1.0V. Therefore, a clipping circuit was added to the output of the gain

stage ensuring that the voltage output never rose above 1.0V, causing damage to the ADC. Also, the ADC device used by the FPGA only had two input channels. To be able to process all three sensor outputs, the signals were time division multiplexed into a single channel. This was accomplished using a multiplexer which sampled the three channels (plus one empty channel) in sequence at a much higher sampling rate than the ADC sampling rate. The value of each sensor sample was output in sequence on a single channel. The FPGA then demultiplexed the single channel back into three channels internally.

A block diagram of the signal conditioning circuit is shown in Figure 4.14. As can be seen, the output from the clipping stage could either be routed to an ADC on a motion capture system or to a mutliplexer stage and then an FPGA ADC. The route chosen depended on whether the system was being trained (routed to motion capture ADC) or tested (routed to FPGA ADC). The motion capture system and the FPGA device are described in sections 4.3.5 and 4.3.6 respectively.
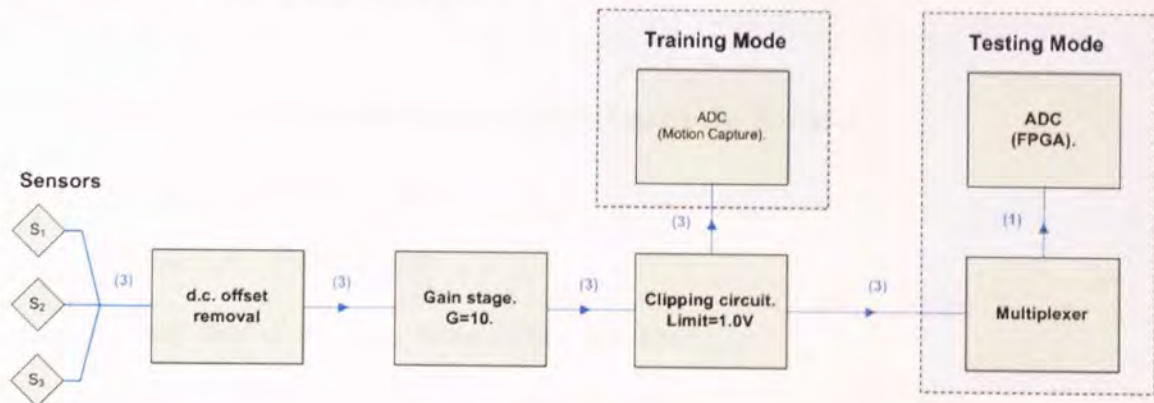
Figure 4.14: *Block diagram of signal conditioning circuit. Numbers indicate number of physical channels between stages.*

4.3.5 Motion Capture System

To be able to train the neural network, data relating to the actual position of the swing was required to be captured along with the corresponding sensor values. To

capture this data a Vicon MX13 (Vicon Peak Ltd, Oxford, UK) motion capture system was used. The motion capture system can capture the movement of an object in 3D space by tracking the position of reflective markers attached to the object under observation. A well calibrated setup can track the markers with an error of less than 1mm. The system used consisted of twelve cameras which were positioned around the volume where the swing and platform were positioned.

A PC workstation was used to process the twelve sets of synchronised 2D video data along with calibration data to determine a single set of 3D coordinates over time for each marker. The displayed markers were then labelled and related such that a 3D representation of the object captured was shown on the screen. The coordinate data was used to provide a training dataset for the neural network.

The markers were positioned on the swing at key points such that a good quality 3D representation could be reproduced in the motion capture software. The marker points were positioned at:

- Either end of the horizontal bar at the top of the A-frame.

- The top of the pivot point.

- On each foot of the frame.

- The top face of the 10kg mass (three markers).

- The outer circumference of the 10kg mass (four markers).

Figure 4.15 shows the resulting 3D representation of the swing. An extra marker can be seen in the middle of the 10kg mass, not described above. This is a virtual marker, calculated as the centre of the four markers placed around the circumference of the mass. The coordinates of this virtual marker are used as the reference point for the swing position in the training data for the neural network. To generate the training dataset, the sensor outputs were captured by an ADC built into the motion capture system which was a 16-bit device, able to capture

over the range ± 1.25V and was fully synchronised with the sampling rate of the cameras at 200Hz.
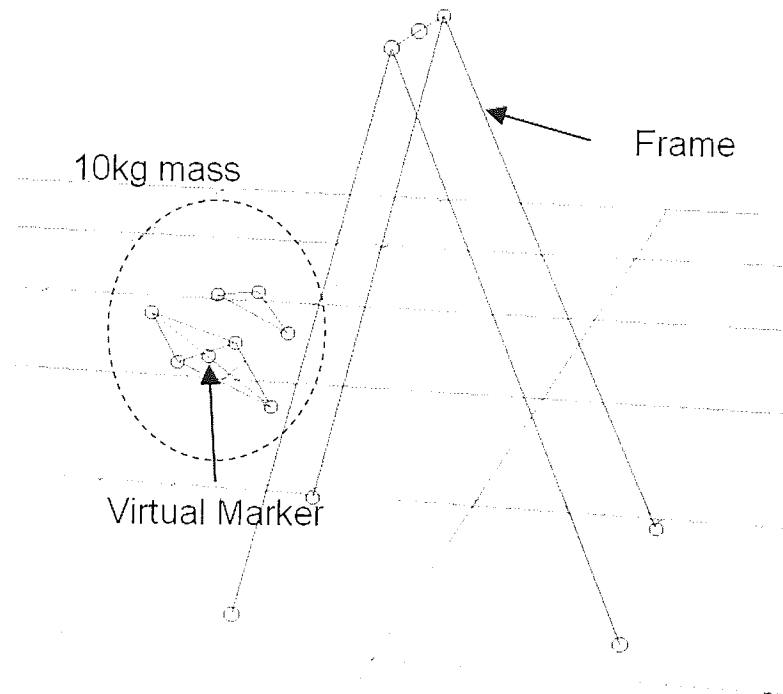
Figure 4.15: *3D representation of the swing in the motion capture software.*

4.3.6 Field Programmable Gate Array

To enable the system to track the swing in real-time as a stand alone embedded device (i.e no external processing provided by a PC or similar), the neural network was implemented on a field programmable gate array (FPGA). An FPGA is a silicon chip based integrated circuit device consisting of a large matrix of interconnected logic gates. The interconnections between the logic gates can be made or broken and their configurations adjusted such that complex logic circuits can be created. Algorithms are used to convert a high level, simple programming

language (e.g 'VHDL') into the mappings of the logic gates required to produce the desired functions.

For this experiment, the methods derived by Petra *et al* [75] were used to generate, synthesise and implement a neural network onto a Xilinx Xtreme FPGA-based embedded system (Nallatech Ltd, Glasgow, UK). The embedded system consisted of a high performance dual channel, 14-bit Analogue-to-Digital Convertor (ADC), a corresponding Digital-to-Analogue Convertor (DAC) and a Xilinx Virtex-II FPGA XCE2V3000 (32,000 logic cell device). A further Virtex-II XC2V80 FPGA was used to provide clock management functions. The embedded system is shown in Figure 4.16.

The system was fully compatible with the Xilinx Blockset and Xilinx System Generator software toolboxes for Simulink (The Mathworks, Inc., MA) enabling the neural network to be trained and constructed in the Matlab/Simulink environment before being synthesised on to the FPGA.

4.4 Method

4.4.1 Mathematical Model

Before the platform and swing were constructed and the sensor circuits implemented, an initial mathematical model of the pendulum and frame was produced to determine the operating range of the sensors (see Figure 4.7) and the level of amplification that may be required. Based on Figure 4.17, the following equations give the resultant vertical force at each foot of the frame and was hence used to determine the dynamic plate deflection when the swing was in motion.

From Figure 4.17 it can be seen that four forces are acting on the pendulum mass, F_{gr}, the radial component of the weight due to the mass itself, F_p, the tensile force on the pendulum, F_c, the centrifugal force and F_m, the tangential
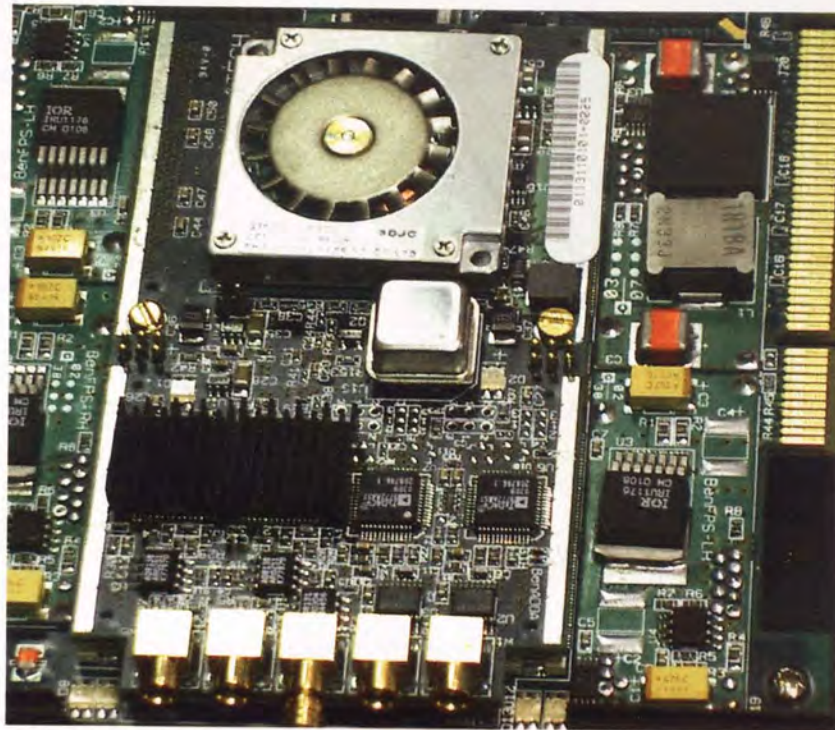
Figure 4.16: *The Nallatech embedded FPGA system.*

force. These forces must be resolved in order to determine the forces acting on the bearing of the frame, O, denoted as F_x, the horizontal force acting on the bearing and F_y, the vertical force acting on the bearing. Given a dynamic system these are calculated as follows [76].

The radial component of the gravitational force is given as:

$$F_{gr} = \bar{m}g\cos\theta \tag{4.3}$$

where θ is the angle between the vertical at the pivot point and the pendulum, $\bar{m}$ is the mass attached at the pendulum end (the rod is assumed to be massless), g is the acceleration due to gravity. The centrifugal force is given as:
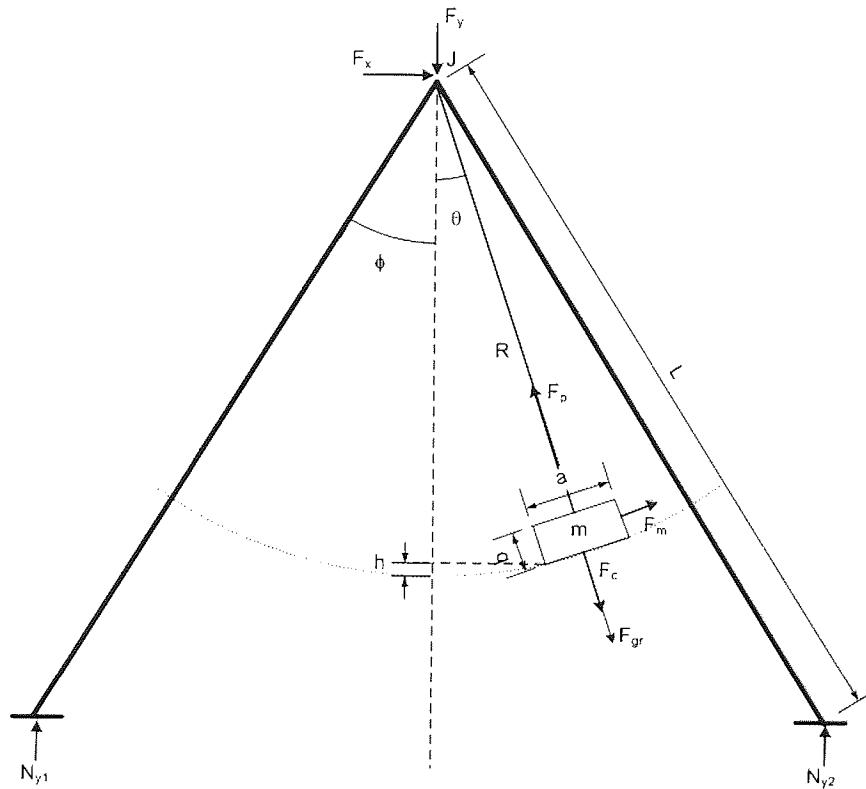
Figure 4.17: *Forces and moments due to the motion of the pendulum.*

$$F_c = \bar{m}\omega^2 R \qquad\qquad (4.4)$$

where R is the rod length. To find ω, conservation of energy principles can be used:

$$\frac{1}{2}J\omega^2 + \bar{m}gh = \frac{1}{2}J\omega_{max}^2 \qquad\qquad (4.5)$$

where J is the moment of inertia about the mass and ω_{max} is the maximum pendulum angular velocity. From figure 4.17 it can be seen that $h = R - R\cos\theta$ so:

$$\omega^2 = \omega_{max}^2 - \frac{2\bar{m}gR}{J}(1 - \cos\theta) \tag{4.6}$$

Defining θ_0 as the initial angle of release, then when $\theta = \theta_0$, $\omega = 0$ so:

$$\omega_{max}^2 = \frac{2\bar{m}gR}{J}(1 - \cos\theta_0) \tag{4.7}$$

Substitute equation 4.7 into equation 4.6 to get:

$$\omega^2 = \frac{2\bar{m}gR}{J}(\cos\theta - \cos\theta_0) \tag{4.8}$$

As the force does not move in the plane of F_c and F_{gr}, then as shown in Figure 4.17, the tensile force must be equal to the sum of the centrifugal force and the gravitational force in the radial direction. Using equations 4.3, 4.4 and 4.8, the tensile force, F_p is given as:

$$F_p = \frac{\bar{m}g}{J}\left[\left(J + 2\bar{m}R^2\right)\cos\theta - \left(2\bar{m}R^2\cos\theta_0\right)\right] \tag{4.9}$$

Finally, the tangential force is created by the moment of inertia about the centre of the mass. The equation of motion of the system is defined as:

$$J\frac{d^2\theta}{dt^2} = \bar{m}gR\sin\theta \tag{4.10}$$

Given a rectangular cross section of the mass with a width, a and height, b, the moment of inertia about the centre of the mass is:

$$J_{CoM} = \frac{\bar{m}(a^2 + b^2)}{12} \tag{4.11}$$

The torque due to the mass is:

$$\tau = J_{CoM} \frac{d^2\theta}{dt^2} \tag{4.12}$$

From equation 4.10:

$$fracd^2\theta dt^2 = \bar{m}gR\sin\theta \tag{4.13}$$

so:

$$\tau = \frac{\bar{m}(a^2 + b^2)}{12} \cdot \frac{\bar{m}gR\sin\theta}{J} \tag{4.14}$$

Finally, the tangential force is found by dividing the torque by the rod length to get:

$$F_m = \frac{\bar{m}^2 g(a^2 + b^2)\sin\theta}{12J} \tag{4.15}$$

The horizontal and vertical component forces acting on the frame bearing can now simply be found as follows:

$$F_x = F_p\sin\theta - F_m\cos\theta \tag{4.16}$$

$$F_y = F_p\cos\theta - F_m\sin\theta \tag{4.17}$$

Defining $M = F_m R$ and using equations 4.16 to 4.17, then by summing the moments the resulting equations for the vertical force at each foot can be calculated as follows:

$$N_{y_1} = \frac{LF_y \sin\phi + M - LF_x \cos\phi}{2L\sin\phi} \tag{4.18}$$

$$N_{y_2} = \frac{LF_y \sin\phi - M + LF_x \cos\phi}{2L\sin\phi} \tag{4.19}$$

where L is the length of the swing legs and ϕ is the angle between the legs.

This model assumes a two dimensional representation of the swing and therefore requires the assumption that the resulting front (N_{y1})and rear (N_{y2}) forces are split equally between the two feet on the front and rear of the swing. Note, damping was not taken into account for this model.

By converting equations 4.18 and 4.19 to a series of summed sine terms it is possible to apply it to Szilard's dynamic plate model [31]. The resulting model makes it possible to determine the plate deflection at any point, due to the motion of the swing.

Implementing the conversion resulted in the following sine series:

$$\begin{aligned} N_{y_1} &= k_0 + (k_1 + k_2)\sin\theta - k_3 \sin\left(\frac{\pi}{2} - \theta\right) \\ &+ (k_4 + k_5)\sin\left(\frac{\pi}{2} - 2\theta\right) - (k_6 + k_7)\sin 2\theta \end{aligned} \tag{4.20}$$

$$\begin{aligned} N_{y_2} &= k_0 - (k_1 + k_2)\sin\theta - k_3 \sin\left(\frac{\pi}{2} - \theta\right) \\ &+ (k_4 - k_5)\sin\left(\frac{\pi}{2} - 2\theta\right) - (k_6 - k_7)\sin 2\theta \end{aligned} \tag{4.21}$$

where:

$$k_0 = \frac{1}{4\tan\phi}\left[\frac{\bar{m}g}{J}\left(J + 2\bar{m}R^2 + \frac{\bar{m}\left(a^2 + b^2\right)}{12}\right)\right] \tag{4.22}$$

$$k_1 = \frac{R}{2L\sin\phi}\left[\frac{\bar{m}^2 g\left(a^2 + b^2\right)}{12J}\right] \tag{4.23}$$

$$k_2 = \bar{m}R^2\cos\theta_0 \tag{4.24}$$

$$k_3 = \frac{\bar{m}R^2\cos\theta_0}{\tan\phi} \tag{4.25}$$

$$k_4 = \frac{1}{4\tan\phi}\left[\frac{\bar{m}g}{J}\left(J + 2\bar{m}R^2\right)\right] \tag{4.26}$$

$$k_5 = \frac{1}{4\tan\phi}\left[\frac{\bar{m}^2 g\left(a^2 + b^2\right)}{12J}\right] \tag{4.27}$$

$$k_6 = \frac{\bar{m}g}{4J}\left(J + 2\bar{m}R^2\right) \tag{4.28}$$

$$k_7 = \frac{\bar{m}^2 g\left(a^2 + b^2\right)}{48J} \tag{4.29}$$

The deflection of a plate due to a harmonic force can be found using equation 3.23. Note, it is assumed the plate is simply supported, rather than clamped, to avoid excessively complicated equations. The result will provide a suitably accurate approximation of the real plate deflection when the swing is in motion.

$$w(x,y,t) = \sum_{r=1}^{\infty}\sin\left(p_r t\right)\sum_{i=1}^{\infty}\sum_{j=1}^{\infty}W_{ijr}\sin\left(\frac{i\pi x}{l_x}\right)\sin\left(\frac{j\pi y}{l_y}\right) \tag{4.30}$$

where p_r is the frequency of the rth sine term, l_x, l_y are the plate dimensions and W_{ijr} describes the mode shape due to the applied force. The load is applied to the plate through the rectangular feet of the frame. Assuming each foot has length c and width d with the foot centre located at (ε, η), the resulting mode shape, P_{ij} for a simple harmonically varying force is given by:

$$P_{ij} = \frac{16p_0}{\pi^2 ij}\sin\left(\frac{i\pi\varepsilon}{l_x}\right)\sin\left(\frac{j\pi\eta}{l_y}\right)\sin\left(\frac{m\pi c}{2a}\right)\sin\left(\frac{n\pi d}{2b}\right) \tag{4.31}$$

where p_0 is the force per unit area.

For a dynamically varying force made up of multiple sine terms we extend this to calculate P_{ijr}, and substitute p_0 (equation (4.31)) for p_{0_r}, the force per unit area of the rth sine term.

$$P_{ij} = \frac{16 p_{0_r}}{\pi^2 ij} \sin\left(\frac{i\pi\varepsilon}{l_x}\right) \sin\left(\frac{j\pi\eta}{l_y}\right) \sin\left(\frac{m\pi c}{2a}\right) \sin\left(\frac{n\pi d}{2b}\right) \qquad (4.32)$$

Finally, defining ω_{ij} as the natural angular frequency of the plate for mode (i, j) and $\tilde{m}$ as the mass per unit area of the plate, W_{ijr} can now be defined as:

$$W_{ijr} = \frac{P_{ijr}}{\tilde{m}\left(\omega_{ij}^2 - p_r^2\right)} \qquad (4.33)$$

In this case four force distributions (area: 0.05m x 0.06m) are used to represent the feet of the swing. Equation 4.30 is used to determine the plate deflection due to each individual force with the resultant deflection given by the sum of these deflections. The predicted deflection of the plate at the chosen sensor locations (as defined in Figure 4.11) are shown in Figure 4.18. Note, that damping is not taken in to consideration.

The results from the model show that the maximum deflection will be approximately 0.5mm and therefore, the sensors were required to be positioned so that they operated in their most sensitive region (as shown in Figure 4.7). Additionally, to take advantage of the full ADC range, an amplifier gain of ten was specified for the signal conditioning circuit.

4.4.2   Neural Network

To couple the sensor outputs and relate the plate deflection data to the pendulum position, a multi-layer perceptron (MLP) neural network was used. A regression network was implemented that consisted of three inputs (one for each sensor), a
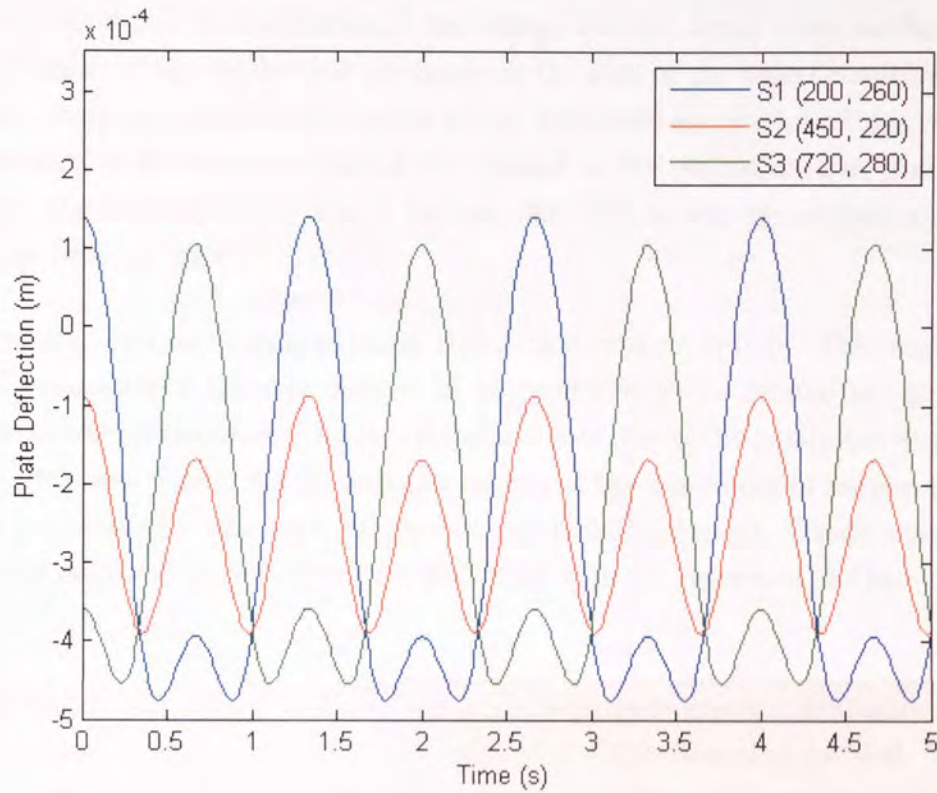
Figure 4.18: *Plate deflection at the three sensor locations as calculated by the mathematical model.*

hidden layer and three outputs describing the pendulum position in X, Y and Z coordinates.

A summary of the neural network implementations for this experiment is shown in Table 4.2.

4.4.2.1   Training

The neural network training data consisted of three inputs, which were the sampled voltage amplitudes from each sensor and three outputs giving the corre-

sponding X, Y and Z coordinates of the swing. For the input data, no further pre-processing of the signals was necessary as the gain of the signal conditioning amplifier stage (along with the clipping stage) was set to ensure the voltage range was between ± 1.0V. Post processing was applied to the output data so that, for example, the Y-coordinate range of between 200-300mm was normalised to give a voltage between ± 1.0V.

The training data was captured using the motion capture system. This enabled a fully synchronised training dataset to be produced which related the sensor outputs to the corresponding three dimensional location of the pendulum at that moment in time. Three, fifteen second captures of the pendulum in motion (one launch per capture) were used to produce the training dataset. These samples were then randomly permutated such that they were not presented to the neural network in time order.

The back-propagation algorithm with a scaled conjugate gradient optimiser was used to train the neural network whilst using the Early Stopping method. This method requires the data captured for training to be split into three sets: training, validation and test. The algorithm trains the network by a number of iterations at a time using the training dataset. After each group of iterations the network's current state is tested against the validation dataset with the resulting error compared to the previous validations. If the error converges or starts to rise again then training is stopped. Finally, the fully trained neural network is presented with the test data. This is data the network was not exposed to during training or validation and so provides a benchmark as to how accurate the neural network is at producing the expected output.

The training data was therefore split into training, validation and test sets, with the chosen proportions as follows: Training, 50%; Validation, 25%; Test, 25%.

The training was done offline in MATLAB using the Netlab add-on package (I. T. Nabney, Aston University, 2004). By training offline, optimisation of the network was possible in order to determine the optimum number of hidden nodes, hence reducing the network complexity. By reducing complexity, generalisation to the

underlying function is more likely and hence reduces the chance of over-fitting (i.e when the network fits to the noise in the system rather than the underlying function). There is no reported method on how to determine the optimum number of hidden nodes. Therefore, in practice the network optimisation was implemented through repeated training of the network with varying numbers of hidden nodes (from 4 to 25). The chosen number of hidden nodes was based on the network showing the lowest generalisation error. A typical optimisation response is shown in Figure 4.19.
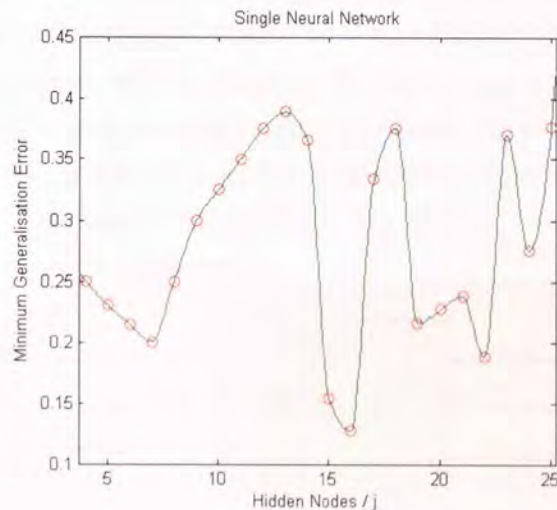
Figure 4.19: *Example of number of hidden nodes versus error (taken from Single architecture tests). Reproduced with kind permission of I. Petra.*

4.4.2.2   Architectures

Three different neural network architectures were investigated in an attempt to achieve the lowest prediction error. First, a 'Single' architecture was implemented whereby a single neural network was used to compute the X, Y and Z outputs concurrently (Figure 4.20). Secondly, a 'Multiple' architecture was implemented whereby a separate network was used to compute each dimension individually (Figure 4.21). Finally a 'Cascaded' architecture was implemented which also

used separate networks for each dimension but was cascaded sequentially, such that the outputs of any previous networks were used as additional inputs to the next network (Figure 4.22). The Cascaded network was ordered by the magnitude of the displacement in each axis. So, the Y-dimension was the first in the sequence followed by the Z-dimension and finally the X-dimension. The X-dimension therefore, had two further inputs compared to the Y-dimension.

The optimisation techniques described previously were used to determine an appropriate number of hidden nodes for each architecture. The optimum number of hidden nodes for the Single architecture was found to be 16 (see Figure 4.19). Thus the configuration will be 3 inputs, 16 hidden nodes and 3 outputs, denoted as (3:16:3). For the Multiple architecture, the optimum configuration was; (3:7:1), (3:7:1) and (3:9:1) for the X, Y and Z dimensions respectively. For the cascaded architecture, the optimum configuration was (3:7:1), (4:6:1) and (5:5:1) for the Y, Z and X dimensions respectively.
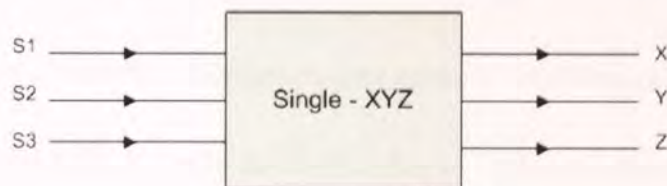
Figure 4.20: *Single neural network architecture*

4.4.3   Testing

The resulting trained networks were converted into an FPGA mapping using the Xilinx Blockset and Xilinx System Generator toolboxes for Simulink. Independent tests were then carried out using the Single, Multiple and Cascaded network designs to determine the accuracy of the predicted position in comparison to the position measured by the motion capture system. It should be noted that the testing between each network was carried out independently due to the limited digital resources of the embedded system. This inhibited the ability to place all
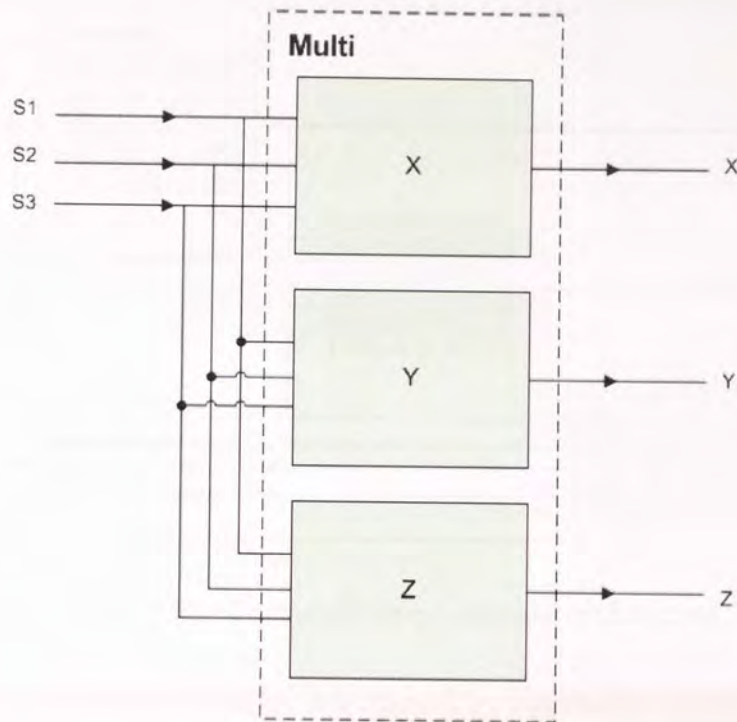
Figure 4.21: *Multiple neural network architecture*

three architectures on to a single device in order to facilitate concurrent measurements for direct comparison.

For each test, the motion capture system was required to be calibrated to give accurate measurements. The positions inferred by the FPGA based implementations of the various neural network designs were compared to the actual position that was obtained from the motion capture system. For further validation, the predicted positions were also compared to both the position of the swing computed by the software based (MATLAB) neural network (using off-line testing) and the position of the swing computed by the Xilinx simulation design. This enabled quantification of the expected performance of the FPGA based neural networks and early interception of potential problems in the training. Both simulations produced position errors that were close to the actual error achieved, indicating the FPGA based neural network was operating as expected when implemented on the FPGA device. The error between the three predicted positions
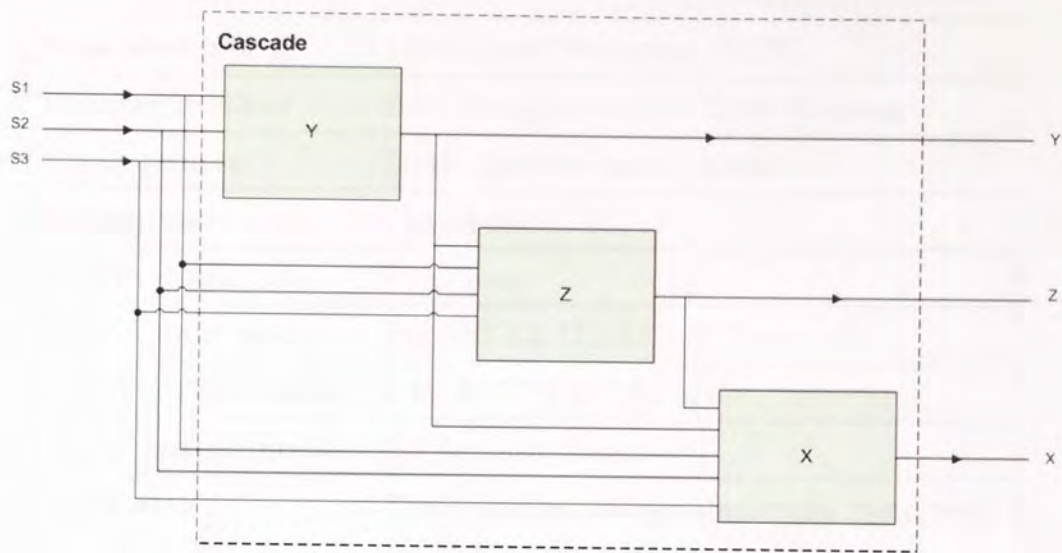
Figure 4.22: *Cascaded neural network architecture*

and the actual measured position determined by the motion capture system are shown in Table 4.3.

4.5 Results

4.5.1 Model Validation

To validate the model, a laser vibrometer was used to determine the actual deflection of the plate when the swing was in motion. The vibrometer was aimed close to one of the rear legs and the plate deflection velocity was determined using optical interference measurement methods. The resulting velocity profile was then numerically integrated to get the plate deflection over time. The measured deflection was compared to that of the simulated deflection at the same location on the plate. The comparison is shown in Figure 4.23 and indicates that the model produces a relatively accurate simulation of the plate response.

Network type	Multi-Layer Perceptron (MLP)
Training method	Back Propagation with Early Stopping
Architectures	Single, Multiple and Cascaded
Hidden node $f(x)$	Tan-sigmoid
Output node $f(x)$	Pure linear
No. of input nodes	S:3, M:3,3,3, C:3,4,5
No. of hidden nodes	S:16, M:7,7,9, C:7,6,5
No. of output nodes	S:3, M:1,1,1, C:1,1,1
Input data	Three sampled voltage amplitudes from conditioned sensor signals
Output data	Three, continuous values in the range [0,1], representing a normalised pendulum position in x, y and z coordinates

Table 4.2: *Summary of the neural network implementation*

4.5.2 Experimental Results

The three neural network architectures described in section 4.4.2 were tested using the FPGA implementation. As indicated previously, the Y dimension represented the location of the pendulum along the length of the plate. The Z dimension represents the height of the swing (from its static vertical position) and has a smaller range of up to approximately 60mm. The swing has no free movement in the X dimension which represents the displacement along the width of the plate. Therefore, any measured displacement in this dimension is down to instabilities in the frame and pendulum when the swing is in motion. The displacement in the X dimension is small with a range of approximately 0-10mm.

The following graphs (Figures 4.24 to 4.26) show the predicted location against the actual location as measured by the motion capture system as well as the error

Axis	Architecture	% Error		
		Matlab Sim.	Xilinx Sim.	FPGA Real Time
X	Single	1.8	2.5	3.8
	Multi	1.2	2.2	1.5
	Casc.	2.9	3.1	3.8
Y	Single	1.3	1.9	2.9
	Multi	1.1	2.0	1.9
	Casc.	1.4	1.5	2.1
Z	Single	4.1	6.6	7.1
	Multi	3.8	4.1	4.1
	Casc.	4.0	4.9	4.7

Table 4.3: *Average percentage errors for each axis and architecture measured by Matlab simulation, Xilinx simulation and the real time hardware implementation*

for each sample. Tables 4.4 to 4.6 shows the percentage error in each dimension for each architecture. The percentage error is calculated as the mean absolute error divided by the mean absolute displacement over the time of the capture.

The results show that the different neural network architectures cause only a small difference in the tracking error, although a marginal improvement in accuracy is achieved by having an independent neural network for each dimension. Regardless of the network architecture, it was found that the back propagation neural network was successfully able to track the position of the pendulum in three dimensions. The best case results show that the swing position can be predicted, in real time, with an error of less than 5%.
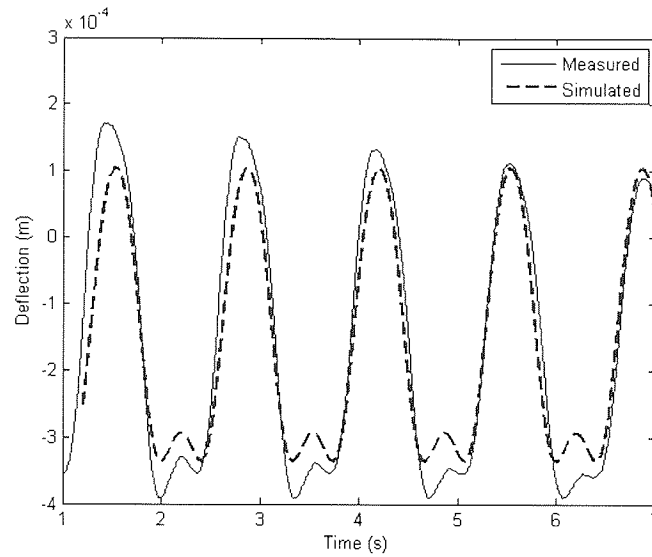
Figure 4.23: *Mathematical model validation results, showing actual measured deflection (black solid) compared to predicted deflection (blue dashed).*

Dimension	Mean Error (mm)	Mean Displacement (mm)	Percentage Error
X	0.3	7.0	3.8%
Y	8.6	271.7	2.9%
Z	1.9	26.7	7.1%

Table 4.4: *Tracking accuracy of the neural network when using a 'single' architecture*
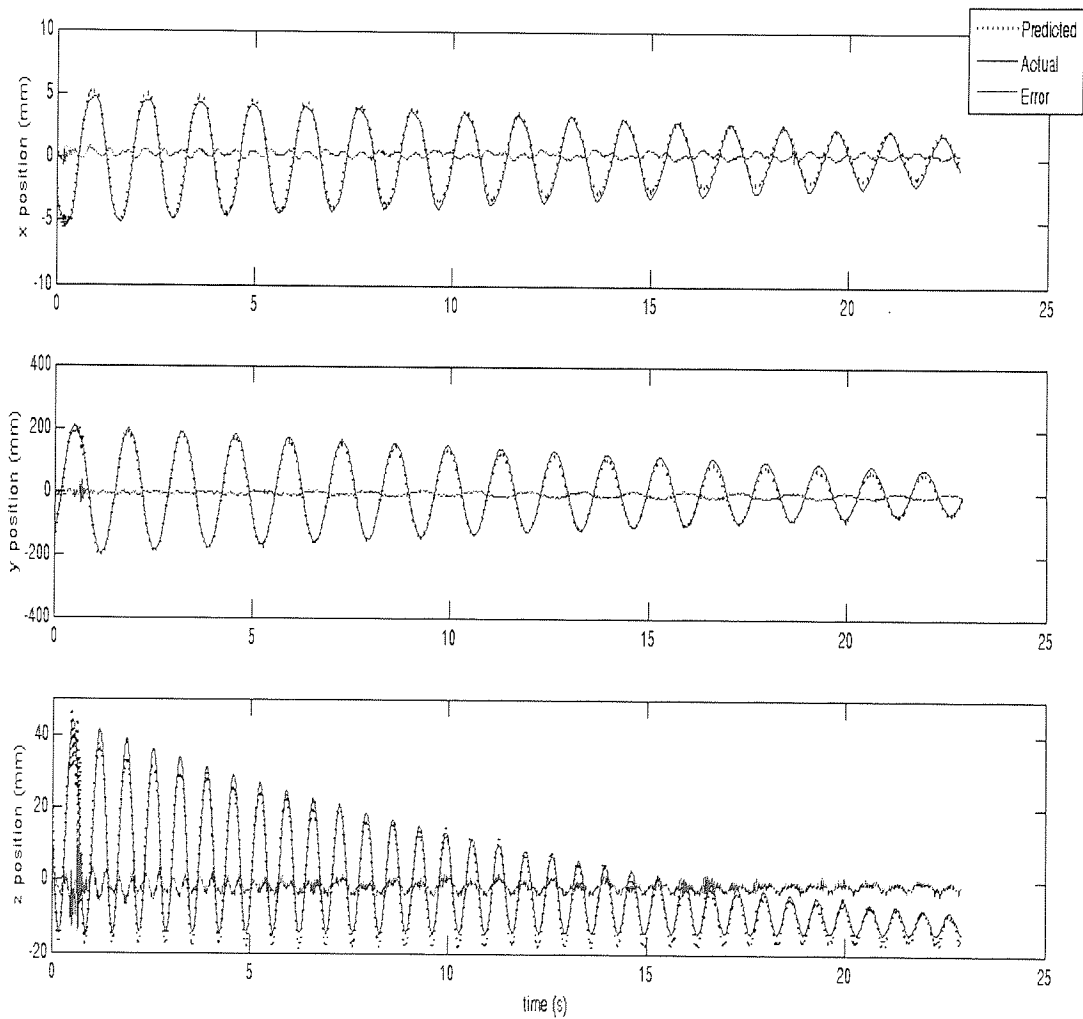
Figure 4.24: *Predicted position (...) against actual position (—) using 'Single' architecture for X, Y & Z dimensions respectively. Light grey line indicates relative error*
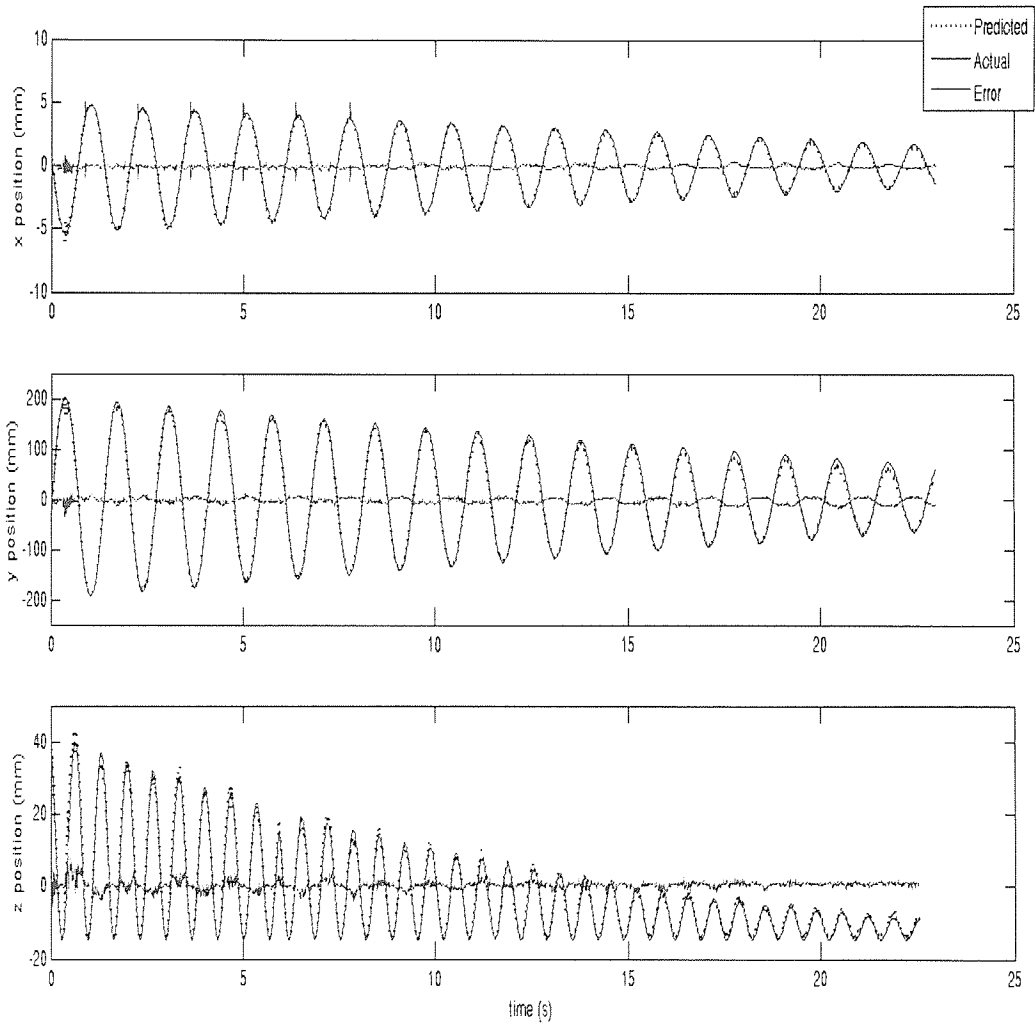
Figure 4.25: *Predicted position (...) against actual position (—) using 'Multi' architecture for X, Y & Z dimensions respectively. Light grey line indicates relative error*
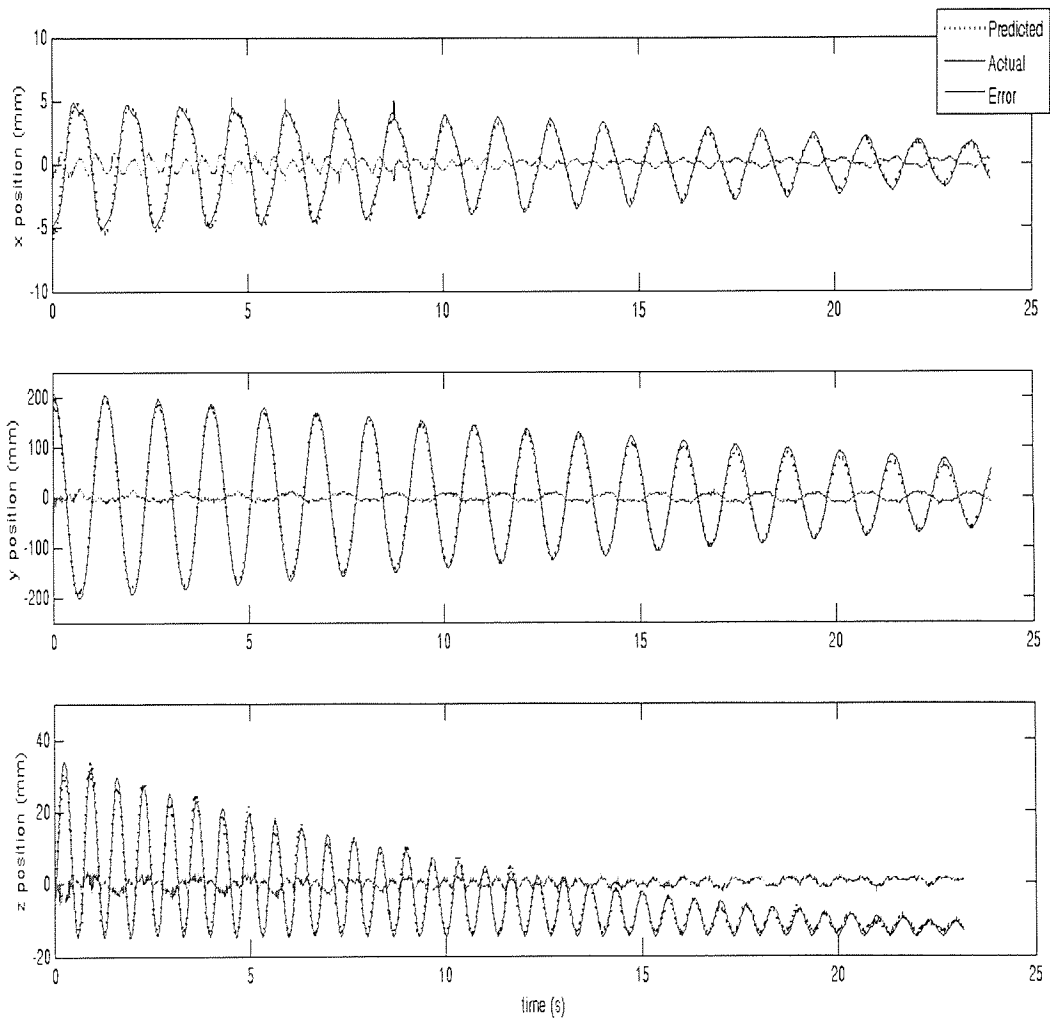
Figure 4.26: *Predicted position (...) against actual position (—) using 'Cascaded' architecture for X, Y & Z dimensions respectively. Light grey line indicates relative error*

Dimension	Mean Error (mm)	Mean Displacement (mm)	Percentage Error
X	0.1	6.7	1.5%
Y	5.2	251.7	1.9%
Z	0.9	20.6	4.1%

Table 4.5: *Tracking accuracy of the neural network when using a 'multiple' architecture*

Dimension	Mean Error (mm)	Mean Displacement (mm)	Percentage Error
X	0.3	6.8	3.8%
Y	6.3	262.9	2.1%
Z	1.0	20.6	4.7%

Table 4.6: *Tracking accuracy of the neural network when using a 'cascaded' architecture*

4.6   Discussion

In this section, a novel platform based instrument has been implemented that could ultimately provide balance and sway measurements of a person during quiet standing using relatively low cost sensors and components. An experiment has been described which enabled a detailed evaluation of the accuracy of the system developed. Using a pendulum mounted on an A-frame to perform the representation of a swaying person during quiet standing, the system achieved >95% tracking accuracy in all three dimensions. An embedded hardware based neural network was implemented, based on the technique developed by Petra *et al* [75] which enabled real-time output of the pendulum position without the presence of a computer workstation.

Extending the system to measure Centre of Mass (COM) or Centre of Pressure (COP), as is commonly the required output from current balance systems, would require some relatively simple additional algorithms. However, the key outcome of this experiment was that distributive tactile sensing has been shown to be a viable method for tracking the motion of an object placed on a relatively large scale surface. In the following chapters, the equipment, signal processing hardware

and analysis methods developed in this experiment, are used as a foundation to explore the possibility of discriminating different gait patterns in people.

Chapter 5

Person identification through the discrimination of gait profile

5.1 Introduction

Person identification, based on biometric data has recently become an important area of research. UK passports are soon to start using biometric data captured from a person's finger print and iris for example. Whilst finger printing and iris scans are now well developed technologies, person identification by their gait profile is a more recent area of research. Most research into identification through gait examines the whole body posture through the gait cycle using video capture and filtering methods (for example, Zhang *et al* [61]).

In this section an experiment is undertaken, whereby it is hypothesised that a small number of people can be individually identified by the deflection pattern created as they walk over a sensing platform. Using a similar experimental setup to that described in Chapter 4, the hypothesis is tested using five volunteers. This experiment moves away from the measurement techniques discussed in the

previous chapters and instead investigates two different classification methods to identify a subject when compared to templates stored in the system. The results show classification accuracies that were reasonable given the similarity of the physical build and age of the volunteers. It is suggested that this method could be used as a convenient and unintrusive identification system where only a small number of people are required to be identified, such as an office or workplace.

This chapter first describes the improvements to the experimental setup implemented due to issues found in the equipment used in the previous experiment (Chapter 4). The first algorithm investigated is the Dynamic Time Warping algorithm which is used to classify a captured gait pattern to one of five people. Secondly, feature extraction along with linear discrimination analysis methods are used in an attempt to improve the classification accuracy.

5.2 Instrumentation Design and Setup

A new platform design was implemented that was a similar, scaled up version of that used in Chapter 4. Several new design features were included that overcame the problems and weaknesses identified when using the original design.

One of the main issues identified when using the original platform was not having the base-plate attached to the frame of the platform. The steel base-plate was used to position the sensors under the platform using brackets with a magnetic base. The original base-plate had dimensions such that the frame of the platform sat around it. The base-plate itself sat flush to the floor of the laboratory and was not connected in any way to the frame. This made the system very sensitive to external movements. For example, if the platform was knocked or moved in any way, the relative position of the platform to the sensors was changed, therefore generating a different deflection profile when the swing was in motion. This effect reduced the repeatability of the swing experiments.

It was important to eliminate this issue in the new platform design. The solution was to sandwich the base-plate between two frames. The lower frame was in contact with the floor and supported the base-plate. The upper frame was used to clamp the base-plate and support the main sensing plate. The two frames were welded to the base-plate to create a solid structure. The top plate was not welded to the plate, but was clamped on the long sides using a rectangular steel bar secured with bolts. To enable cable access to and from the sensor circuits, 30mm diameter holes were created in each side of the upper frame. The platform design is shown in Figure 5.1.
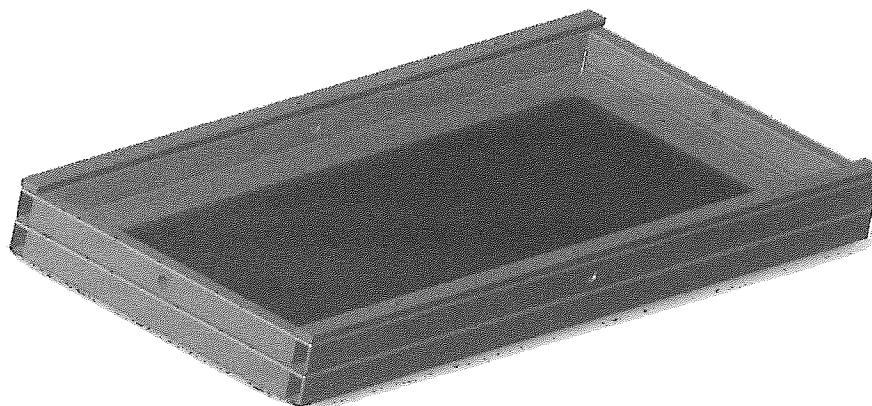
Figure 5.1: *Mechanical drawing of the platform with a sandwiched base plate.*

By integrating the sensor base-plate to the frame of the platform, the sensors were now only sensitive to the effects caused by deflection of the top plate with respect to the whole frame, rather than any movement to the platform itself due to arbitrary knocks. Also, only a displacement large enough to overcome the magnetic holding force of the sensor brackets was able to knock the sensors out

of their set location. This enabled more reliable and repeatable results to be produced.

5.2.1   Platform Dimensions

The platform was designed such that it was able to record two foot strikes (i.e. one left foot and one right foot strike) as the subject walked over the platform. To calculate the required platform length, research data was used to determine the mean step length of an adult male. Murray *et al* [77] found this to be approximately 78cm from a sample of 120. This was effectively doubled to ensure the plate would always capture at least one left and one right foot strike. It was also important that the subject could walk naturally without the width of the plate causing them to narrow their stride. In this case shoulder width was used to give a reasonable estimate of adult stride width. Anthropometric data was used to determine the 95th percentile width of 0.5m [78]. An extra 200mm was added to account for the clamp width, variation of stride width in different people and also to ensure the foot strikes did not occur too close to the platform edge, reducing the plate deflection.

The resulting plate dimensions were 1.50m x 0.70m. The height of the plate due to the double frame implementation was 0.13m. The height of the platform from the floor would require the subject to step on to the platform and therefore, would have significant effects on natural gait. To encourage natural walking as much as possible, two further platforms were constructed and placed before and after the sensing platform. These were referred to as the *gait initiation platform* and *gait termination platform* respectively. The platforms were simple wooden constructions with adjustable feet to enable them to sit flush and level with the sensing platform, eliminating any trip hazards.

The midgait protocol is a commonly used method to measure the natural gait of a subject within a laboratory environment [79]. However, this method requires an 8-10m walkway with the measurement taken at the midpoint of the walkway.

Due to space constraints, the experiments discussed in this chapter used the 'two-step gait initiation' protocol as proposed by Meyers-Rice *et al* [80]. This method proposes a short gait initiation, where the measurement is taken on the subject's second step. They show that although the pressure and force profiles are slightly altered, the two-step method, in comparison with a one-step initiation produces more representative results to that of a midgait measurement.

The gait initiation platform was constructed to an appropriate length, enabling a minimum of two strides before a foot strike on to the measurement plate. In practice, it was found that two or three practice runs was sufficient for the subject to find the optimal start position on the gait initiation platform such that the foot strike on the measurement platform was positioned within the target area. The gait termination platform was constructed to a slightly shorter length, but still allowing two further steps after the second step on the sensing platform. The overall walkway length was 4.30m. Figure 5.2, shows the anticipated step locations when using the walkway.
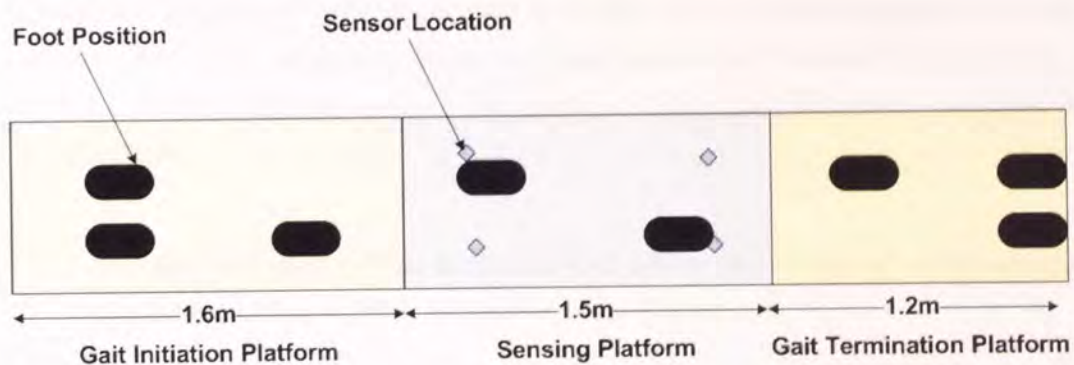
Figure 5.2: *Anticipated foot strike locations.*

The sensing plate had a thickness of 3mm. Using Ansys FEA software (Ansys Inc., PA, USA) a model was generated to assess the potential deflection depth of the plate when in use. The plate was defined by the properties given in Table 5.1.

To determine the optimum sensor operating range, the static plate deflection was

Property	Value
Length	1.42m
Width	0.62m
Thickness	0.003m
Material	Steel
Element Type	Shell93
Mesh (Elements per side)	8

Table 5.1: *Plate properties for FEA model. Note: length and width are adjusted to assume plate is supported by the inner edge of the frame supports.*

calculated for when an 'average' adult male walked over the platform. Ogden *et al* [81] state that an average adult male has a weight of 86kg. Keller *et al* [82] researched into the various ground reaction forces (GRF) generated during walking, jogging and running at different speeds. Their work has shown that the mean GRF generated by an adult male at $1.5ms^{-1}$ is 1.23 times the subject's body weight. Therefore, using the above data and assuming $9.81m/s^{-2}$ for gravity, a 1038N force was applied to the FEA model of the plate. The force was applied in two areas:

1). The approximate location where the first heel strike will occur on the sensing platform (0.23m, 0.26m) as indicated on Figure 5.2.

2). The centre of the plate to determine the maximum plate deflection.

From the simulation, location (1) returned a maximum deflection of 4.7mm. Location (2) returned the overall maximum deflection as 6.0mm.

Therefore, whereas the experiment discussed in Chapter 4 generated only small plate deflections and was required to use the most sensitive operating range of the sensor response curve, the much larger deflections in this experiment required the sensors to be positioned further from the plate surface (approximately 10mm)

with the sensors operating in the asymptotic part of the response curve. The operating range was as shown in Figure 5.3. The second stage amplifier gain was also reduced to unity, ensuring a suitable operating range of between zero and one volt.
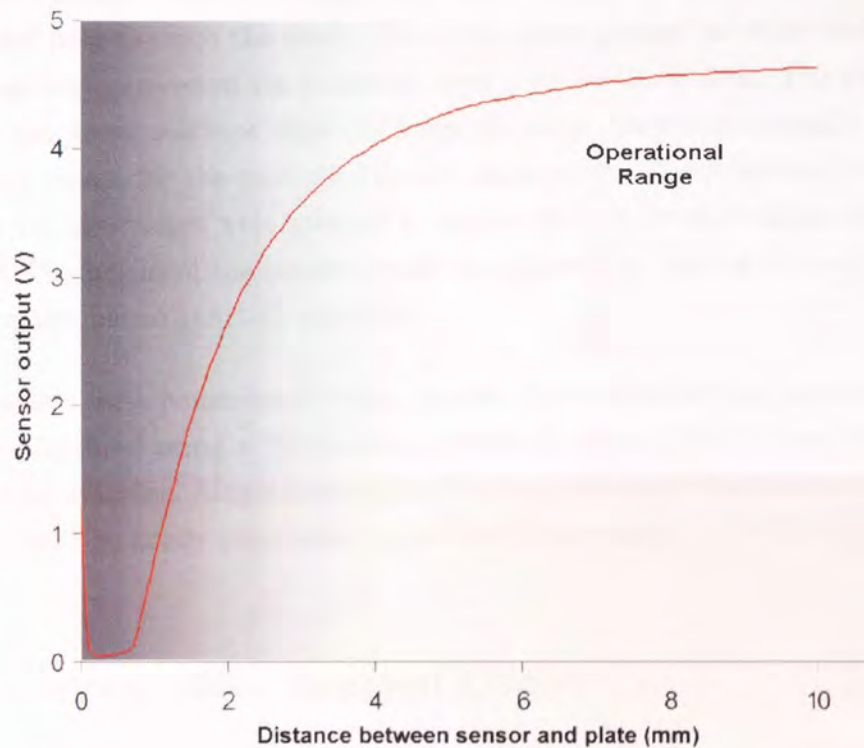
Figure 5.3: *Valid sensor operating range shown by unshaded area.*

5.2.2 Sensor Bracket Design

The sensor brackets used in the experiment discussed in Chapter 4 were found to be difficult to adjust accurately. Ideally, the brackets needed to be finely adjusted in height so that optimum distance between the sensor and the sensing plate could be achieved and therefore operate on an appropriate part of the sensor operating curve. When used in practice, the simple nut and bolt clamping method used in

the original design was found to be fiddly and difficult to make small adjustments with.

A new bracket was designed for this set of experiments. The design was based on a two-piece flanged implementation (see Figure 5.4). The inner piece contained a threaded hole through the shaft. The outer piece housed an Allen bolt. The two pieces were connected via a dovetail type joint on three sides. The tolerance between the joints was kept tight (0.15mm) to ensure there was virtually no free movement except for the controlled height adjustment. The joints and interface between the two pieces were greased to ensure smooth vertical adjustment was possible. The height of the bracket could be adjusted by turning the bolt, which drove the two pieces apart or together.

The brackets were constructed using Accura Si10 photo-setting polymer resin and manufactured using a 3D Systems (South Carolina, USA) Viper Si2 rapid prototyping machine. Magnets were glued into a recession in the base so that the bracket could be firmly positioned on the steel base-plate.

5.2.3   Sensor Offset Removal Circuit

As part of the redesign process, the sensor offset circuit design was revisited. Although the high-pass filter circuit performed well in the previous experiment, it did require a dynamic signal to operate correctly. A signal that remained at a constant amplitude (for example static applications) was subject to droop.

A review of devices available that might improve the circuit design revealed a prototype component available from Maxim Integrated Products Inc. (California, USA). The component (DS4305) was a programmable voltage reference using 'sample and infinite hold' technology. The unique feature of the device was the ability to apply a voltage on the input which, by asserting the adjust pin, was sampled and thereafter continuously output on the output pin. Non-volatile
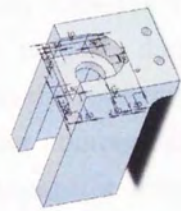
(a) Top part
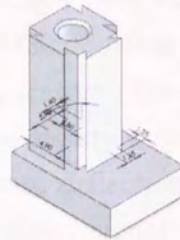
(b) Base part
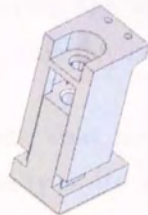
(c) Assembled bracket
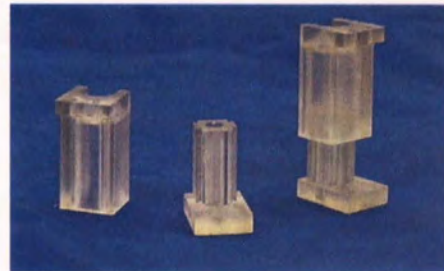
(d) Manufactured parts

Figure 5.4: *The new sensor brackets, design pictures and photo of the manufactured parts.*

memory built in to the device stored the sample voltage level enabling the same voltage to be output after a power-cycle.

The devices came mounted on an evaluation PCB, and hence no further design was required for these devices. A specially designed panel was created using the Viper Si2 rapid prototyping machine to hold upto four of the evaluation boards along with cable routing paths and connectors that enabled the devices to be easily interfaced to the original comparator PCB used for the manual adjustment circuit (see section 4.3.4.1). The sensor offset voltages were sampled during the steady state (i.e. no plate deflection) with the DS4305 devices to provide a continuous output to the reference inputs of the comparators. The sensor signal was used for the other comparator input. During the steady state this would give a theoretical comparator output of zero. Any plate deflections would result in just the relative change in voltage between the sensor signal and the reference signal being output from the comparator. Therefore, this circuit operated in a similar way to the manual adjustment circuit described in section 4.3.4.1. However, rather than having the need to manually adjust potentiometers to zero the comparator output, this device did it automatically, via a push of a button.

It was found however, that the DS4305 struggled to accurately remove the offset voltage, with a steady state output of between zero and 0.2V for each device after sampling the offset voltage. With a signal amplitude of around one volt, this resulted in a significant offset. Also, with the errors varying between devices, this led to problems with neural network training and repeatability of experiments as found in earlier experiments.

After evaluating the above device and the high-pass filter based circuit, it was decided that, for this application the high-pass filter circuit still provided the most stable and accurate offset removal method.

5.3 Dynamic Time Warping

5.3.1 Introduction

It has been shown that a person's gait can be used as a means of biometric identification [83; 84; 85]. However, these methods generally use motion capture or standard video cameras to analyse the whole body movement of the subject. In this experiment, an attempt is made to identify a small group of people using just the deflection data captured by the sensors under the platform. In essence, the experiment is examining the viability of identifying the person from their foot profile as they walk.

To identify a person, the method devised required some form of reference dataset to be able to compare the test data to. Each person would have their own reference dataset. A scoring technique would then be required to determine which reference dataset had the closest match to the test dataset. Closely related applications were investigated. It was found that handwriting or signature recognition had similar requirements for classification. A research of the literature suggests there are several proven techniques for hand writing recognition. These are:

- Dynamic Time Warping (DTW)
- Hidden Markov Models (HMM)
- Neural Networks

Traditionally, the DTW algorithm has successfully been used for handwriting and optical character recognition [65; 86]. However, more recently it has been claimed that generally HMM gives a better classification performance for patterns with a lot of detail [87]. A HMM is a more complex algorithm to develop over DTW however. For this application, the gait profile is of a simpler form than that of a hand written word and therefore it was decided that the DTW algorithm would be investigated as a tool for classifying the gait profile.

Neural networks (NN) have also been found to be an effective classification tool, but usually require the data to be pre-processed using further algorithms such as feature extraction. Neural networks are therefore investigated further in Chapter 6.

5.3.2   An overview of the DTW algorithm

Dynamic Time Warping is a distance measurement algorithm, similar to the Euclidean distance method and can be used to classify a time series. However, the Euclidean distance is known to be sensitive to distortion in the time axis [63]. A time series that is more compressed or elongated in time, in comparison to the template (due to the event happening faster or slower for example) could therefore be misclassified using Euclidean distance.

DTW gets around this problem by enabling the time axis to be warped non-linearly such that the similarity of two signals can be compared even if they are out of phase, or one if signal is more compressed or elongated than the other. The phase difference, compression or elongation can occur at local points on the signal or to the signal as a whole. It can be seen therefore that DTW is a potentially optimal method of classifying a gait profile, which is likely to be subject to changes in width due to the subject walking at different speeds during the test.

Two time series vectors are defined, one representing the template, $\mathbf{T}$ and the other representing the test data to classify, $\mathbf{R}$:

$$\mathbf{R} = \{r_1, r_2, \ldots, r_i, \ldots, r_n\}$$
$$\mathbf{T} = \{t_1, t_2, \ldots, t_j, \ldots, t_m\}$$

An $n \times m$ matrix can now be created where element (i, j) contains the squared distance between r_i and t_j:

$$d(r_i, t_j) = (r_i - t_j)^2$$

We now define a path, $\mathbf{P}$ through the matrix that minimises the cumulative distance between $\mathbf{R}$ and $\mathbf{T}$. $\mathbf{P}$ is defined as:

$$\mathbf{P} = \{p_1, p_2, \ldots, p_k, \ldots, p_K\} \text{ where } max(n, m) \leq K \leq n + m - 1$$

The kth element of $\mathbf{P}$, is a coordinate pair $(i, j)_k$.

The minimum cost path is found using a dynamic programming algorithm. To ensure efficiency of the algorithm, the following constraints must be applied:

1). The warping path must start at the first point of both time series and end at the last point, i.e. $\mathbf{P}(1) = (1, 1)$ and $\mathbf{P}(K) = (n, m)$

2). The path must monotonically increase in time.

A local slope constraint is applied so that each element only has a limited range of predecessors. So, if element p_k is (i, j), then the possible predecessors in $p_{(k-1)}$ are: $(i - 1, j)$, $(i, j - 1)$ or $(i - 1, j - 1)$. This is shown in Figure 5.5.
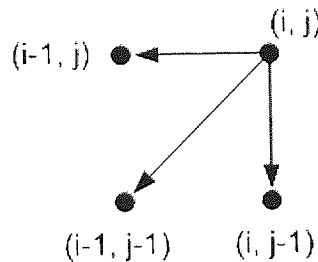
Figure 5.5: *Local slope constraints applied to the DTW algorithm*

In addition to this a global constraint is applied, in the form of the Sakoe-Chiba band [88]. This constrains the path $\mathbf{P}$, such that it remains within the grey area shown in Figure 5.6 and therefore is limited in how far it can diverge from the diagonal. This constraint increases the processing performance of the algorithm and also stops excessive warping of the time scale.
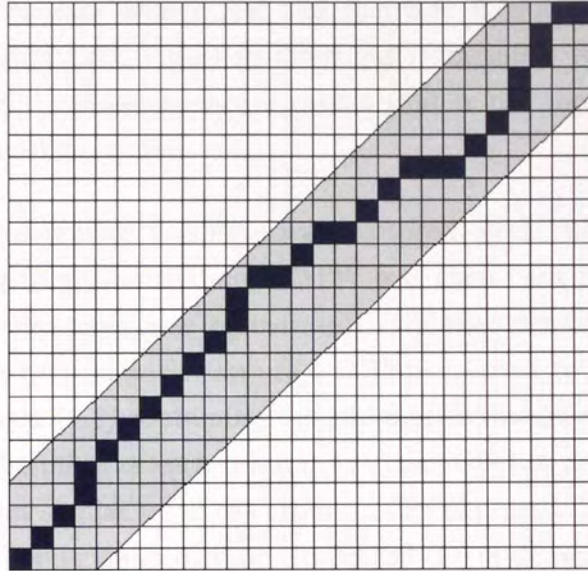
Figure 5.6: *An example of a DTW path constrained by the Sakoe-Chiba band (grey area).*

The minimum cumulative distance, D at element (i, j) can now be defined as:

$$D(i,j) = d(r_i, t_j) + min\{D(i-1, j-1), D(i-1, j), D(i, j-1)\} \qquad (5.1)$$

The total distance is found in the last element, $D(n, m)$.

5.3.3 Template Design

DTW relies on an accurate set of templates to compare the test data to. The template which shows the lowest cost (i.e. cumulative distance) is identified as the class that the test data belongs to. In this experiment, each person involved in the identification test was required to have a template produced and stored for comparison with the test data.

A person's gait can vary widely [55] and therefore it would be unwise to take a single capture and accept that as their gait template. A small stumble or unusual weight shift could produce a profile that is not representative of that person's normal walking style.

To ensure a representative template was captured, each subject was asked to walk over the platform fifteen times. DTW was then used to determine which of the fifteen profiles was most representative of that person's walking profile. A pairwise comparison of each capture was implemented to produce a 15 x 15 matrix with element (i, j) containing the cumulative distance between capture i and capture j. The mean of each column was calculated to determine the profile which was the most similar to all the other profiles captured for that person. The column with the lowest mean distance indicated the most representative profile.

A graphical representation was also produced in the form of a colour-map which helped spot any anomalies in the result, such as a single extreme result that may disproportionately affect the mean value. An example of the colour map is shown in Figure 5.7. Lighter values in the colour map indicate a closer match and in the example shown it can be seen that capture seven is probably an anomalous result due to it being a poor match to any of the other captures.

5.3.4   Method

For this experiment, four sensors were placed under the sensing plate to capture the deflection as the person walked over. The sensors were positioned as shown in Figure 5.2 and labelled using standard compass point notation: NW, NE, SW, SE. The positioning meant that sensors SW and SE primarily captured the first foot strike, while sensors NW and NE captured the second foot strike. It was found that there was very little crosstalk in the sense of the south sensors detecting the second foot strike and the north sensors detecting the first foot strike.

141
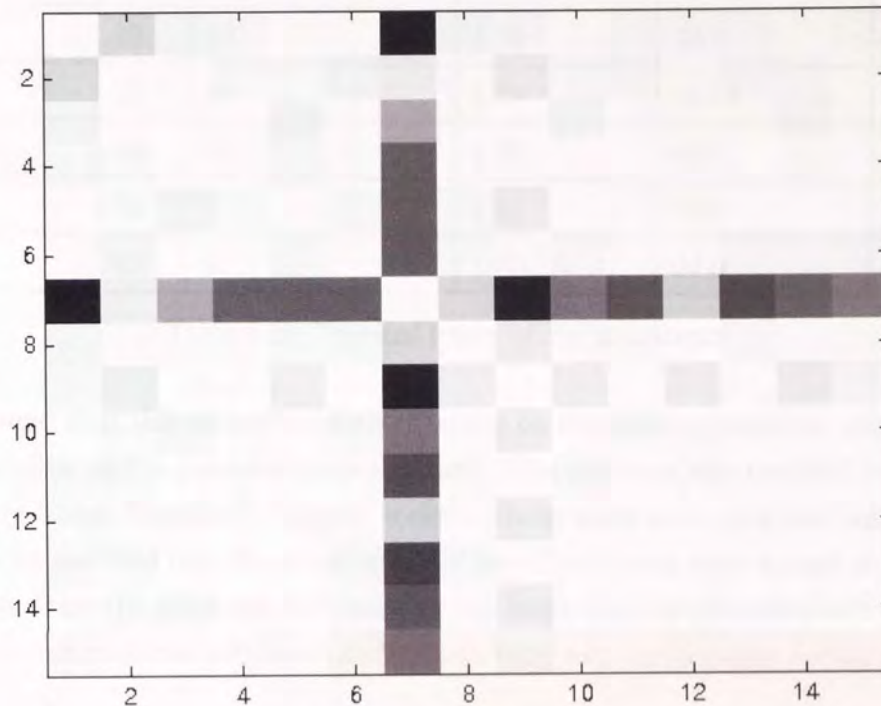
Figure 5.7: *An example colourmap used to determine the best template. The lighter shaded boxes indicate a closer match between the profiles being compared.*

A National Instruments (Texas, US) data acquisition card (DAQ) was used to capture the sensor data. The DAQ had a sampling rate of 100Hz and was interfaced directly to the Matlab environment to enable live testing.

Five volunteers were recruited to test the system. All the volunteers were male and aged between 28 and 40 years of age. The age, height, weight and Body Mass Index (BMI) of each volunteer were recorded and is shown in Table 5.2. None of the volunteers claimed to have any specific walking disorder.

To avoid the system profiling each person due to their shoe type rather than walking style, the volunteers were required to walk in their socks. However, initial

Volunteer	Age	Shoe Size (UK)	Height (m)	Weight (kg)	BMI
A	28	10	1.79	70.8	22.1
B	28	11	1.78	111.5	35.2
C	35	9	1.75	85.3	27.9
D	32	8	1.63	73.0	27.5
E	40	9	1.80	64.0	19.8

Table 5.2: *Physical traits of the volunteers*

tests found that this caused volunteers to slip on the sensing platform, producing poor profiles and a potential safety hazard. The problem was rectified by using a pair of Totes Toasties® 'slipper socks'. These were worn over the volunteers own socks and had non-slip grips on the soles. Crash mats were placed to form a pathway from the platform end, back to the beginning, to provide a soft surface for the comfort of the volunteer and also to bury any surrounding cables present in the area.

For this experiment, a single sensor (SW) was used to capture and compare the first foot strike only. No restriction was placed on whether the left or right foot should strike the plate first, however, a record was kept for analysis if required. The sensor data was captured using the NI data acquisition card and the Matlab Data Acquisition Toolbox. A database was created in Matlab to store the captured profiles from each person. The database enabled easy retrieval of the large amounts of data collected.

Before the DTW algorithm was applied, some conditioning of the captured signals was required. First the signal was low pass filtered to remove any noise. Using Matlab, a 3rd order Butterworth filter was applied with a cut-off frequency of 15Hz.

Secondly, any trailing zeros were removed from the captured data, leaving only the data containing the plate deflection caused by the foot strike. Note, this

Actual	Predicted Class				
Class	A	B	C	D	E
A	10	0	4	3	7
B	0	22	2	0	0
C	0	0	23	1	0
D	0	0	4	11	9
E	0	0	0	7	17

Table 5.3: *Confusion Matrix showing classification accuracies*

meant the conditioned time series vectors were not of equal length. However, the features of DTW allow the different length vectors to be directly compared.

The conditioned signals were then compared using DTW to determine the most representative capture (as described in section 5.3.3). The chosen signal was stored as the template for that person in the database.

5.3.5 Results

A total of 120 test captures were produced, with each volunteer walking over the platform 24 times. The system recorded the prediction for each walk and had an overall classification accuracy of 69.2%. Further investigation is warranted to view the individual accuracies of classifying each volunteer.

Table 5.3 gives the confusion matrix showing the classification performance of the system when tested with the five subjects discussed above. Figure 5.8 shows a misclassification mapping which gives a clearer view of the relationships.

From the results it can be seen that Volunteer A had the worst classification performance with the confusion matrix showing that the system correctly classified A ten times. It falsely classified A as C four times, as D three times and as E
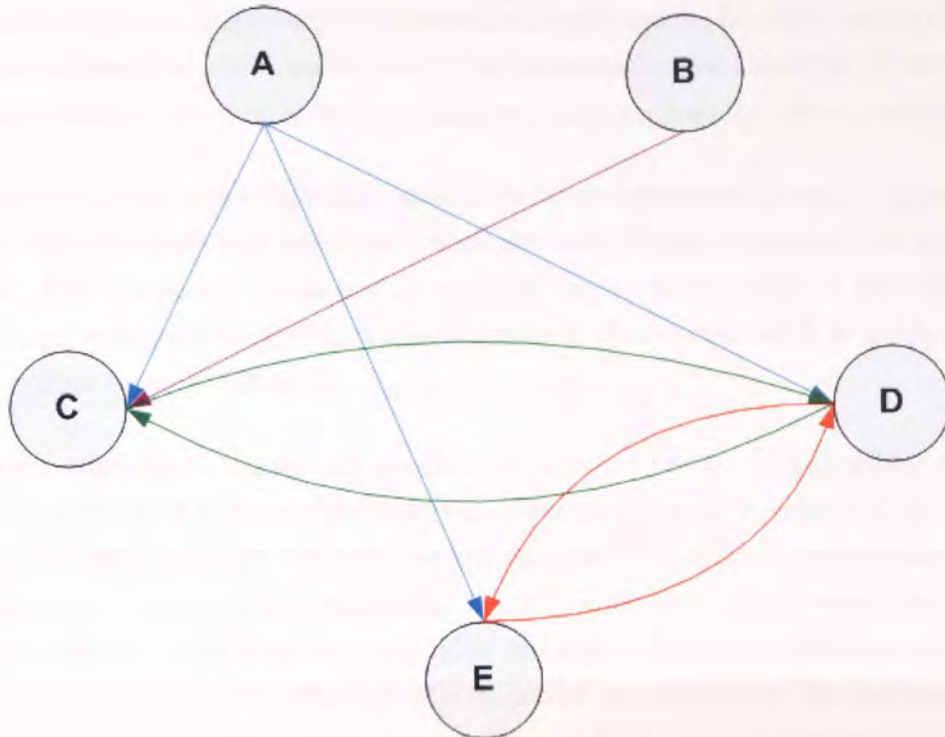
Figure 5.8: *Misclassification mapping. Arrows point from actual class to predicted class.*

seven times. Interestingly, looking at the A column, it can be seen that no other volunteer is ever misclassified as A.

These results suggest that volunteer A had a particularly variable walking style causing them to be misclassified with several other volunteers. The template used for volunteer A must have had considerable differences to those of volunteers C, D and E for there to be no misclassification of those volunteers to A. Overall the underlying issue with A's poor performance is likely to be due to how representative the template was to A's natural walking style. This could be down to a poor choice of template, or down to the variability of A's walking style. Assuming the latter, the method of choosing a single representative template is flawed if that person has a wide variation in their gait. A more robust method of template generation is attempted in Chapter 6.

Volunteer B had a high number of correct classifications. In addition to this, no volunteers were falsely classified as B. One explanation for this level of accuracy could be due to B's weight being significantly higher than the other volunteers.

Figure 5.8 shows a misclassification loop between volunteers D and E (shown in red). This indicates that these two volunteers have similar templates and walking style. This similarity would not be expected upon examination of the physical builds of volunteers D and E. Table 5.2 reveals that volunteer E is much taller and lighter than volunteer D.

Finally, volunteer C shows yet another unexpected result. C has achieved the highest number of correct classifications. However, looking at column C in Table 5.3 shows that three out of the four other volunteers have been misclassified as C at least once. One possible suggestion is that C has many similar walking traits to A, B and D, such that the variations in these volunteer's walking styles has caused misclassifications. This hypothesis would also mean that the high number of correct classifications indicates that volunteer C has a very consistent walking style. An alternative reason for these results is that C's template is the most representative of all the volunteers' walking styles. This means that C has a very generic gait pattern with few unique features, causing the generic shape of the other volunteers' profiles to outweigh the small local differences in the distance calculations.

5.3.6   Discussion

Through a detailed analysis of the classification results it has been possible to make several observations about the DTW algorithm when applied to the application of human gait identification. Some of these observations are contradictory. For example, it could be deduced from the results of volunteer B, that the algorithm depends on the overall amplitude, rather than differences in foot profile shape as the primary classifier. Further analysis showed that normalising the amplitude of the data reduced the classification performance and therefore backed

up this hypothesis. However, the occurrence of the misclassification loop for volunteers D and E in Figure 5.8 contradicts the suggestion due to the physical differences between these subjects.

It has also been found that the method used here can have its accuracy severely reduced if a person using the system has either a significantly variable or generic walking style, as shown by A and C respectively. A variable walking style will limit the classification errors to the person exhibiting those properties only. However, a person exhibiting a generic walking style can cause widespread misclassification errors across subjects.

A possible way to avoid the 'generic walker' problem is to only examine the important localised areas of the profile where differences are likely to occur rather than the shape as a whole. Section 5.4 investigates this feature extraction method. To improve the reliability of classification for volunteers with a variable walking style, a more robust template needs to be generated. Chapter 6, revisits the distance algorithm method and aims to improve the shortcomings identified through the experiments discussed here.

5.4 Feature Extraction

5.4.1 Introduction

In the previous section, the Dynamic Time Warping method was used to compare the overall shape of a person's foot profile as they walked over the surface. The results showed varying levels of success between volunteers. Of the volunteers with high misclassification rates, one was identified as having a high variation in their walking style, therefore being misclassified as several other volunteers. It was suggested that another volunteer (C) had very few unique features in their walking profile, resulting in a generic walking style. This caused other volunteers to be misclassified as C, probably because their overall foot profile always closely matched that of C, reducing the significance of any unique features that volunteer exhibited.

To avoid the problems associated with the previous method, a feature based approach was considered. Feature extraction and analysis involves picking out particular features from a set of data that will aid discrimination of the two classes. The features are combined making up a feature vector that is used for classification.

Feature extraction techniques have applications in a great number of areas. Hand writing recognition was identified in the previous section as an area that has similar datasets to that of the experiments discussed in this chapter. Feature extraction is used extensively in the application of hand writing recognition. Feature sets vary between papers. For example, Huang and Yan use geometric features [89], Verma *et al* used the stroke direction and contour [90], while Pervouchine and Leedham found that examining the features in a grapheme such as 'th' was more effective at identifying the writer than looking at individual letters [91].

In a more closely related application, Huang *et al* use feature extraction techniques in an attempt to identify a person from video image data [92]. Using

canonical space transforms, they reduce the dimensionality of the image data and create classification templates based on a person's gait. A 100% recognition rate was achieved when tested on six volunteers (36 trials).

Feature extraction itself is more of a complimentary method used alongside other common classification techniques such as neural networks. In this section, appropriate features of the foot profiles are investigated and techniques generated to extract those features from the data. Linear discrimination techniques are then used to classify the features extracted from a set of unknown foot profiles in an attempt to identify the volunteer.

5.4.2   Identifying Features

The feature vector had to provide as much information about the gait profile as possible without being overly long (and hence causing slow computation times). The most significant characteristics of the gait profile were the two peaks caused by the heel-strike (HS) and toe-off (TO) events. As in the previous section, the data from the SW sensor was used for analysis. From the data available, the most likely differences occurring between volunteers would be in the size, shape and ratios between the two peaks.

A Matlab based program was written to automatically extract the features from each capture (see Appendix B). The original signal required a comprehensive filtering technique to be applied, to remove noise and ensure that false peak detections did not occur. A moving average (MA) filter was therefore applied to smooth the curve without causing significant distortion to the overall shape. The data was also normalised such that the amplitude was between zero and one. The algorithm developed used peak detection techniques to identify the HS and TO peaks as well as the resulting trough between. The points where the maximum gradients occurred were then identified for each section of the curve joining the peaks and troughs. These values were then used to construct the following feature vector:

g_1, g_2, g_3, g_4	Maximum gradient amplitudes
p_1, p_2, p_3	Peak/trough amplitudes (normalised)
$r_1 = (p_1 - p_2)/p_1$	HS peak : trough ratio
$r_2 = (p_3 - p_2)/p_3$	TO peak : trough ratio
w_1, w_2, w_3	Peak/trough widths

resulting in a twelve element vector, $\mathbf{x} = \{g_1, g_2, g_3, g_4, p_1, p_2, p_3, r_1, r_2, w_1, w_2, w_3\}$.

An example foot profile is shown in Figure 5.9 with the identified peaks, troughs and gradients marked by the algorithm. The derived features described above are also shown.
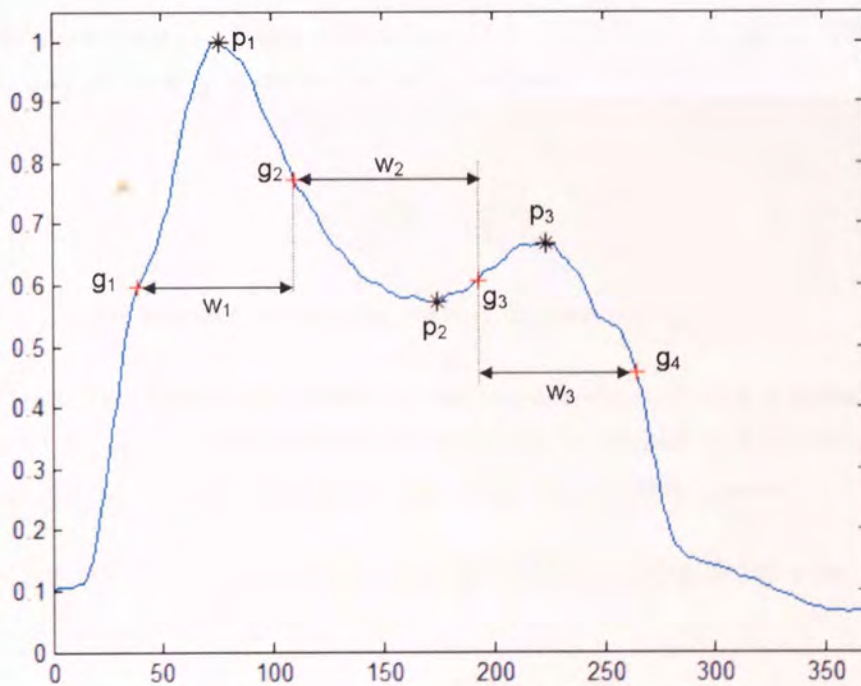
Figure 5.9: *Example profile showing the features extracted.*

5.4.3 Discrimination Analysis

The algorithm developed enabled fast extraction of the described features from a captured dataset. The next stage was to identify an appropriate method that would generate representative templates for each volunteer and also classify newly captured data appropriately.

Simple but very effective algorithms for feature based classification are the Discriminant Analysis methods. The Quadratic Discrimination rule was considered first. This function assumes that the elements of the feature vector are normally distributed and assigns a vector to a class using probability based decision rules [93].

Assume there are C classes defined as $Q = \{q_1, \ldots, q_j, \ldots, q_C\}$. The *a priori* probability of class q_j is defined as $p(q_j)$, where:

$$p(q_j) = \frac{n_j}{\Sigma_j \, n_k} \tag{5.2}$$

where n_j is the number of training vectors in class q_j.

Now define the observation vector $\mathbf{x}$, where each element of $\mathbf{x}$ is a feature of the captured dataset. The requirement is to assign $\mathbf{x}$ to class q_j if the probability of class q_j given $\mathbf{x}$, $p(q_j|\mathbf{x})$ is greatest out of all the possible classes.

The *a posteriori* probabilities, $p(q_j|\mathbf{x})$ can be found using Bayes rule:

$$p\left(q_j|\mathbf{x}\right) = \frac{p\left(\mathbf{x}|q_j\right) p(q_j)}{p\left(\mathbf{x}\right)} \tag{5.3}$$

Since $p(\mathbf{x})$ is independent of class, $\mathbf{x}$ is assigned to class q_j if:

$$p\left(\mathbf{x}|q_j\right) p\left(q_j\right) > p\left(\mathbf{x}|q_k\right) p\left(q_k\right) \qquad k = 1, 2, \ldots, C; k \neq j \tag{5.4}$$

151

Each class, q_j has an associated set of n_j training vectors, $\mathbf{X_j} = \{\mathbf{x_1}, \ldots, \mathbf{x_i}, \ldots, \mathbf{x_{n_j}}\}$. Assuming the class distributions are normal and taken from a sample with mean $\mathbf{\bar{x}}$ and covariance matrix $\mathbf{\hat{\Sigma}_j}$ where:

$$\mathbf{\bar{x}_j} = \frac{1}{n_j} \sum_{m=1}^{n_j} \mathbf{x_m} \tag{5.5}$$

and

$$\mathbf{\hat{\Sigma}_j} = \frac{1}{n_j} \sum_{m=1}^{n_j} (\mathbf{x}_m - \mathbf{\bar{x}_j})(\mathbf{x}_m - \mathbf{\bar{x}_j})^T \tag{5.6}$$

then the 'plug-in' method is used to determine $p(\mathbf{x}|q_j)$ using the sample mean and covariance vectors:

$$p(\mathbf{x}|q_j) = \frac{1}{(2\pi)^{\frac{p}{2}} \left|\mathbf{\hat{\Sigma}_j}\right|^{\frac{1}{2}}} exp \left\{ -\frac{1}{2} (\mathbf{x} - \mathbf{\bar{x}_j})^T \mathbf{\hat{\Sigma}_j^{-1}} (\mathbf{x} - \mathbf{\bar{x}_j}) \right\} \tag{5.7}$$

where p is the number of elements in $\mathbf{x}$.

By substituting (5.7) in to (5.4) and taking logs, then feature vector $\mathbf{x}$ is assigned to class q_j if $\phi_j > \phi_k$, for all $k \neq j$, where:

$$\phi_j = log(p(q_j)) - \frac{1}{2} log\left(\left|\mathbf{\hat{\Sigma}_j}\right|\right) - \frac{1}{2} (\mathbf{x} - \mathbf{\bar{x}_j})^T \mathbf{\hat{\Sigma}_j^{-1}} (\mathbf{x} - \mathbf{\bar{x}_j}) \tag{5.8}$$

For the experiment, $n_j = 10$ training sets were used for each class (volunteer). On calculation of the sample covariances, it was found that the data from two volunteers resulted in their covariance matrices being singular, possibly due to the low sample sizes. To get round this an assumption was made that each class had the same covariance matrix. Therefore, the individual covariance matrices

were replaced by a single, pooled within-class covariance matrix. This is defined as:

$$\mathbf{S_W} = \sum_{j=1}^{C} \frac{n_j}{n} \hat{\Sigma}_j \tag{5.9}$$

From this, the discriminant function (5.8) is now simplified to a linear discriminant function, defined as:

$$\phi_j(\mathbf{x}) = log(p(q_j)) - \frac{1}{2}\bar{\mathbf{x}}_j^T \mathbf{S}_W^{-1} \bar{\mathbf{x}}_j + \mathbf{x}^T \mathbf{S}_W^{-1} \bar{\mathbf{x}}_j \tag{5.10}$$

where n is the total number of training samples used. Again, $\mathbf{x}$ is assigned to class q_j if $\phi_j > \phi_k$ for all $k \neq j$.

5.4.4 Results

A total of thirty five captures were recorded for each volunteer. Ten randomly chosen samples from each volunteer were used to generate the sample mean vectors and the sample covariance matrices. The pooled within-group sample covariance matrix was then generated using equation (5.9). These were stored and used to classify the 125 test captures. To reduce the possibility of the ten randomly samples used for training being misrepresentative, the test was run five times. Each time a new set of ten random training captures were used for each class. The results for each volunteer are shown in Table 5.4, while the confusion matrix for all the tests combined is shown in Table 5.5. Finally, the overall classification accuracy for each volunteer is presented in Table 5.6.

The results show that using this method, the classification accuracy is fairly equal between the volunteers. Only volunteer D has a noticeably lower classification accuracy in comparison to the other volunteers. Overall, when compared to the

Volunteer—Test	Test 1	Test 2	Test 3	Test 4	Test 5
A	23	23	22	23	20
B	22	17	20	21	15
C	18	15	19	24	23
D	14	15	14	13	17
E	21	23	22	20	18

Table 5.4: *Number of correct classifications (out of 25) for each volunteer over five tests.*

Volunteer	A	B	C	D	E
A	111	0	8	3	3
B	5	95	12	13	0
C	4	0	99	22	0
D	23	10	18	79	1
E	7	1	13	0	104

Table 5.5: *Confusion matrix showing classifications between volunteers*

Volunteer	Percentage Correct
A	88.8%
B	76.0%
C	79.2%
D	58.4%
E	83.2%
Overall	77.1%

Table 5.6: *Percentage classification accuracy for each volunteer*

DTW method discussed in section 5.3, this method has yielded an 8% increase in classification accuracy. Interestingly, volunteer A, who was identified as having a highly variable walking style previously, now has the highest overall classification accuracy, with consistently high scores across all five tests. Volunteer C, who was identified as a possible generic walker with few unique features to his walking style has scores which vary widely between tests. It therefore appears that A's results are sensitive to which captures are used for the training data. Volunteer C is still the second highest class to which false classifications have occurred, the highest being D.

5.4.5 Discussion

The results show that using feature extraction with the linear discrimination method has improved the classification accuracy of identifying a person in comparison to the Dynamic Time Warping method discussed in section 5.3. It was hypothesised that less false classifications (due to Volunteer C) would occur since specific features were being examined that should have reduced the 'generic walker' factor. This wasn't the case however and Volunteer C was still subject to many misclassifications with all the other volunteers being misclassified as C several times. On the otherhand, the feature extraction method has potentially improved Volunteer A's accuracy, with that class now showing the highest classification accuracy. It is difficult to say why that is the case, except that maybe despite the variability, some of the extracted features remain relatively constant for this person.

5.5 Conclusion

In this chapter, two well established pattern recognition techniques, Dynamic Time Warping (DTW) and Discrimination Analysis have been applied to the

area of person identification through the measurement of gait. The techniques used enabled classification through both shape matching (DTW) and feature extraction. Reasonable results were achieved through both methods, with the Linear Discrimination method used on extracted features producing a greater classification accuracy of just under 78%. It is recognised however, that the number of classes used in this experiment is small. It would be expected that increasing the number of possible classes would rapidly reduce the accuracy of the system.

It has been hypothesised that two walking styles have been identified which can also have a negative effect on the classification accuracy. First, if a person has a wide variation in their gait, then it is likely that person will achieve a low classification rate, due to the difficulties in producing a representative template. It appeared that linear discrimination was more able to cope with this variation, with volunteer A achieving a much improved classification rate when tested using this method. In this case, the problem is restricted only to those with a variable walking style. The second identified problem style, labelled the Generic Walker style can be present in only one person but affect the classification rate of several other volunteers. In this situation the person has a very generic walking style with few unique features in comparison to other users of the system. This causes other users to be commonly misclassified as the unique features of their own walking template are outweighed by that of the generic walker's. The feature extraction method appeared to have little effect on improving this.

The experiments discussed here indicate further research is required for person identification to be possible through the measurement of a foot profile. It is recommended however, that this method could be successfully used as a complimentary technique alongside one of the many other biometric measurement systems available.

The experiments have also provided a very good foundation for the research to be discussed in the following chapter. This chapter has shown that it is possible to detect small differences in gait and successfully classify the data exclusively

through the measurement of these small differences. The following chapter concentrates on discriminating changes in gait of a single person, due to some external effect. The results and issues identified from the experiments discussed in this chapter are taken into account and improvements to the algorithms are implemented.

Chapter 6

Identifying changes in gait due to some influencing factor

6.1 Introduction

In this chapter, the techniques originally discussed in Chapter 5 are investigated further with the aim of developing a system that can detect a small change in a single person's gait when they are subjected to some influencing factor. In the following experiments, the subject is first required to walk with and without a heavy tray (as shown in Figure 6.1) and then, in the second experiment, with and without a backpack style bag (as shown in Figure 6.2). Both these items are expected to create small but detectable changes in a person's gait due to changes in stance and balance. Being able to detect these small changes provides the basis of applying these methods to a medical environment, such as discriminating between various walking conditions which inhibit a person's normal gait.

Two experiments are undertaken. As in the previous chapter, one experiment uses a feature extraction method to classify the data, whilst the second experiment

returns to using a shape matching algorithm to determine the class.

Figure 6.1: *Using a heavy tray to affect normal walking*
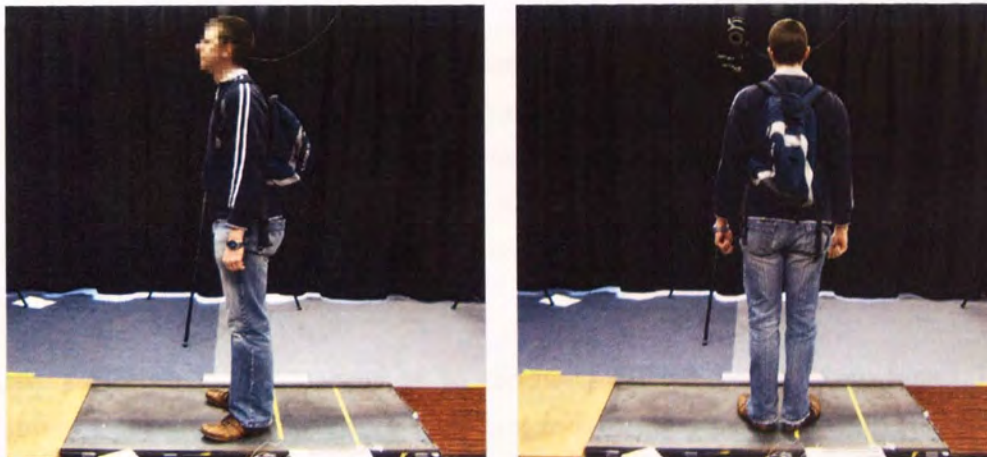
Figure 6.2: *Using a heavy backpack to affect normal walking.*

6.2   Experimental Set up

The majority of the equipment remains unchanged and as described in section
5.2. However, in these experiments the distributive sensing techniques are re-
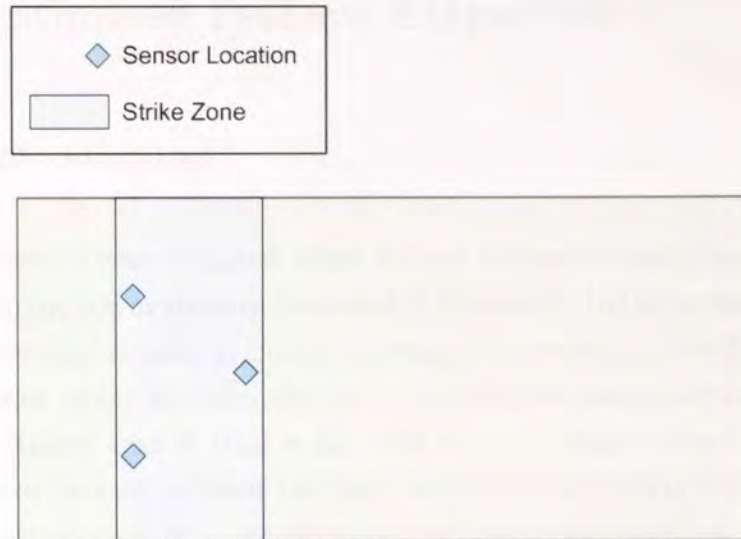
Figure 6.3: *Sensor locations and the 'strike zone'*

introduced using multiple sensors. The sensors were relocated to optimally capture data relating to the plate deflection during the first foot strike on the platform. Figure 6.3 shows the location of the three sensors used. The sensors were placed in a triangular formation so that it would be possible to discriminate differences between the plate deflection occurring to the left and right of the foot strike and also between front and back.

A new 'strike zone' was marked on to the platform measuring 30cm long. The volunteer was requested to ensure their first foot strike occurred within this zone. Note, there were no restrictions on where the foot could land along the width of the plate. Volunteers were given a sufficient number of practice runs to find an appropriate starting point on the gait initiation platform to let their foot land naturally within the strike zone. An additional requirement was to ensure that it was the left foot that landed in the strike zone. No subjects had any problems with determining an appropriate start point so that the requirements were met whilst maintaining a natural walking style. The sensors were located under the strike zone and positioned so that in most cases the foot strike would occur within the triangle formed by the sensors.

6.3 Optimised Feature Extraction

6.3.1 Introduction

Promising results were achieved using feature extraction techniques along with linear discrimination analysis as described in Chapter 5. In this section the feature extraction method is used to identify a change in one person's walking style due to some causal event. In the experiment, the volunteer was required to walk with a tea tray, loaded with a 10kg mass, held by both hands. The volunteer was also requested to walk without the tray, in their natural style, resulting in two possible classifications. It is hypothesised that by carrying the tray, the volunteer was no longer able to swing their arms whilst walking, causing some instability during walking and hence having an effect on the gait profile [67].

6.3.2 Methodology

In this experiment, rather than investigating individual sensor data, the features are extracted from data calculated from the differences between sensors. This results in two separate waveforms for analysis:

{L - R} The difference between the left and right sensors.

{F - B} The difference between the front and back[1] sensors .

A moving average filter is applied to the above waveforms to remove noise and smooth the curve. In addition to this, after removing any trailing zeros before and after the foot strike data, the resulting waveform was normalised in both magnitude *and* time. Time normalisation was achieved, by generating a vector

---

[1] the back deflection magnitude is taken as the mean of the left and right sensors

Feature	Description
$LRpk_1$, $LRpk_2$, $LRpk_3$	Normalised magnitudes of peaks/troughs
$LRratio$	Ratio between first and second peak
$LRgrad_1$, $LRgrad_2$, $LRgrad_3$, $LRgrad_4$	Peak gradients
$LRpc90_1$, $LRpc90_2$	Occurance of 90% peak magnitude in normalised time
$LRpc10_1$, $LRpc10_2$, $LRpc10_3$	Occurance of 10% peak magnitude in normalised time
$FBpk_1$, $FBpk_2$	Normalised magnitudes of peaks/troughs
$FBratio$	Ratio between first and second peak
$FBgrad_1$, $FBgrad_2$, $FBgrad_3$, $FBgrad_4$	Peak gradients
$FBpc90_1$, $FBpc90_2$	Occurance of 90% peak magnitude in normalised time
$FBpc10_1$, $FBpc10_2$, $FBpc10_3$	Occurance of 10% peak magnitude in normalised time

Table 6.1: *Extracted features used to classify data, prefix LR indicates feature extracted from {L-R data}, prefix FB indicates feature extracted from {F-B} data*

on the time interval [0,1] which had the same number of equally spaced elements as the processed waveform.

The second stage involved extracting the features from the processed waveform. The feature vector was made up of a combination of features from the two derived waveforms. In addition, the features extracted were revised slightly from the previous experiment. The new feature vector consisted of twenty five feature elements, listed in Table 6.1. Figures 6.4 and 6.5 show a typical {L-R} and {F-B} waveform respectively, along with some of the associated features.
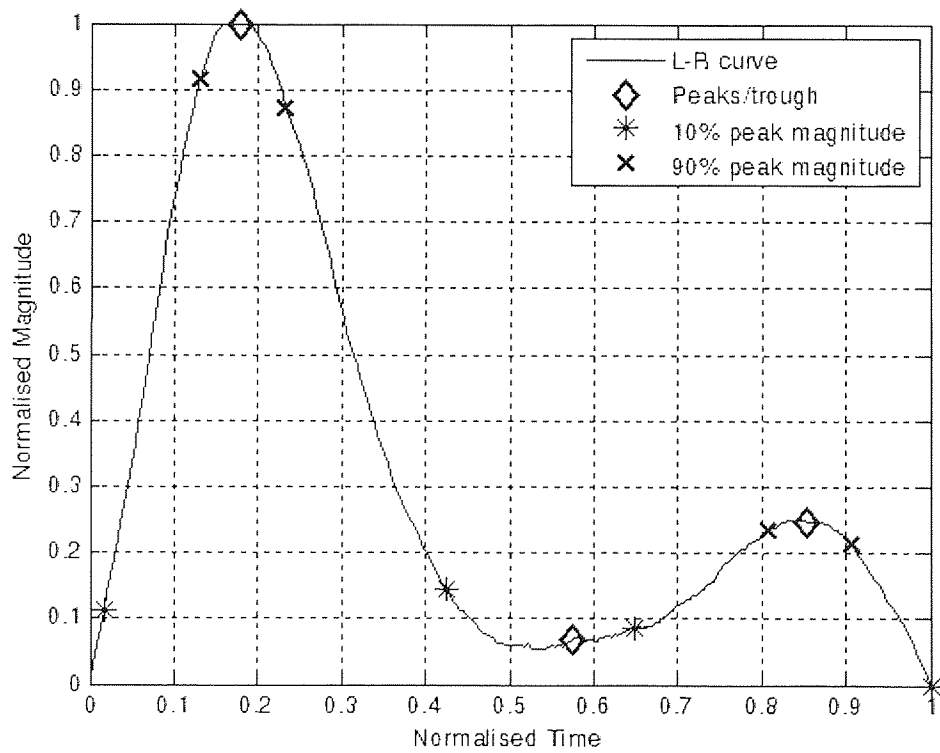
Figure 6.4: *A typical {L-R} curve showing detected features*
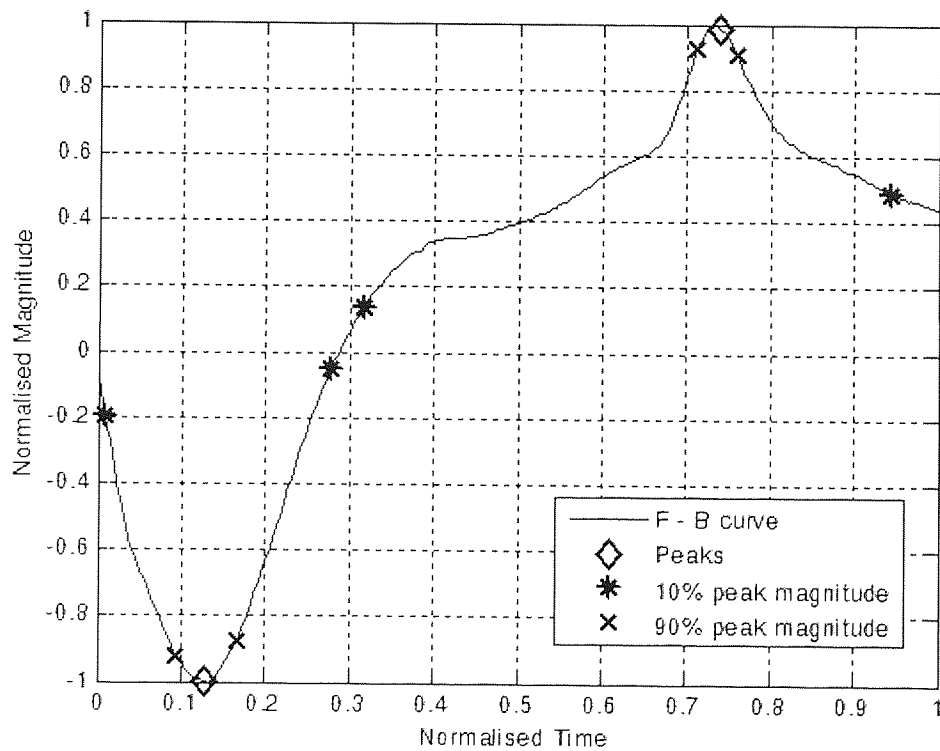
Figure 6.5: *A typical {F-B} curve showing detected features*

	Number of feature vectors	
Class	Training	Test
Natural	43	27
With Tray	45	20

Table 6.2: *Number of feature vectors used for each class in training and testing.*

A total of 135 valid captures were taken, consisting of 70 natural walking captures and 65 walking with a tray captures. The formatting and feature extraction algorithms described above were applied to the captured datasets. A randomised selection method was then used to split the dataset into training and test data. Approximately 65% of the data was used for training, with the remaining 35% used to test the resulting classifer. The number of vectors assigned to each group is shown in Table 6.2.

The linear discrimination algorithm discussed in Chapter 5, was used for this experiment. Using the training vectors, a feature means vector was calculated for each class along with a pooled within-class covariance matrix. All the data was stored as a database style structure using Matlab (see Appendix B).

A Matlab program was written with a GUI front-end to enable live tests to be carried out (see Appendix A and Appendix B). The software was able to display its classification decision to screen within 2-3 seconds of the volunteer walking off the platform. A second script was also written that enabled batch testing of previously captured data.

6.3.3   Optimisation

After initial tests using all twenty five features to classify the captures, optimisation techniques were investigated in an attempt to discover which features contributed most to the classification. Features that contribute little to the clas-

sification decision effectively add noise to the system and therefore, by identifying and removing these redundant features an increase in accuracy is possible.

To find which features made a significant contribution to the classification, the SPPS software package (SPSS Inc., Chicago, Illinois, US) was used to calculate the Wilk's Lambda for each feature using the training dataset. Wilk's Lambda is a measure of the difference in the between-group means for each feature. The smaller the lambda value for a given feature, the more that feature contributes to the discrimination between the two classes. The Wilk's lambda can be transformed to approximate an F distribution to see which features make a significant contribution to the discrimination.

6.3.4 Results

6.3.4.1 Pre-Optimisation

In this experiment, the data can belong to one of two classes; natural walking (class: Natural) or walking with a tray (class: Tray). As shown in Table 6.2, a total of 47 test vectors were used to assess the performance of the classifier. Because of the two possible classifications, binary classifier notation is introduced and used to assess the performance of this system.

Table 6.3, identifies the two possible classes as positive and negative events and relates these to the possible outcome of this experiment. The notation of positive and negative events derives from the common usage of these measurements in medical trials. In this experiment, the aim is to identify when the person is carrying a tray. Therefore, for notation's sake, the event where the person carries the tray will be identified as positive, whilst the negative event is defined as the person walking naturally. Hence, a True Negative event occurs when the classifier correctly identifies the person walking naturally.

166

Outcome	Label	Event
True Positive	TP	Tray class correctly identified
True Negative	TN	Natural class correctly identified
False Positive	FP	Natural class incorrectly identified as Tray
False Negative	FN	Tray class incorrectly identified as Natural

Table 6.3: *Possible outcomes using binary classifier notation as applied to this experiment*

Actual Class	Predicted Class	
	Natural	Tray
Natural	22	5
Tray	3	17

Table 6.4: *Contingency table showing classification accuracy*

The classifier performance can now be presented as a contingency table shown in Table 6.4.

Using this table, it is now possible to calculate the specificity and sensitivity of the classifier. Specificity is a measure of how accurate the classifier is at identifying a True Negative result and is calculated in equation 6.1.

$$Sp = \frac{TN}{TN + FP} \tag{6.1}$$

Sensitivity is a measure of how accurate the classifier is at identifying a True Positive result and is calculated using equation 6.2.

$$Se = \frac{TP}{TP + FN} \tag{6.2}$$

The results achieved show that the sensitivity of this classifier is 0.85. The speci-

ficity is 0.82. In this case, the classifier appears to be well balanced, with the sensitivity and specificity both having similar and high values (the maximum sensitivity/specificity is one, indicating perfect classification). Large variations between the two values indicates the classifier is more biased to choosing a particular class. In certain situations this can be useful, for example where the classifier is detecting an illness, it may be preferred that the system had a high sensitivity over specificity in order to minimise the number of people who have the illness being falsely classified as not ill.

Related measures of accuracy are the Positive Predictive Value (PPV) and Negative Predictive Value (NPV). In this experiment, PPV states the probability of the person carrying the tray when the system states they are. Similarly, NPV states the probability that the person is walking naturally when the system states that is the case. $PPV = TP/(TP + FP)$ and is found to be equal to 0.82 for this experiment. $NPV = TN/(TN + FN) = 0.84$. Note, that unlike sensitivity and specificity, PPV and NPV are affected by the number of vectors present in each class. Therefore, despite the classifier being more sensitive, the NPV is found to be higher than the PPV. A contributing factor to this result is the difference between the test data class sizes. A clear, graphical approach to sensitivity, specificity and predictive values is provided by Loong [94].

The overall accuracy of the system (the number of correct classifications out of the total number of tests) was found to be 83.0%.

6.3.4.2 Optimising the Feature Vector

Using the Wilks Lambda statistic transformed to the F distribution, each of the 25 features were analysed using the training set to see which ones provide a significant ($p < 0.1$) contribution to the classification. The Wilks Lambda, F and confidence level for each feature is shown in Table 6.5.

The results show that of the original 25 features, ten have been found to make a

Feature	Wilk's Lambda	F	df1	df2	Significance
$LRpk_1$	0.994	0.505	1	86	0.479
$LRpk_2$	0.998	0.196	1	86	0.659
$LRpk_3$	1.000	0.010	1	86	0.920
$LRratio$	0.999	0.091	1	86	0.764
$LRgrad_1$	0.996	0.360	1	86	0.550
$LRgrad_2$	1.000	0.004	1	86	0.949
$LRgrad_3$	**0.957**	**3.905**	**1**	**86**	**0.051**
$LRgrad_4$	0.997	0.290	1	86	0.592
$LRpc90_1$	0.973	2.371	1	86	0.127
$LRpc90_2$	1.000	0.002	1	86	0.963
$LRpc10_1$	0.985	1.329	1	86	0.252
$LRpc10_2$	0.977	1.990	1	86	0.162
$LRpc10_3$	0.999	0.094	1	86	0.759
$FBpk_1$	**0.895**	**10.066**	**1**	**86**	**0.002**
$FBpk_2$	1.000	0.026	1	86	0.871
$FBratio$	**0.894**	**10.201**	**1**	**86**	**0.002**
$FBgrad_1$	**0.923**	**7.214**	**1**	**86**	**0.009**
$FBgrad_2$	0.984	1.424	1	86	0.236
$FBgrad_3$	**0.908**	**8.715**	**1**	**86**	**0.004**
$FBgrad_4$	**0.888**	**10.844**	**1**	**86**	**0.001**
$FBpc90_1$	0.995	0.409	1	86	0.524
$FBpc90_2$	**0.951**	**4.384**	**1**	**86**	**0.039**
$FBpc10_1$	**0.941**	**5.357**	**1**	**86**	**0.023**
$FBpc10_2$	**0.922**	**7.242**	**1**	**86**	**0.009**
$FBpc10_3$	**0.866**	**13.358**	**1**	**86**	**0.000**

Table 6.5: *Wilk's Lambda, F statistic and significance for each feature. Emboldened entries show significant ($p < 0.1$) features.*

Actual Class	Predicted Class	
	Natural	Tray
Natural	23	4
Tray	5	15

Table 6.6: *Contingency table showing classification accuracy after optimisation*

Sensitivity	0.75
Specificity	0.85
PPV	0.79
NPV	0.82
Overall	80.9%

Table 6.7: *Classifier performance results for optimised feature set*

significant contribution to the discriminatory power of the classifier. It's interesting to note that all but one of the significant features is taken from the {F-B} curve. Therefore, it is suggested that while walking with a tray has little effect on the side-to-side sway of the person, there are differences in the distribution of weight when going from the heel strike towards the toe-off position, when compared to natural walking. Closer examination shows the differences occurring in the first peak magnitude, the ratio between the peaks, the gradients and the peak widths (determined by the 10% and 90% values) in the {F-B} curve.

6.3.4.3 Post-Optimisation

Using the same data as previously for training and testing, the linear discrimination algorithm was run again using just the ten optimised features. The results are displayed as a contingency table in Table 6.6. The sensitivity, specificity, PPV and NPV values are presented in Table 6.7.

Contrary to the expected outcome, the optimisation process in this case has

170

Actual	Predicted Class	
Class	Natural	Tray
Natural	16	9
Tray	20	5

Table 6.8: *Contingency table showing classification accuracy from live tests*

reduced the performance of the classifier. Although there has been a slight improvement in the ability to classify natural walking, the sensitivity of the system and hence the ability to identify the Tray class has reduced considerably. Similarly, there has been a slight reduction in both the PPV and NPV. Therefore, although statistically only the identified ten features made a significant contribution, the overall smaller contribution made by some or all of the other features were important in discriminating the two classes.

6.3.4.4 Live Tests

The real-time software was also tested on live captures, with the volunteer walking over the platform fifty times; twenty five times with the tray, twenty five without. The live test used the same training data and hence, mean vector and covariance matrix as that discussed in the results above. The tests used the full twenty five element feature vector rather than the optimised vector as the results showed this provided better discrimination between the two classes. The results are shown in Tables 6.8 and 6.9.

The live tests produced a considerably lower classification accuracy than that shown in offline testing. As time was the only variable that differed from the offline testing (the live test was carried out several days after the original data was captured), then it may be assumed that lower accuracy is down to repeatability problems in the system. However, it is equally possible that there may be a psychological factor involved. The volunteer was aware that the system was being

Sensitivity	0.20
Specificity	0.64
PPV	0.23
NPV	0.62
Overall	42%

Table 6.9: *Classifier performance results for live tests*

tested at this stage and therefore a willingness for the system to perform could affect the natural gait of the person as they become conscious of their actions.

6.3.5 Discussion

This section has discussed the experiments undertaken in an attempt to detect small differences in gait occurring when the volunteer is subjected to some external effect. In this case, the volunteer was requested to walk over the platform whilst carrying a tea tray containing a 10kg mass. The volunteer was also asked to walk naturally over the platform without the tray. Feature extraction techniques along with the linear discrimination method were used to classify the captured gait profiles into either the Tray or Natural class.

The results indicate varying degrees of success. Initial offline testing using the full twenty five feature vector was found to have a good overall performance, with it correctly classifying 83% of the test data. Additionally, measuring sensitivity and specificity indicated that the system was well balanced with both these values at a similarly high level.

Optimisation techniques in the form of Wilk's Lambda were then used in an attempt to improve the classifier performance by removing features that weren't making a significant contribution to the classification. Wilk's Lambda transformed on to an F distribution indicated that only ten of the features were making

a significant ($p < 0.1$) contribution to the discriminatory power of the classifier, with all but one of these being features of the {F - B} curve. Unfortunately, the results of the optimisation technique were disappointing with the sensitivity of the system dropping considerably, while the specificity only rose marginally. This suggested that the overall effect of the features that made little individual contribution made a significant contribution to the discriminatory power. Other optimisation techniques that could be introduced in future experiments could include analysing the correlation between the features and removing any features that are found to be highly correlated, hence providing no unique contribution to the classification.

The final experiment involved carrying out a set of live tests. The full, twenty five feature vector was used due to it producing the best performance in offline testing. It was expected that the live test results would be similar to those achieved in offline testing. However, although the set up was identical (the offline test data was captured using the same setup and used the same training data), the results achieved were considerably worse than those achieved in offline testing, with the live tests only achieving an overall classification accuracy of 42%. This could be due to repeatability problems. However, improvements made to the platform for these experiments and a robust, low drift electronics design would make this unlikely. Therefore, it is suggested that problems may have occurred due to the volunteer being aware of the testing process and become conscious of their walking style, possibly trying to enhance the difference between their natural walk and that when carrying the tray, but on the contrary, making them worse.

Overall, the feature extraction used with linear discrimination, appeared to work well. Although, some experimental flaws were identified it would appear that small improvements could provide a robust classification method. The LDA algorithm itself was found to be a simple but effective method in discriminating the features between classes. There are disadvantages with using LDA, namely that it can only successfully classify data that is linearly separable. For the person identification experiment, a pooled within-groups covariance matrix had to be used due to some of the separate covariance matrices being singular. This can re-

duce the classification performance slightly, although with this experiment, both methods were compared with no significant difference found between the results.

The biggest challenge of this experiment was developing a flexible feature extraction algorithm. The algorithms developed used various methods to detect peaks and troughs in the signal and measure specific gradients or points on the curve related to those peaks. This system works fine if the overall shape of the curve is the same for both classes with the differences appearing in the gradients, peak amplitudes and widths etc. However, for the tray walk experiment, although the features extracted did provide a good level of discrimination, it was noted that generally the {L - R} curve produced when walking with a tray was a different shape to that of natural walking and had an extra peak present just before the heel strike peak occurred. The rigidity of feature extraction method meant that this would either go unnoticed or even cause errors in the extraction algorithm. This meant that unique features of the curve only present due to tray walking were unable to be used, as the algorithm could only measure differences in the features present in *both* classes. Although this could be remedied, one of the thesis aims is to develop a method that can be generalised to other (as yet unknown) effects on a person's gait. The feature extraction method is very much limited in its generalisability as the developer needs to know which features to look for and compare.

In the final chapter, the shape classification method is revisited. Using the results and observations found in the previous experiments, a much more robust and generalisable method is developed for detecting small changes in gait.

6.4 Normalised Distance Method

6.4.1 Introduction

In the first Person Identification experiment (section 5.3) a distance measurement algorithm was used in the form of Dynamic Time Warping (DTW). The DTW algorithm provided an added feature, in that the time axis could be 'warped' and therefore the data could be matched to a template regardless of local or global differences in the width (i.e. time duration) of the profile. This method gave promising results, but had flaws particularly in the technique used to define a template for each person. The template was chosen from a training set by in-dentifying the most representative template out of those available. This method generated poor results for those people with widely varying walking styles. It was also observed from the feature extraction methods applied, that an affected walk-ing profile may exhibit changes in the peak and trough widths. Using DTW would effectively filter out those features due to the time warping principle, therefore potentially losing important information from the captured profile.

In this final experiment, the distance algorithm is revisited in an attempt to iden-tify and classify small changes in gait based on the overall shape of the captured gait profile, rather than the fixed features. To overcome previous flaws and lim-itations, a more robust template generation method is suggested along with a simple, but effective distance calculation. The captured profile is normalised in both time and amplitude to enable direct comparison of the overall shape, in-cluding differences in peak and trough widths. Neural network methods are also introduced in an attempt to couple the three sensor outputs which are likely to have a non-linear relationship.

6.4.2   Experimental Setup

In this experiment the hardware set up remained identical. However, in the previous experiment, the volunteer found that carrying the tray for a long period of time caused discomfort. Therefore, in this experiment the influencing factor is changed to the wearing of a backpack containing a 10kg mass inside. The bag was padded in the area which had contact with the person's back and also had padded straps. This was found to provide an acceptable level of comfort during the trials. The volunteer was required to wear the bag using both straps and also used a waist strap to provide a secure fit. The bag was put on and removed using a table provided at waist height, to reduce the need for any excessive bending. The two classes were redefined as Natural for natural walking and Backpack for walking whilst wearing the backpack.

A new piece of software was written using MATLAB (see Appendix B). A GUI was designed, this time enabling the user to select whether the capture was to be used for training, validation (offline testing) or test. The data was then automatically structured into a database ready for processing. Screenshots are shown in Appendix A.

6.4.3   Method

6.4.3.1   Template

The main flaw with the original distance calculation algorithm was in the template design. In the person identification experiment, the template was selected from a sample of training data based on how representative it was to the other captures within the training set. This was based on the mean DTW distance as described in section 5.3. In this experiment a template is generated which is based on all the captures within the training set. Also, a specific template was created for each of the sensors, so a single training capture would consist of three vectors.

Each vector was filtered using a moving average filter to remove noise and smooth the curve. The amplitude was then normalised between zero and one for each vector. Time was also normalised to a value between zero and one. However, this time each vector had to be of equal length. Therefore, it was decided that each capture would be mapped on to an $m = 200$ element vector over the time interval $[0, 1]$. Two hundred was chosen as it was found that the length of the extracted foot profile would in the majority of cases be over 200 samples long (but usually less than 300). Any captures found to be less than two hundred samples long in the experiment were discarded. Given n training captures, the resulting dataset was three sets of $n \times m$ matrices. Based on the n training captures, the mean of each of the 200 elements was calculated to produce a mean vector:

$$\bar{\mathbf{x}} = \{\bar{x}_1, \bar{x}_2, \ldots, \bar{x}_k, \ldots, \bar{x}_m\} \tag{6.3}$$

where:

$$\bar{x}_k = \frac{1}{n} \sum_{i=1}^{n} t_{i,k} \tag{6.4}$$

and, given the jth training capture vector, $\mathbf{T_j} = \{t_{j,1}, t_{j,2}, \ldots, t_{j,k}, \ldots, t_{j,m}\}$ $j = 1, 2, \ldots, n$.

Similarly, a vector of standard deviations was also generated:

$$\hat{\sigma} = \{\sigma_1, \sigma_2, \ldots, \sigma_k, \ldots, \sigma_m\} \tag{6.5}$$

A mean ($\bar{\mathbf{x}}$) and standard deviation ($\hat{\sigma}$) vector was generated for each of the three sensors. The mean vector was used as the template for that class and is a representation of all the training captures. In addition to this, the standard deviation (s.d) vector is added and subtracted from the mean vector to produce a 'soft' boundary above and below the template curve. Figures 6.6 to 6.8 show
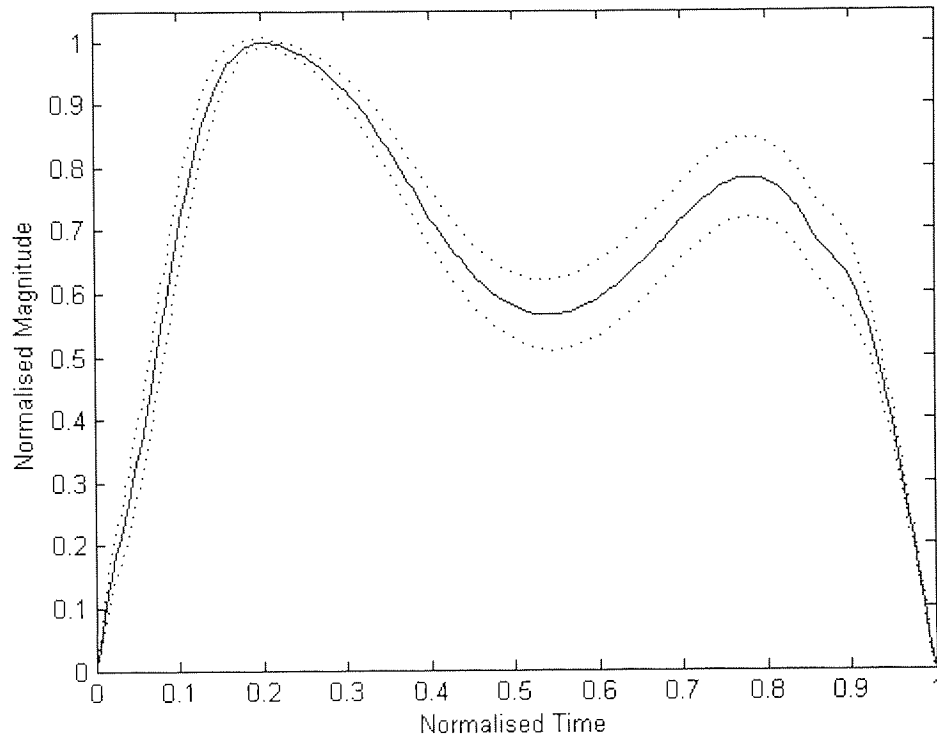
Figure 6.6: *Typical Left sensor template. Solid line is mean of all samples. Dotted line is mean ± 1 s.d of all samples.*

typical Left, Right and Front sensor templates for when the volunteer is wearing the backpack. These plots give a visual representation of how much variance there is in the walking style for different parts of the profile (it should be noted however, that normalisation distorts the s.d curves at the extreme points of the plot).

6.4.4   Distance Calculation

It was decided that time warping was no longer required due to the normalisation and mapping of the time axes to a fixed 200 sample vector between zero and one,
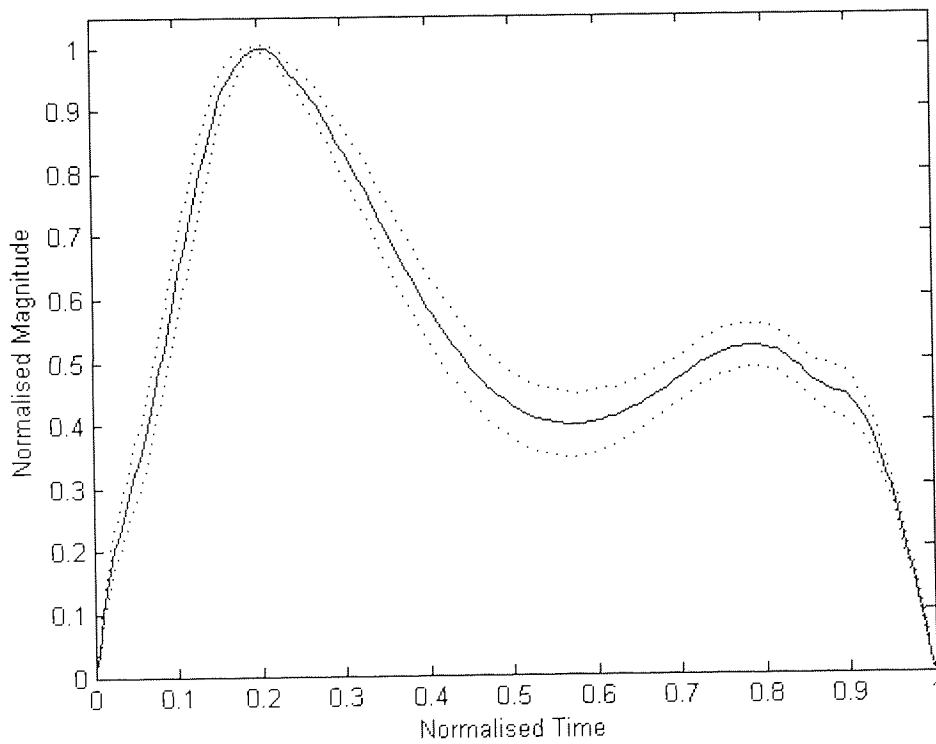
Figure 6.7: *Typical Right sensor template. Solid line is mean of all samples. Dotted line is mean ±1 s.d of all samples.*
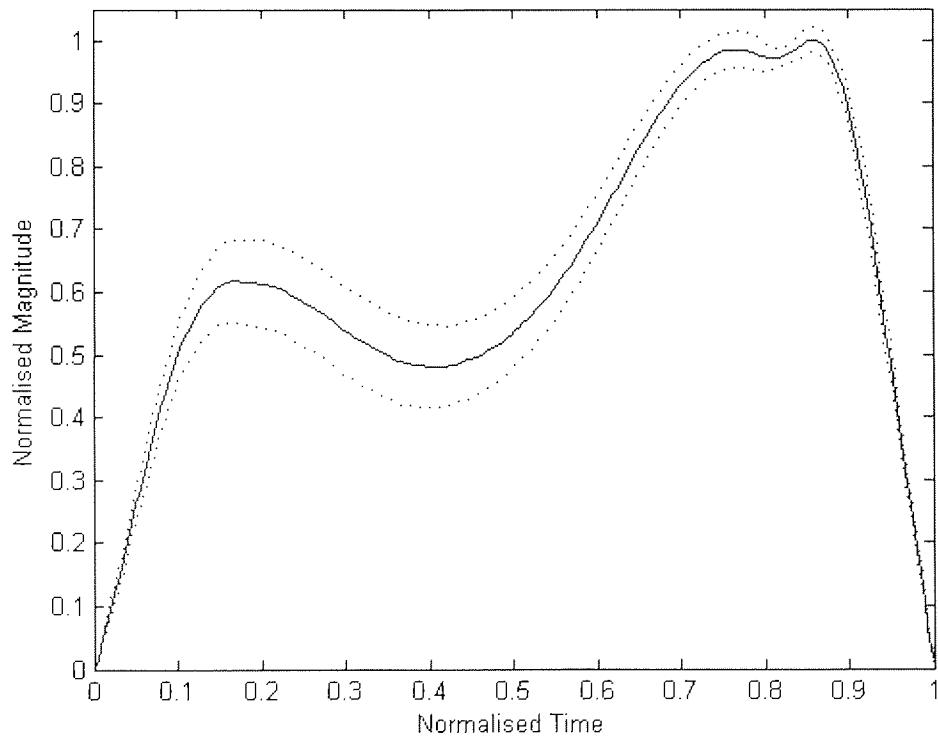
Figure 6.8: *Typical Front sensor template. Solid line is mean of all samples. Dotted line is mean ±1 s.d of all samples.*

enabling direct sample to sample comparisons to be made.

The captured data used for test, **R** was processed the same way as that of the template data. The absolute distance between each sample in the test data vector and the corresponding sample in the template vector was calculated and divided by the standard deviation for that sample, as shown in equation 6.6. By dividing by the standard deviation, the variation in a person's walking style is taken in to account, hence weighting the distance score to that template appropriately.

$$d_k = \frac{|r_k - \bar{x}_k|}{\sigma_k} \quad k = 1, 2, \ldots, m. \tag{6.6}$$

Each comparison of the test data to a template produces an overall cost value, defined as the mean value of the distances defined in (6.6) as follows:

$$C^R = \frac{1}{m} \sum_{k=1}^{m} d_k \tag{6.7}$$

Finally, the captured data and the mean vector are both differentiated. The two resulting curves are compared in the same way as the time based data producing another cost value, C^{dR}, defined in 6.8.

$$C^{dR} = \frac{1}{m-1} \sum_{k=1}^{m-1} \frac{|\delta r_k - \delta \bar{x}_k|}{\delta \sigma_k} \tag{6.8}$$

This effectively compares the gradients of the capture with that of the template and was found to produce an increase in accuracy. The resulting overall cost C is calculated as:

$$C = C^R \cdot C^{dR} \tag{6.9}$$

The cost C, was calculated for each of the three sensors and originally, for each class (Natural or Backpack) such that the data was assigned to the class which had the lowest sum of three costs. However, disappointing results led to further investigation. Kohle and Merkl [55] suggest that the number of degrees of freedom is a direct cause of the variability in walking and therefore, unrestricted, natural walking is likely to show the most variable profile in contrast to someone with a walking disorder. This suggestion led to the Natural walking template to be dropped as it would seem likely to prove hard to define a definitive template for natural walking. Instead, only the affected walking class, i.e. the Backpack class, had a template.

6.4.5 Neural Network

Using the above method meant the system then required some form of threshold level between the classes. If the distance scores from the three sensors were found to be less than the threshold, then they would be assigned to the Backpack class, otherwise they would be assigned to the Natural class. It would be possible to define a simple linear threshold for each sensor, however, this approach was too simplistic. It was likely that the boundary between the classes would be non-linear in this case and hence a neural network was introduced to the system. Using a neural network provided the system with the ability to:

Define a non-linear boundary between the two classes. For this experiment, it was likely that the relationship between the sensors and the distance thresholds between the two classes was non-linear. Neural networks were able to define non-linear relationships between the inputs and outputs and therefore provided a better a classification accuracy than using a linear method.

Determine a coupled relationship between the three sensors. Rather than investigate the sensor outputs individually, the distributive sensing method was used in this experiment to consider the three sensor outputs together. Using

a neural network, enabled the system to identify complex coupled relationships between the sensors and relate them to the classes.

Remove the dependency on where the foot strikes. One of the non-linear relationships mentioned above was likely to be due to the position of the foot strike on the plate. Ideally, it was hoped that no further restriction was required on where the foot landed within the strike zone. The neural network was therefore used to identify how the cost values from the three sensor outputs changed with respect to each other when the foot landed in different places within the strike zone.

A feedforward multi-layer perceptron (MLP) using back propagation was identified as the network architecture that produced the highest classification accuracy. Radial Basis Function networks were also investigated, but gave inferior results in comparison. The network architecture consisted of three input nodes, a single hidden layer (number of nodes defined below) and a single output node. As this was a classification network, a log-sigmoid transfer function was used both on the hidden layer and output layer nodes.

A summary of the neural network implementation is shown in Table 6.10.

6.4.5.1   Training

Training data was generated by capturing repeated walking trials, both with and without the backpack. First, 50 walking trials with a backpack were captured and stored. This data was used purely to generate the 'affected walking' templates for each sensor as described in section 6.4.3.1. Following this, another 100 walking trials were captured, 50 with a backpack and 50 without. These captures were each compared to the template to generate an associated set of three cost values as described in section 6.4.4. This dataset was used to train the neural network, with each training vector consisting of three cost values in the range [0,1] as inputs

and a class value as the associated output (binary output: zero for natural, one for backpack).

Both Bayesian Regularisation (BR) and Early Stopping (ES) training methods were investigated for this experiment. The BR function in Matlab was stated to be optimised for function fitting networks rather than those with pattern recognition [95]. Therefore, both BR and ES methods were investigated to see which gave the best results.

Using offline testing, ten trials were carried out. For this comparison, a total of 150 captures were used. Using the stored 100 neural network training vectors, 70 were used for training, 30 for validation (early stopping only). For testing, the 50 stored template vectors were used. The 50 test captures remained the same for each trial, whilst the training and validation sets were picked randomly from the group of 100 available vectors. Table 6.11 shows the number of misclassification errors for each training method. The results clearly show that the BR method was much more reliable and accurate than the ES method, which produced highly variable results. The BR method produced less misclassification errors in all but one of the tests and was therefore chosen as the training method for the network implemented in this experiment.

6.4.5.2   Hidden Nodes

The final stage of the neural network design was to determine the optimum number of hidden nodes. As there is no specific way of determining this, the offline data was used to train and test a network with between 2 and 26 hidden nodes, increasing in steps of two. The number of hidden nodes chosen is the one showing the lowest number of misclassification errors. Figure 6.9 shows a bar chart with the mean number of errors after ten trials against the number of hidden nodes and indicates that two hidden nodes is the optimum number.
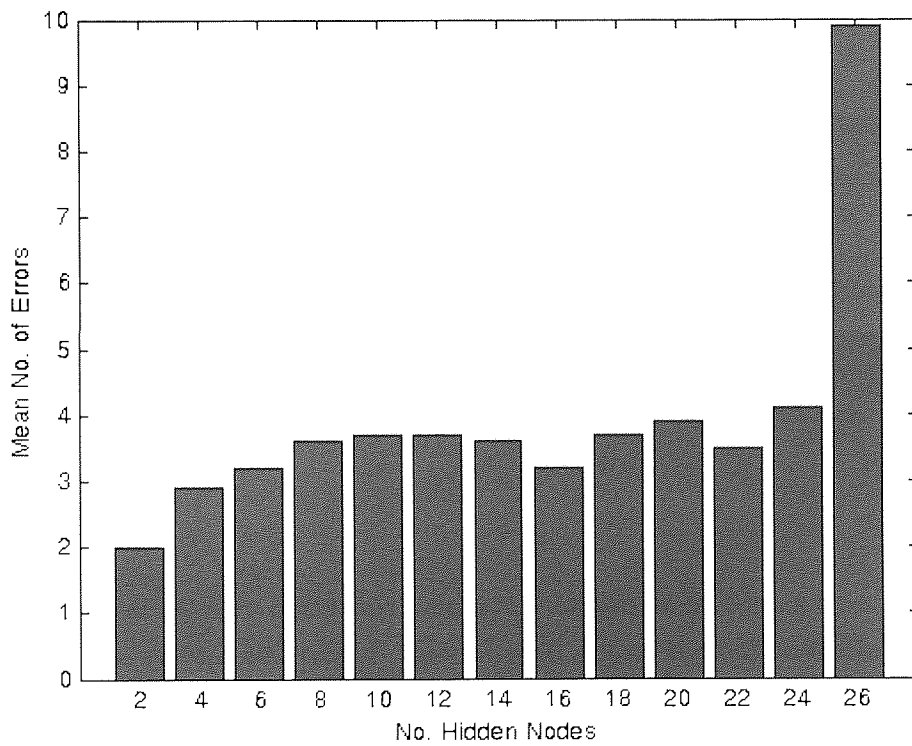
Figure 6.9: *Mean number of errors after ten trials vs number of hidden nodes*

Network type	Multi-Layer Perceptron (MLP)
Training method	Back Propagation with Bayesian Regularisation
Hidden node $f(x)$	log-sigmoid
Output node $f(x)$	log-sigmoid
No. of input nodes	3
No. of hidden nodes	2
No. of output nodes	1
Input data	Three 'cost' values calculated from distance between template and captured sensor data (see 6.4.4)
Output data	Discrete value, representing the classification. Natural: 0, Affected: 1

Table 6.10: *Summary of the neural network implementation*

6.4.6 Results

With the neural network optimised, and a representative Backpack class template generated, the system was tested. As indicated above, the offline testing showed very promising results with only two misclassifications out of a total of fifty unseen trials. However, previous experiments tended to show that offline testing produced more optimistic results than when tested live. Several live tests were carried out for this experiment. It should be noted that due to the randomised start weights of the neural network, the network was trained differently each time. Therefore, several training attempts were required before a well balanced network was produced. Initial results were unbalanced, with some showing good classification for the Backpack class, but poor for the Natural (Backpack: 100%, Natural:48%) and others vice-versa (Backpack: 57%, Natural: 88%). Hanson and Salamon [96] originally stated that using multiple neural networks in parallel

Trial	Early Stopping	Bayesian Regularisation
1	42	5
2	9	12
3	14	2
4	13	4
5	5	3
6	6	4
7	28	4
8	25	4
9	11	5
10	5	3

Table 6.11: *Number of misclassification errors when using Early Stopping training compared to Bayesian Regularisation*

(referred to as a neural network ensemble) could increase the overall classification accuracy of the system. However, experimentation with this suggestion did not provide a significant improvement in results. The following results were produced from the multi-layer perceptron neural network after optimisation, using two hidden nodes and Bayesian Regularisation training.

The results from the optimised neural network are shown in the contingency table (Table 6.12) after 46 live trials; 23 natural walking and 23 walking with a backpack. The associated classification performance is shown in Table 6.13 and shows a good level of accuracy. Additionally, both classes are well balanced with the specificity and sensitivity values very close together.

Actual	Predicted Class	
Class	Natural	Backpack
Natural	20	3
Backpack	2	21

Table 6.12: *Contingency table showing classification accuracy*

Sensitivity	0.91
Specificity	0.87
PPV	0.88
NPV	0.91
Overall	89%

Table 6.13: *Classifier performance results for optimised feature set*

6.4.7 Discussion

In this experiment, the issues identified in previous experiments have been taken into account and a robust method has been implemented to discriminate small changes in gait. Using simple but effective methods, a distance algorithm was developed that compared the data to a template generated as a mean vector from fifty training samples. In addition a standard deviation vector was used to take into account the variability of the person's walking style. A neural network was then used to couple the sensor data and cope with the non-linearities present within the system. Promising results were achieved, with an overall accuracy of just under 90% in live testing and 96% in offline testing. The results showed that one of the main dependencies on accuracy was training and optimisation of the neural network. Although the results presented were from an optimised network, its possible that deeper analysis of the network architecture could improve results further. In addition the training data used for both the template and neural networks could be pruned to remove 'outliers' in the data. However, in this case it was decided that only by including all the (valid) data, could a truly

representive result be achieved.

It should also be pointed out at this stage that one of the disadvantages of this method is the amount of training data required; in this case fifty trials to generate the template and one hundred (separate) trials for the neural network. However, the nature of the system means that live captures can continue to be stored during use to provide further training data over time when accompanied with the correct class, leading to an adaptive system that can learn gait patterns over time.

Another aim of this experiment was to produce a technique that could be generalised to various similar applications. As long as a change in gait occurs it is proposed that this method can be applied to any application where a diversion from natural walking occurs. It is suggested that one application of the system is to provide a form of screening tool, to detect possible walking disorders at an early stage. Research of the literature also suggests that variability in gait is a useful predictor of falls and fear of falls in older adults [97; 98]. Using the inbuilt variability measure within this system, it could possibly be applied to this area of research as well.

6.5   Conclusion

This final section has investigated the possibility of detecting and discriminating small changes in a person's gait. Initially, the feature extraction method developed in section 5.4 was extended. In this case the differences between three sensors were calculated and the features extracted from the two resulting vectors. Discrimination analysis was used again to classify between natural walking and walking with a tray. Overall classification rates were high with an 83% accuracy. However, it was hypothesised that the performance could be increased further by removing redundant features. This was done by calculating the Wilk's Lambda for each feature to test it's significance. Ten significant features were found and used to run further tests. However, the resulting accuracy dropped

to 81%. Therefore, the non-significant features, when combined were probably making an important contribution to the discriminatory power of the function.

It was suggested that despite the high accuracy achieved, feature extraction methods weren't generalisable to any scenario. Different walking disorders would potentially affect different features of the gait pattern and hence would need to be identified and somehow extracted for each different application. Therefore, a distance based algorithm was developed which relied on the overall shape of the gait pattern and hence was potentially more generalisable. The algorithm developed created templates on gait patterns that were fully normalised and mapped onto a 200 element vector. The template was created by taking multiple captures and calculating the mean and standard deviation of each of the two hundred elements. The cost was calculated by the distance of the captured gait profile from the mean template, weighted by the standard deviation. The same was done for the first derivative of the captured profiles and the two costs multiplied together to give an overall cost. This was done for each of the three sensors.

It was found that better results were achieved by only storing a template for the 'abnormal' gait. Neural networks were then used to couple the sensor data and define the cost threshold, hence using the distributive tactile sensing method to discriminate between normal and abnormal gait. Accuracies of 89% were achieved. This algorithm can also learn adaptively so future captures can be used to tweak the gait templates. This makes the final algorithm a highly flexible and accurate method that acheives the main aims of the project.

Chapter 7

Conclusion and Summary

7.1 Concluding Remarks

In this thesis a system has been designed, developed and tested that is able to discriminate between different gait patterns when a person walks over a sensing platform. Using a small number of low cost sensing elements and the distributive tactile method, the system provides a practical solution for gait analysis and overcomes some of the limitations found in a force plate. Several experiments and investigations were required to progressively develop the system and meet the aims of the project.

In Chapter 3 a mathematical model was developed to test the viability of using the distributive tactile sensing method on a large scale dynamic project. The model was designed to test the possibility of being able to track a moving load (object) as it passed across the surface of the plate. The load was to be tracked by analysing the deflection of the plate caused by the load using a small number of sensing elements. The amplitude of the applied force was varied harmonically, which for the experiment had a profile in the form of a square wave.

A method developed by Szilard [31] was taken and extended to that of a moving

load and also to take into account damping. Using this data, a novel method of analysis was developed that was able to use the deflection data from six locations under the plate to determine the location of the load at any point in time. The method developed was primarily based around data reduction techniques including sensor optimisation using genetic algorithms and Karhunen-Loeve decomposition. Neural networks were used to relate the reduced data vectors to an actual position on the plate. Results showed, that whilst being dependent on the window size, it was possible to track the moving load with an accuracy of up to 98%. This relates to just 18mm positional error on the plate.

In Chapter 4, the first experimental setup was developed. This experiment was designed to be controllable and hence have a minimum number of variables. However, it also had be relevant to the overall project and provide an extensible solution towards the main aims of the project. Following on from the mathematical model, this experiment investigated whether the position of a pendulum could be tracked using the deflection of the plate caused by the frame the pendulum was mounted on.

Various sensor methods were investigated, with infra-red distance measuring sensors being the chosen devices due to their high analogue resolution, simple construction and previous use in distributive tactile sensing applications. The distributive tactile sensing method was used to capture and analyse the data. This time a neural network was implemented on a field programmable array (FPGA) device enabling real-time output of the swing location. To train the neural network a Vicon MX13 motion capture system was used to capture the position of the pendulum in three dimensions over time. Using this accurate training method, it was found that real-time tracking of the pendulum was possible with a minimum accuracy of 95%. This compares favourably with the results produced by Betker et al [51], who achieved 90% accuracy when measuring Centre of Mass using accelerometers. It would be relatively straight forward to extend the position calculations in this experiment to provide centre of pressure or centre of mass measurements. With the ability to output these measurements, the system could then be applied to the measurement of sway in a person during quiet standing.

In Chapter 5 the limitations of the equipment developed in the previous experiment are identified and improved upon. In particular, the plate is scaled up to a size that can comfortably accommodate a person's stride, with the base plate containing the sensing elements sandwiched in the frame, to reduce susceptibility to external disturbances. A classification experiment is then developed, whereby the gait pattern alone is used to identify one of five volunteers.

From this experiment, it was hypothesised that certain walking styles could affect the accuracy of the system. In particular, a person with a widely varying walking style could be misclassified as one of many different people. A walking style identified as the 'generic walker' was found to be most destructive in terms of affecting the system accuracy however. A generic walker has a very standard walking style with few unique features. When using a shape matching algorithm such as DTW, this can cause other members to be easily misclassified as the generic walker. When applied to this novel application, feature extraction with linear discrimination achieved the best results with a 78% overall classification accuracy. In comparison DTW achieved a 70% accuracy. Both these results were accomplished using a single sensor and therefore it is suggested that applying the methods used in Chapter 6 would improve the accuracy further.

In Chapter 6, more subtle changes in gait were investigated by attempting to discriminate a change in a person's walking. The experiment involved a person walking naturally and then walking with a backpack or heavy tray which caused small changes in their gait pattern. Distributive tactile sensing was found to be a successful technique in discriminating between the two types, while the use of a neural network was found to be essential to cope with the non-linearities involved. Two methods were investigated for this experiment: optimised feature extraction and a normalised distance method combined with neural networks. The feature extraction method produced an overall classification accuracy of 83%. However, when the features were optimised using statistical methods, the accuracy was reduced to 81%. Furthermore, live tests showed a dramatic decrease in accuracy to just 42%. The normalised distance method on the otherhand performed well in both offline and live testing, achieving 96% and 89% respectively. In a similar

experiment, Lafuente *et al* [56] achieved slightly lower accuracies (75%) when using discrimination analysis for gait classification while their neural network method had an accuracy of almost 10% lower than that accomplished with the novel normalised distance method.

Based on captured results and published work, it was found the system accuracy is improved if normal walking is not 'classified', i.e. no template is stored for normal walking. This is due to the high variability in normal walking due to the unrestricted degrees of freedom. On the other hand affected walking will usually be restricted, particularly when due to a pathological or neurological issue. Therefore affected walking is less variable and more likely to match a template when present.

7.2 Algorithms

In Chapter 3, Genetic algorithms were used to optimise the sensor locations. Although, genetic algorithms are useful in various applications, it is a very subjective method that relies on the researcher to correctly identify the appropriate cost function to achieve effective results. Therefore, although it is an optimisation method, there is no guarantee that the results provide the most optimum outcome. In the method described, the genetic algorithm results were used as a guide as to where to place the sensors.

Karhunen-Loeve decomposition (KLD) was used as a data reduction technique to convert large time series datasets into much smaller vectors. As well as the method being used for generating proper orthogonal functions, it is also suitable for producing small vectors that are appropriate for input to neural networks. Along with the use of a windowing method, KLD was found to generate suitable variation in the resulting vectors for a neural network to relate the vector to a location on the plate.

Dynamic time warping (DTW) has previously been used in handwriting and signature identification applications. It works as a cost based function where the distance between the captured data and a template is compared. DTW extends this by being able to warp the time axes such that it can compare the distances between adjacent samples as well. Because of this DTW was identified as a potentially powerful algorithm that would be able to cope with people ambulating over the surface at different walking speeds. DTW was also used to identify the most representative template from a number of captures, although this was found to be an ineffective method overall. The results showed that for person identification, DTW achieved 70% overall accuracy but was found to be affected by different walking styles.

Feature extraction is also a commonly used method in handwriting identification. Feature extraction is not a classification algorithm in itself and is usually used in combination with neural network or discrimination analysis. This method was found to achieve a slightly higher overall accuracy in the person identification experiment in comparison to DTW. In particular it appeared to be more effective in correctly classifying the variable walker. Statistical methods were used to optimise the feature vector in the experiment described in Chapter 6, such that the features that contributed most to the classification were identified, enabling redundant features to be discarded and hence reduce noise in the system. This can improve classification accuracy. In this experiment however, the accuracy was reduced, indicating that the combined contribution of the discarded features was important to the correct classification.

The main limitation of the feature extraction method was that it was a very 'fixed' method whereby the features had to be present in all the classes (albeit at different values) in order for it to be effective. This is especially the case with algorithms that automatically extract the features. The algorithm became unreliable if a feature did not exist or if they occurred out of sequence. One of the aims of the project was to develop a method that could be easily generalised to any form of gait classification, this was not possible using the feature extraction method.

In the final experiment a novel algorithm is implemented that is based on the observations of the previous algorithms investigated. The algorithm had the following features:

1). Used the distributive tactile sensing method - i.e three sensors were used to provide plate deflection data from different locations on the surface.

2). Used a shape matching/distance algorithm - enabling a generalisable method to be developed.

3). Used neural networks to couple the sensor data, define the classification threshold and cope with other non-linearities in the system, such as foot strike location.

4). Templates based around mean values from multiple captures, enabling continuous 'fine-tuning' over time

To ensure walking speed and a person's weight were not used in the classification, the resulting data were fully normalised in time and amplitude. Unlike DTW, this method did allow for differences in speed locally. For example a faster heel strike duration and slower toe-off was able to be discriminated using this algorithm, whereas DTW would have warped the time axis appropriately and therefore removed a potentially important change. To account for variability in a person's walking, the algorithm used the standard deviation calculated from the training captures as a weighting factor for the distance calculation. Finally, the template for normal walking was discarded due to the expected high variability normal walking is known to have in comparison to affected walking.

The developed algorithm produced higher accuracies than any of the previous tested methods, with an accuracy of just under 90% in live tests. By incorporating the above features, the algorithm was found to be suitably sensitive to small changes in the gait pattern. It also has the potential to be applied to clinical applications by simply generating a different template for the affected gait pattern required to be classified.

7.3 Limitations

Due to the priorities of the research, it has not been possible to test the discrimination methods on larger sample sizes. In particular, it is unlikely that the person identification experiment could be successfully applied to a large number of subjects. However, it is suggested that if some of the later methods developed were applied to this experiment, then greater accuracies would be achievable with a reasonably sized sample. It should also be noted that the volunteers involved in the experiment were of a similar physical form and age. Larger samples would bring greater variation and therefore provide to a certain extent more distinguishable gait patterns.

It would have been useful to test the final system on a real pathological or neurological gait disorder. The long ethics process and low availability of volunteers did not make this possible however. It is suggested that accuracies may even improve when tested with real physical gait problems. The tests described in this thesis only created a small change or restriction in a person's walking, while there was evidence that the results were affected by their awareness of the test being carried out.

Although it may be possible to calibrate the system to provide force or moment measurements, it is unlikely that the results attained would have the accuracy of a force plate. However, the aims of the project were not to create a system that improves upon the measurements provided by a force plate. Instead, the project aimed to go a step further and be able to discriminate different gait patterns rather than just provide raw measurements. Another aim was to attempt to overcome some of the physical limitations of the force plate. Both of these aims have been achieved.

7.4 Applications

The mathematical model describes a novel method of tracking an object as it moves along a surface. This could be applied to tracking the motion of people walking over a bridge for example or in an industrial setting, used to track objects on a conveyor belt. The method developed eliminates the need for a camera based system and instead uses low cost sensors to measure the surface deflection.

As described in Chapter 4, the pendulum tracking experiment could be very easily extended to the measurement of balance of sway in people. By using a larger platform, like the one used in the walk discrimination experiments and a different set of training data that relates deflection to centre of mass or centre of pressure, the system could be used to measure the sway in a person during quiet standing. Similarly, it could also be used for sports training applications such as the monitoring of stance during a golf swing or bowling a cricket ball.

Biometrics is an ever growing industry. However, most biometric measurement systems are intrusive. Finger print and iris identification, currently require conscious interaction with the system. The experiment in Chapter 5 describes the possibility of a platform based system that could be used to identify a person from their gait pattern. This could be implemented in low population areas such as an office. Instead of the person being required to consciously interact with the system, they are identified by simply walking over the active surface as they enter the building.

The completed system, described in Chapter 6 has applications in gait analysis as stated in the main project aims. The ability to discriminate between different types of gait pattern or small changes in a gait pattern mean that the system could be used as an initial screening tool for identifying walking disorders or as a system that is able to determine the change in a person's walking over time be it an improvement, degradation or pre and post operation.

7.5   Suggested Further Work

Before the developed system can be applied as a medical tool, the following suggestions should be implemented.

1). Test the system with a real gait disorder in comparison to normal walking or another gait disorder. This will enable the researcher to get a sense of the real accuracies that can be achieved.

2). Extend the sensing data to capture a full stride (two foot strikes). This could provide the system with a lot of extra data and hence improve discrimination accuracy.

3). Investigate the physical size limitations of the platform. Can the platform be extended to capture several strides? The ultimate aim would be to have an active floor made up of multiple platforms that could measure gait without limitation. This would dramatically improve accessibility to those with severe walking disorders, the elderly with limited balance or young children who would be able to move around freely.

Bibliography

[1] R. DeMeis, Piezos step up gait analysis - treadmill force plates measure real-world patient mobility (August 1998).
URL http://www.designnews.com/article/CA119243.html 2.2

[2] R. Kram, A. J. Powell, A treadmill-mounted force platform, Journal of Applied Physiology 67 (1989) 1692–1698. 2.2

[3] R. Kram, T. M. Griffin, J. M. Donelan, Y. H. Chang, Force treadmill for measuring vertical and horizontal ground reaction forces, Journal of Applied Physiology 85 (2) (1998) 764–769. 2.2

[4] F. Dierick, M. Penta, D. Renaut, C. Detrembleur, A force measuring treadmill in clinical gait analysis, Gait and Posture 20 (2004) 299–303. 2.2

[5] B. L. Davis, P. R. Cavanagh, Decomposition of superimposed ground reaction forces into left and right force profiles, Journal of Biomechanics 26 (1993) 593–597. 2.2

[6] A. Belli, P. Bui, A. Berger, A. Geyssant, J. R. Lacour, A treadmill ergometer for three-dimensional ground reaction forces measurement during walking, Journal of Biomechanics 34 (2001) 105–112. 2.2

[7] G. Paolini, U. D. Croce, P. O. Riley, F. K. Newton, D. C. Kerrigan, Testing of a tri-instrumented-treadmill unit for kinetic analysis of locomotion tasks in static and dynamic loading conditions, Medical Engineering and Physics 29 (2007) 404–411. 2.2

[8] V. Wank, U. Frick, D. Schmidtbleicher, Kinematics and electromyography of lower limb muscles in overground and treadmill running, International Journal of Sports Medicine 19 (1998) 455–61. 2.2

[9] F. Alton, L. Baldey, S. Caplan, M. C. Morrissey, A kinematic comparison of overground and treadmill walking, Clinical Biomechanics 13 (1998) 434–440. 2.2

[10] A. Matsas, N. Taylor, H. McBurney, Knee joint kinematics from familiarised treadmill walking can be generalised to overground walking in young unimpaired subjects, Gait and Posture 11 (2000) 46–53. 2.2

[11] A. G. Schache, P. D. Blanch, D. A. Rath, T. V. Wrigley, R. Starr, K. L. Bennell, A comparison of overground and treadmill running for measuring the three dimensional kinematics of the lumbo-pelvic-hip complex, Clinicial Biomechanics 16 (2001) 667–680. 2.2

[12] T. Warabi, M. Kato, K. Kiriyama, T. Yoshida, N. Kobayashi, Treadmill walking and overground walking of human subjects compared by recording sole floor reaction force, Neuroscience Research 53 (2005) 343–348. 2.2

[13] P. O. Riley, G. Paolini, U. D. Croce, K. W. Paylo, D. C. Kerrigan, A kinematic and kinetic comparison of overground and treadmill walking in healthy subjects, Gait and Posture 26 (1) (2007) 17–24. 2.2

[14] H. H. C. M. Savelberg, M. A. Vorstenbosch, E. H. Kamman, J. G. van de Weijer, H. C. Schambardt, Intra-stride belt-speed variation affects treadmill locomotion, Gait and Posture 7 (1998) 26–34. 2.2

[15] V. Lavcanska, N. F. Taylor, A. G. Schache, Familiarization to treadmill running in young unimpaired adults, Human Movement Science 24 (2005) 544–557. 2.2

[16] C. S. Nicolopoulos, E. G. Anderson, S. E. Solomonidis, P. V. Giannoudis, Evaluation of the gait analysis fscan pressure system: clinical tool or toy?, The Foot 10 (2000) 124–130. 2.2

[17] R. E. Ellis, S. R. Ganeshan, S. J. Lederman, A tactile sensor based on thin-plate deformation, Robotica 12 (1994) 343–351. 2.3, 3.1

[18] P. N. Brett, R. S. Stone, A technique for measuring contact force distribution in minimally invasive surgical procedures, Proc. Instn Mech Engrs Part H 211 (1997) 309–316. 2.3, 3.1

[19] X. Ma, P. N. Brett, M. T. Wright, M. V. Griffiths, A flexible digit with tactile feedback for invasive clinical applications, Proc. Instn Mech Engrs Part H: J. Engineering in Medicine 218 (2004) 151–157. 2.3, 3.1

[20] P. N. Brett, Z. Li, A tactile sensing surface for artificial neural network based automatic recognition of the contact force position, Proc. Instn Mech Engrs Part I 214. 2.3, 4.3.3.1, 4.3.3.1

[21] P. Tongpadungrod, T. Rhys, P. Brett, An approach to optimise the critical sensor locations in one-dimensional novel distributive tactile surface to maximise performance, Sensors and Actuators A 105 (2003) 47–54. 2.3, 3.3.3, 4.3.3.1, 4.3.3.1

[22] M. A. Hilal, H. S. Zibdeh, Vibration analysis of beams with general boundary conditions traversed by a moving force., Journal of Sound and Vibration 229 (2000) 377–388. 2.4

[23] A. V. Pesterev, B. Yang, L. A. Bergman, C. A. Tan, Revisiting the moving force problem, Journal of Sound and Vibration 261 (2003) 75–91. 2.4

[24] J. A. Gbadeyan, S. T. Oni, Dynamic behaviour of beams and rectangular plates under moving loads, Journal of Sound and Vibration 182 (5) (1995) 677–695. 2.4

[25] Y. H. Lin, Comments on 'dynamic behavior of beams and rectangular plates under moving loads', Journal of Sound and Vibration 200 (5) (1995) 721–728. 2.4

[26] J. S. Wu, M. L. Lee, T. S. Lai, The dynamic analysis of a flat plate under a moving load by the finite element method, International Journal for numerical methods in engineering 24 (1987) 743–762. 2.4

[27] X. Q. Zhu, S. S. Law, Dynamic behaviour of orthotropic rectangular plates under moving loads, Journal of Engineering Mechanics 129 (2003) 79–87. 2.4

[28] L. Sun, Analytical dynamic displacement response of rigid pavements to moving concentrated and line loads, International Journal of Solids and Structures 43 (2006) 4370–4383. 2.4

[29] H. C. Kwon, M. C. Kim, I. W. Lee, Vibration control of bridges under moving loads, Computers and Structures 66 (1998) 473–480. 2.4

[30] L. Fryba, Vibration of Solids and Structures under Moving Loads, Thomas Telford Ltd, London, 1999. 2.4

[31] R. Szilard, Theory and analysis of plates, classical and numerical methods, Prentice-Hall, New Jersey, 1974. 2.4, 3.1, 3.2, 3.5, 4.4.1, 7.1

[32] T. H. T. Chan, S. S. Law, T. H. Yung, An interpretive method for moving force identification, Journal of Sound and Vibration 219 (3) (1999) 503–524. 2.4

[33] L. Yu, T. H. T. Chan, S. S. Law, Moving force identification based on the frequency-time domain method, Journal of Sound and Vibration 261 (2003) 329–349. 2.4

[34] X. Q. Zhu, S. S. Law, Time domain identification of moving loads on a bridge deck, Journal of Vibration and Acoustics 125 (2003) 187–198. 2.4

[35] T. H. T. Chan, L. Yu, S. S. Law, T. H. Yung, Moving force identification studies, I: Theory, Journal of Sound and Vibration 247 (1) (2001) 59–76. 2.4

[36] T. H. T. Chan, L. Yu, S. S. Law, T. H. Yung, Moving force identification studies, II: Comparitive studies, Journal of Sound and Vibration 247 (1) (2001) 77–95. 2.4

[37] B. T. Wang, Prediction of impact and harmonic force acting on arbitrary structures: theoretical formulation, Mechanical Systems and Signal Processing 16 (2002) 935–953. 2.4

[38] K. Choi, F. K. Changf, Identification of impact force and location using distributed sensors, American Institute of Aeronautics and Astronautics Journal 34 (1996) 136.
URL http://pdf.aiaa.org/jaPreview/AIAAJ/1996/PVJAPRE13033.pdf
2.4

[39] M. D. Graham, I. G. Kevrekidis, Alternative approaches to the karhunen-loeve decomposition for model reduction and data analysis., Computers and Chemical Engineering 20 (5) (1996) 495–506. 2.4

[40] P. Gallina, Neural network painting defect classification using karhunen-loeve transformation, Optics and Lasers in Engineering 32 (1999) 29–40. 2.4

[41] N. Smaoui, S. Al-Enezi, Modelling the dynamics of nonlinear partial differential equations using neural networks, Journal of Computation and Applied Mathematics 170 (2004) 27–58. 2.4

[42] S. Ondimu, H. Murase, Reservoir level forcasting using neural networks: Lake Naivasha, Biosystems Engineering 96 (2007) 135–138. 2.4

[43] M. O'Farrell, E. Lewis, C. Flanagan, W. B. Lyons, N. Jackman, Combining principal component analysis with an artificial neural network to perform online quality assessment of food as it cooks in a large-scale industrial oven, Sensors and Actuators B: Chemical 107 (2005) 104–112. 2.4

[44] J. L. Miller, Parkinson's disease primer, Geriatric Nursing 23 (2) (2002) 69–75. 2.5, 4.1

[45] A. L. Adkin, B. R. Bloem, J. H. J. Allum, Trunk sway measurements during stance and gait tasks in parkinson's disease, Gait and Posture 22 (2005) 240–249. 2.5, 4.1

[46] S. R. Lord, Vision, balance and falls in the elderly (November 2003).
URL http://www.cmellc.com/geriatrictimes/g031209.html 2.5, 4.1

[47] R. Paillex, A. So, Changes in the standing posture of stroke patients during rehabilitation, Gait and Posture 21 (2005) 403–409. 2.5, 4.1

[48] S. Freitas, S. A. Wieczorek, P. H. Marchetti, M. Duarte, Age-related changes in human postural control of prolonged standing, Gait and Posture 22 (2005) 322–330. 2.5, 4.1

[49] P. A. Goldie, T. M. Bach, O. M. Evans, Force platform measures for evaluating postural control: reliability and validity, Archives of physical medicine and rehabilitation 70 (7) (1989) 510–517.
URL http://www.ncbi.nlm.nih.gov/entrez/query.fcgi?db=PubMed&cmd=Retrieve&list_uids=2742465&dopt=Citation 2.5

[50] R. Moe-Nilssen, J. L. Helbostad, Trunk accelerometry as a measure of balance control during quiet standing, Gait and Posture 16 (2002) 60–68. 2.5, 4.1, 4.3.3.1

[51] A. L. Betker, Z. M. K. Moussavi, T. Szturm, Center of mass approximation and prediction as a function of body acceleration, IEEE Transactions on Biomedical Engineering 53 (2006) 686–693. 2.5, 4.1, 4.3.3.1, 7.1

[52] R. E. Mayagoitia, J. C. Lotters, P. H. Veltink, H. Hermens, Standing balance evaluation using a triaxial accelerometer, Gait and Posture 16 (2002) 55–59. 2.5, 4.1

[53] R. Moe-Nilssen, A new method for evaluating motor control in gait under real-life environmental conditions. part 1: The instrument, Clinical Biomechanics 13 (1998) 320–327. 2.5

[54] W. I. Schollhorn, Applications of artificial neural nets in clinical biomechanics, Clinical Biomachanics 19 (2004) 876–898. 2.6

[55] M. Kohle, D. Merkl, Analyzing human gait patterns for malfunction detection, in: SAC '00: Proceedings of the 2000 ACM symposium on Applied computing, ACM Press, New York, NY, USA, 2000, pp. 41–45. 2.6, 5.3.3, 6.4.4

[56] R. Lafuente, J. M. Belda, J. Sanchez-Lacuesta, C. Soler, J. Prat, Design and test of neural networks and statistical classifiers in computer aided movement

analysis: a case study on gait analysis, Clinical Biomechanics 13 (1997) 216–229. 2.6, 7.1

[57] F. Dobson, M. E. Morris, R. Baker, H. K. Graham, Gait classification in children with cerebral palsy: A systematic review, Gait and Posture 25 (2007) 140–152. 2.6

[58] S. Armand, E. Watelain, M. Mercier, G. Lensel, F. Lepoutre, Identification and classification of toe-walkers based on ankle kinematics, using a data-mining method, Gait and Posture 23 (2006) 240–248. 2.6

[59] M. Alwan, S. Dalal, S. Kell, R. Felder, Derivation of basic human gait characteristics from floor vibrations, in: Summer Bioengineering Conference, Sonesta Beach Resort in Key Biscayne, Florida, 2003. 2.6

[60] M. D. Addlesee, A. Jones, F. Livesey, F. Samaria, The ORL active floor, IEEE Personal Communications 4 (5) (1997) 35–41. 2.6

[61] R. Zhang, C. Vogler, D. Metaxas, Human gait recognition at sagittal plane, Image and Vision Computing 25 (2007) 321–330. 2.6, 5.1

[62] C. Bauckage, J. K. Tsotsos, F. E. Bunn, Automatic detection of abnormal gait, Image and Vision Computing In Press (2007) In Press. 2.6

[63] C. Ratanamahatana, E. Keogh. Making Time-Series Classification More Accurate Using Learned Constraints. In Proceedings of the 2004 SIAM International Conference on Data Mining. 2.6, 5.3.2

[64] C.A. Ratanamahatana and E. Keogh. Everything you know about Dynamic Time Warping is Wrong. In Proc. 3rd Workshop of Mining Temporal and Sequential Data, 2004. 2.6

[65] R. Niels, Dynamic Time Warping: An intuitive way of handwriting recognition?, Master's thesis, Radboud University Nijmegen, Faculty of Social Sciences, Department of Artificial Intelligence / Cognitive Science, http://dtw.noviomagum.com (Nov.-Dec. 2004).
URL citeseer.ist.psu.edu/niels04dynamic.html 2.6, 5.3.1

[66] W. L. Wu, F. C. Su, Potential of the back propagation neural network in the assessment of gait patterns in ankle arthrodesis, Clinical Biomechanics 15 (2000) 143–145. 2.6

[67] S. M. Hsiang, C. Chang, The effect of gait speed and load carrying on the reliability of ground reaction forces, Safety Science 40 (2002) 639–657. 2.6, 6.3.1

[68] M. T. Elliott, X. Ma, P. N. Brett, Tracking the position of an unknown moving load along a plate using the distributive sensing method, Sensors & Actuators A: Physical In Press (2007) In Press. 3.1

[69] C. Wolter, M. A. Trindade, R. Sampaio, Obtaining mode shapes through the Karhunen-Loeve expansion for distributed parameter linear systems, Shock and Vibration 9 (2002) 177–192. 3.3.2

[70] D. J. C. MacKay, A practical Bayesian framework for backprop networks, in: Advances in Neural Information Processing Systems 4, 1992, pp. 839–846. 3.3.4.1

[71] B. M. Cowie, D. J. Webb, B. Tam, P. Slack, P. N. Brett, Fibre Bragg grating sensors for distributive tactile sensing, Measurement Science and Technology 18 (2007) 138–146.
URL stacks.iop.org/MST/18/138 4.3.3.1, 4.3.3.1

[72] Accelerometers — Honeywell Sensotec frequently asked questions.
URL http://www.sensotec.com/accelerometer_faq.asp 4.3.3.1

[73] Acceleration sensor series (model: Apa300) reference guide (amplifier circuit design information), 20-10 Nakayoshida, Shizuoka, Japan 422-8654 (December 17 2003). 4.3.3.1

[74] Texas Instruments: Information for medical applications, pages 17-18 (30 Jun 2004).
URL http://focus.ti.com/lit/ml/slyb108a/slyb108a.pdf 4.3.4.2

[75] I. Petra, D. J. Holding, X. Ma, P. N. Brett, K. J. Blow, Fast and accurate tactile sense feedback estimation for innovative flexible digit for clinical applications, Electronics Letters 42 (14) (2006) 790–792. 4.3.6, 4.6

[76] Z. Losonc, The basic properties of the pendulum (August 2003).
URL http://www.gyogyitokezek.hu/fe/pendtutor1.htm 4.4.1

[77] M. P. Murray, A. B. Drought, R. C. Kory, Walking patterns of normal men, Journal of Bone and Joint Surgery 46 (1964) 335–360. 5.2.1

[78] K. H. E. Kroemer, Engineering physiology, bases of human factors/ergonomics, 3rd Edition, Van Nostrand Reinhold, 1997. 5.2.1

[79] S. C. Wearing, S. Urry, J. E. Smeathers, D. Battistutta, A comparison of gait initiation and termination methods for obtaining plantar foot pressures, Gait and Posture 10 (1999) 255–263. 5.2.1

[80] B. Meyers-Rice, L. Sugars, T. Mcphoil, M. W. Cornwall, Comparison of three methods for obtaining plantar pressures in nonpathologic subjects, Journal of the American Podiatric Medical Association 84 (10) (1994) 499–504.
URL http://www.japmaonline.org/cgi/content/abstract/84/10/499
5.2.1

[81] C. L. Ogden, C. D. Fryar, M. D. Carroll, K. M. Flegal, Mean body weight, height and body mass index, united states 1960-2002, Advance data from vital and health statistics 347 (2004) 9. 5.2.1

[82] T. S. Keller, A. M. Weisberger, J. L. Ray, S. S. Hasan, R. G. Shiavi, D. M. Spengler, Relationship between vertical ground reaction force and speed during walking, slow jogging and running, Clinical Biomechanics 11 (5) (1996) 253–259. 5.2.1

[83] S. Sarkar, P. J. Phillips, Z. Liu, I. R. Vega, P. Grother, K. W. Bowyer, The HumanID Gait Challenge Problem: Data sets, performance and analysis, IEEE Transactions on Pattern Analysis and Machine Intelligence 27 (2) (2005) 162–177. 5.3.1

[84] L. Wang, H. Ning, T. Tan, W. Hu, Fusion of static and dynamic body biometrics for gait recognition, IEEE Transactions on Circuits and Systems for Video Technology 14 (2) (2004) 149–158. 5.3.1

[85] L. Lee, Gait analysis for classification, Ph.D. thesis, Department of Electrical Engineering and Computer Science, Massachusetts Institute Of Technology (Lee2003). 5.3.1

[86] T. M. Rath, R. Manmatha. Features for word spotting in historical manuscripts. Proceedings of the Seventh International Conference on Document Analysis and Recognition. 3-6 Aug. 2003 Page(s):218 - 222 vol.1. 5.3.1

[87] F. Jiang, H. Yao, G. Yao, Multilayer architecture in sign language recognition system, in: ICMI '04: Proceedings of the 6th international conference on Multimodal interfaces, ACM Press, New York, NY, USA, 2004, pp. 352–353. 5.3.1

[88] H. Sakoe, S. Chiba, Dynamic programming algorithm optimization for spoken word recognition, IEEE Transactions on Acoustics, Speech, and Signal Processing 26 (1) (1978) 43–49. 5.3.2

[89] K. Huang, H. Yan, Off-line signature verification based on geometric feature extraction and neural network classification, Pattern Recognition 30 (1) (1997) 9–17. 5.4.1

[90] B. Verma, M. Blumenstein, M. Ghosh, A novel approach for structural feature extraction: Contour vs. direction, Pattern Recognition Letters 25 (2004) 975–988. 5.4.1

[91] V. Pervouchine, G. Leedham, Extraction and analysis of forensic document examiner features used for writer identification, Pattern Recognition 40 (2007) 1004–1013. 5.4.1

[92] P. S. Huang, C. J. Harris, M. S. Nixon, Recognising humans by gait via parametric canonical space, Artificial Intelligence in Engineering 13 (1999) 359–366. 5.4.1

[93] A. R. Webb, Statistical Pattern Recognition, 2nd Edition, John Wiley & Sons, Ltd., 2002. 5.4.3

[94] T. W. Loong, Understanding sensitivity and specificity with the right side of the brain, British Medical Journal 327 (2003) 716–719. 6.3.4.1

[95] H. Demuth, M. Beale, Neural Network Toolbox: User's Guide, 8th Edition, The Mathworks, 2004. 6.4.5.1

[96] L. K. Hansen, P. Salamon, Neural network ensembles, IEEE Transactions on pattern analysis and machine intelligence 12 (10) (1990) 993–1001. 6.4.6

[97] B. E. Maki, Gait changes in older adults: predictors of falls or indicators of fear., Journal of the American Geriatric Society 45 (3) (1997) 313–20.
URL http://www.ncbi.nlm.nih.gov/entrez/query.fcgi?cmd=Retrieve&db=PubMed&list_uids=9063277&dopt=Citation 6.4.7

[98] J. M. Hausdorff, M. E. Nelson, D. Kaliton, J. E. Layne, M. J. Bernstein, A. Nuernberger, M. A. F. Singh, Etiology and modification of gait instability in older adults: a randomized controlled trial of exercise, Journal of Applied Physiology 90 (2001) 2117–2129. 6.4.7

Appendix A

Photographs of the experimental setup

A.1 Person Identification User Interface

Figure A.1 shows the graphical user interface developed for running the person identification experiment. Key features of the user interface are numbered and described below:

1). This gives the name of the identified person once a prediction has been made along with numerical values for the score for diagnostic purposes.

2). For extra impact, a photo of the identified person is displayed, along with an audio voice stating the person's name.

3). To keep track of the results during testing, it was possible to record whether the system had correctly identified the person.
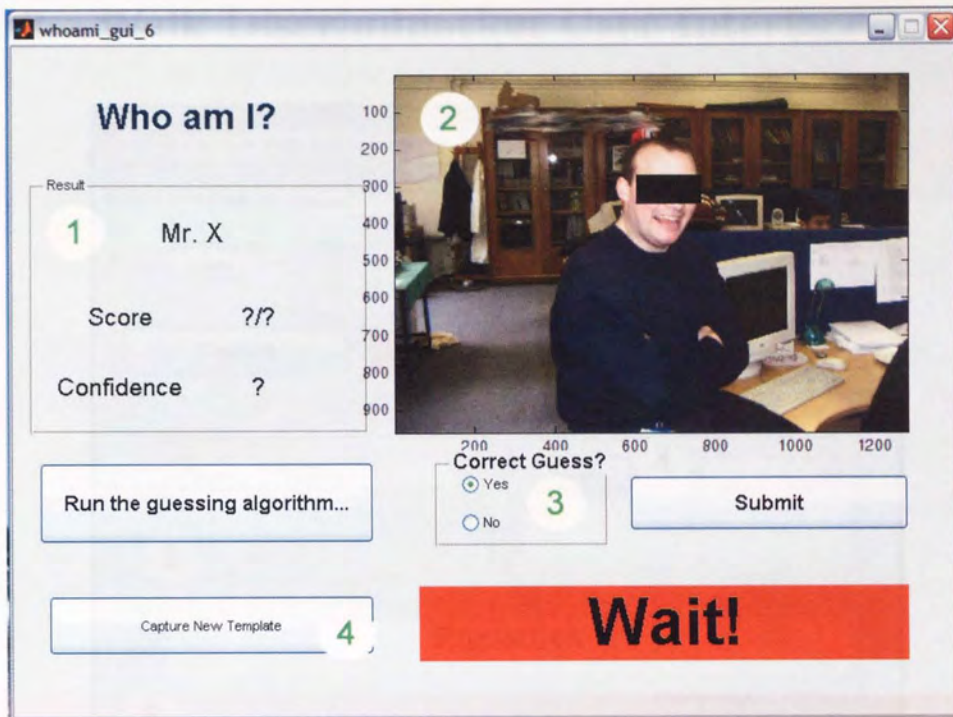
Figure A.1: *Screenshot of the person identification GUI*

4). The GUI was also used for training the system and capturing data to be used for a new template.
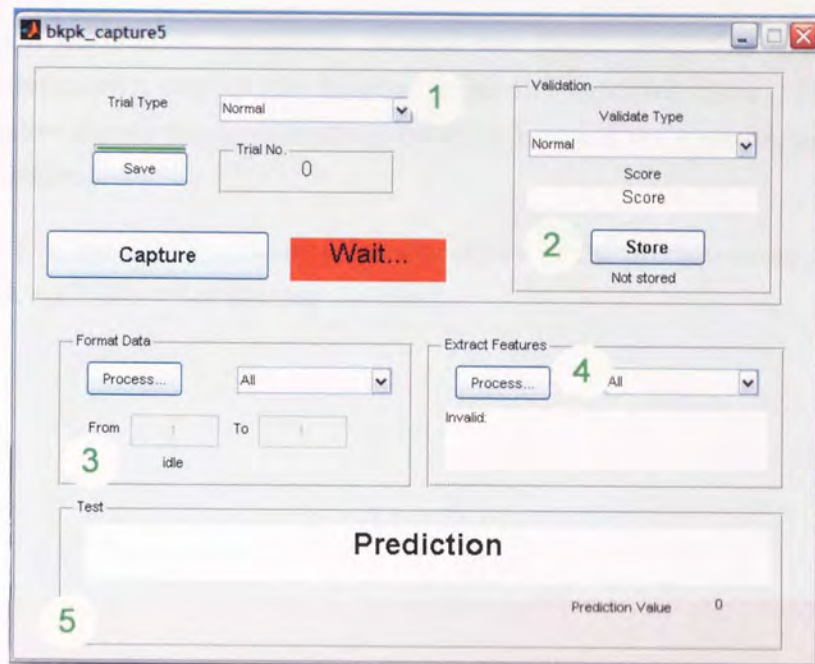
A.2 Walk Discrimination User Interface

Figure A.2: *Screenshot of the walk discrimination GUI*

Figure A.2 shows the more advanced graphical user interface developed for discriminating small changes in a person's gait. The key features of the interface are numbered and described below:

1). This GUI had several modes of operation, including different training methods, offline-testing and live testing. For training/off-line testing a running count of captures was displayed as well as an option to save the captured data.

2). For offline-testing the user was required to identify the actual result to the system, so it was possible to measure the accuracy. The score window displays the distance scores calculated for each sensor when the captured data is compared to the template.

3). For training, the GUI was now able to fully format the captured data before it was stored, for example apply the moving average filter, normalise, etc.

4). When the feature extraction method was being used, this option would automatically extract the features from the captured data. The invalid window shows the captures that failed to have all the features successfully extracted.

5). For live testing, the classification was shown in the prediction window along with an audio voice stating the class.

A.3   The Sensing Platform

Figure A.3: *The full walkway with the gait initiation platform, sensing platform and gait termination platform respectively.*

Figure A.4: *The sensing platform with the top plate removed showing the baseplate containing the sensors and electronic signal conditioning circuits*

Figure A.5: *Panoramic view of the experimental area, with the sensing plate and motion capture system.*

Figure A.6: *The platform in action.*

Appendix B

Matlab Scripts and Example Databases

B.1 DVD Request

Appendix B is available on DVD/CD format only. Copies of the disc are available through Dr. Xianghong Ma at Aston University. Please send requests to:

Dr. Xianghong Ma
Bio-Medical Engineering Research Group
School of Engineering and Applied Science
Aston University
Aston Street
Birmingham
UK
B4 7ET

Or email: x.ma@aston.ac.uk

B.2   DVD Contents

The DVD contains the following files:

Chapter 3 - Mathematical Model	
gen_data_100706.m	Batch processing script for generating plate deflection data for multiple load speeds
szilard_damping10hz_100706.m	Generates plate deflection data based on Szilard (1974). Uses a 0.05m grid. Takes speed as input
con_Pmn_cxy_damped_100706.m	Creates the training data by extracting data from chosen sensor locations and applying windowing and KLD methods
KL_fun.m	Karhunen-Loeve Decomposition algorithm
mNN_Fpos_damped.m	Neural Network training algorithm
mNN_F_Test_damped.m	Neural Network testing script

Table B.1: *Index of Chapter 3 Matlab scripts*

Chapter 4 - Pendulum Tracking Experiment	
szilard_swing4.m	szilard_swing4.m
mNN_train.m	Offline Neural Network training algorithm
mNN_test.m	Offline Neural Network testing algorithm

Table B.2: *Index of Chapter 4 Matlab scripts*

Chapter 5 - Dynamic Time Warping Experiment	
whoami_gui_6.m	Main GUI control script for the person identification experiment
whoami_gui_6.fig	Main GUI for the person identification experiment
whoami_struct_multi.m	Main algorithm which calculates cost of capture using DTW when compared to each template in order to predict the person that walked over the surface
gen_data.m	Loads all training captures for the persons template, formats it, chooses the best and then stores it in the DB
best_template_auto.m	Compares training data using DTW to determine most representative template
person_db.mat	Database for this experiment

Table B.3: *Index of Chapter 5 (DTW) Matlab scripts*

Chapter 5 - Feature Extraction Experiment	
whoami FX_gui.m	Main controlling script for calling feature extraction and interpreting the result
whoami FX_gui.fig	GUI for Feature Extraction experiment
whoami_fx.m	Main controlling script for calling feature extraction and interpreting the result
feat_extrac3.m	Algorithm to extract the features of the captured data
ext_vectors_live2.m	Run discrimination analysis to classify captured features
whoami_fx_train.m	Captures training data, calls feature extraction routine and stores them in the database
daqcapture.m	Function to set up and control the NI data acquisition card. Returns captured data
person_FX_db.mat	Database for this experiment

Table B.4: *Index of Chapter 5 (Feature Extraction) Matlab scripts*

Chapter 6 - Feature Extraction Experiment	
tray_class_gui.m	Main GUI control script for the two class feature extraction experiment
tray_class_gui.fig	Main GUI for the two class feature extraction experiment
tray_trial_capture111006.m	Captures the data, runs the feature extraction algorithm and then makes a classification using the linear discrimination method
feature_vec_gen2.m	Extracts features from the waveform to make a feature vector
feat_extrac_tray3.m	Extracts features from the waveform to make a feature vector
daqcapture.m	Function to set up and control the NI data acquisition card. Returns captured data
train_data_compile.m	Collects together all the data stored in trials and transfers it to a seperate training data section
get_all_features111006.m	Takes all the features from the training data section and computes the sample mean, covariance and a-priori probability for use with linear discrimination
person_tray_db111006.mat	Database for this experiment

Table B.5: *Index of Chapter 6 (Feature Extraction) Matlab scripts*

Chapter 6 - Normalised Distance Experiment	
bkpk_capture6.m	Main GUI control script for the two class normalised distance experiment
bkpk_capture6.fig	Main GUI for the two class normalised distance experiment
daqcapture.m	Function to set up and control the NI data acquisition card. Returns captured data
bkpk_proc_signals.m	Separates right, left and front sensor signals from captured data set. Stores in database
bkpk_normcurve.m	Removes leading and trailing zeroes, normalises data in time and amplitude
md_templates.m	Calculate distance score between captured data and template for each sensor
bkpk_NN_train.m	Neural network training routine
bkpk_NN10_Golden.mat	Optimised neural network structure
bkpk_data_db191206.mat	Database for this experiment

Table B.6: *Index of Chapter 6 (Normalised Distance) Matlab scripts*